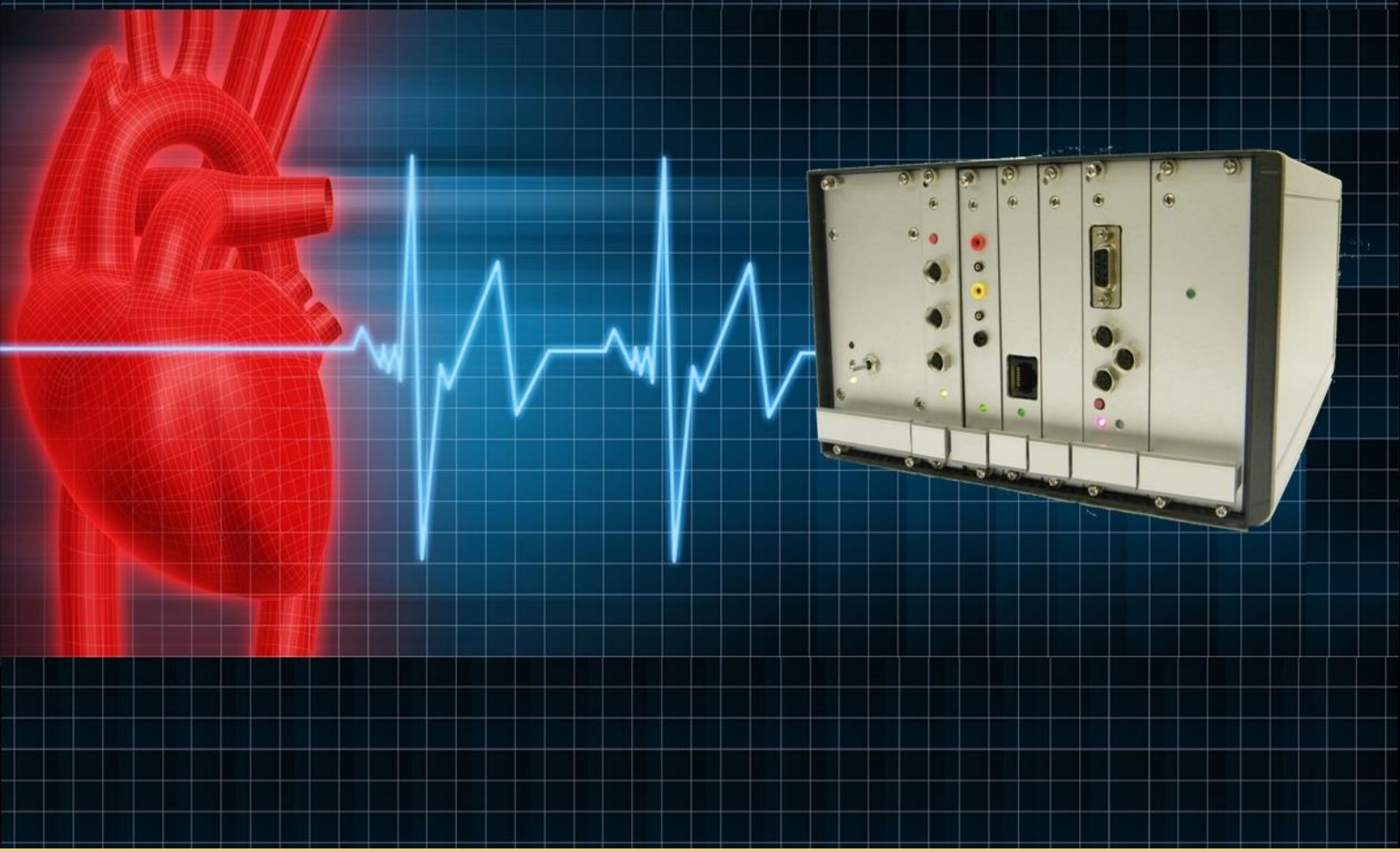

Pedro Miguel Reis Pereira

DAQ software tools for the management of a multichannel platform in hemodynamic studies

Dissertation submitted in partial fulfillment of the

requirements for the MSc degree in Biomedical Engineering

2013

· U C ·

UNIVERSIDADE DE COIMBRA

DAQ software tools for the management of a multichannel platform in hemodynamic studies

Scientific Advisors:

PhD Professor Carlos M. B. A. Correia

PhD João Manuel Rendeiro Cardoso

Scientific Supervisor:

MsC Vânia Maria Gomes de Almeida

Dissertation submitted to the Faculty of Sciences and Technology of the University of Coimbra in partial fulfillment of the requirements for the MsC degree in Biomedical Engineering

Para os meus pais,

Agradecimentos

Em primeiro lugar, gostaria de agradecer aos meus supervisores Prof. Dr. Carlos Correia e Dr. João Cardoso por todo apoio dado ao longo deste ano e por me terem acolhido neste fantástico grupo.

Um especial agradecimento à minha supervisora Vânia Almeida, por tudo o seu incessante apoio e grande disponibilidade que sempre mostrou ao longo de todo o ano.

Aos meus colegas de trabalho Pedro Santos, Pedo Vaz, Mariana Sequeira e Neide com quem partilhei o meu local de trabalho, um muito grande obrigado por tornarem aquele local uma partilha de sabedoria.

Aos meus amigos e colegas de curso que acompanharam no meu percurso académico, e tornaram estes últimos 5 anos, numa experiência fantástica. Aos meus amigos Beto, Fox, David,Pina, Gondomar, Dani, Pacífico, Alzheimer, Margarida e Sara, que me acompanharam ao longo deste magnífico percurso académico e com quem espero partilhar muitos mais sucessos no futuro. A eles deixo o meu grande obrigado, pois sem eles ao meu lado tudo seria mais difícil.

Um eterno obrigado à família, principalmente aos meus Pais e ao meu irmão, por todos os sacrifícios e por toda ajuda que me deram durante estes últimos 5 anos. Sem eles nada disto seria possível.

Obrigado a todos!

Abstract

Arterial stiffness assumes an important role as marker of cardiovascular diseases (CVD), which according to the World Health Organization (WHO) are the leading cause of death worldwide. The most studied parameters are the pulse wave velocity (PWV) and the augmentation index (AIx). These parameters can be retrieved from the arterial pulse waveform analysis.

A multichannel platform was assembled with four different modules, enabling the measurement of various important hemodynamic parameters. The platform incorporates electrocardiography (ECG), a photoplethysmography (PPG), arterial pressure waveform (APW) analysis and pulse wave velocity (PWV) measurements. This system provides a more complete cardiovascular condition assessment by the integration of several technologies and methodologies used in the traditional clinical path of cardiovascular patients.

A graphical user interface (GUI) was developed in Matlab and integrated with a custom database, allowing to acquire and to save data from all of the modules present on the multichannel platform.

Primary studies were performed using the previous interface following a protocol for two different acquisitions: one comprising the APW, ECG and PPG measurements and another with the PWV, ECG and PPG measurements.

Studies from the heart rate variability derived from the PPG and the ECG from the same acquisitions showed excellent results, which validates the reliability of the PPG and ECG modules. Repeatability tests performed to the APW showed satisfactory results. Results extracted from the second derivative of the photoplethysmogram waveform for vascular assessment are in accordance with values found in literature.

Keywords : Arterial Stiffness, Multichannel platform, Hemodynamic parameters, Graphical user interface.

Resumo

A rigidez arterial é um óptimo marcador das doenças cardiovasculares, que de acordo com a Organização Mundial da Saúde são uma das maiores causas de morte em todo o mundo. Os parâmetros mais estudados são a velocidade de onda e o índice de aumentação. Estes parâmetros podem ser obtidos através da análise da forma de onda.

A platforma multicanal foi construída com quatro módulos diferentes, permitindo medir vários parâmetros hemodinâmicos importantes. A platforma encorpora um electrocardiomógrafo, um fotopletismógrafo, um módulo para a análise da onda de pressão arterial e um módulo para a medição da velocidade da onda de pulso. Este sistema providencia uma avaliação mais completa da condição cardiovascular, através da integração de várias tecnologias e metodologias usadas tradionalmente em rastreio clínico.

Uma interface gráfica foi desenvolvida em Matlab e integrada numa base de dados, permitindo adquirir e gravar os dados de todos os módulos presentes na plataforma multicanal.

Foram relizados estudos primários usando a interface anterior, seguindo um protocolo para duas diferentes acquisições: uma compreendendo a medição da forma da onda de pressão arterial, o electrocardiomógrafo e do fotopletismografo, e outra com as medições da velocidade da onda de pulso, do electrocardiomógrafo e do fotopletismógrafo.

Estudos da variabilidade do batimento cardíaco derivado do fotopletismograma e do electrocardiograma para as mesma acquisições, mostraram excelentes resultados, o que comprova a fiabilidade dos módulos do fotopletismógrafo e do electrocardiomógrafo. Testes de repetibilidade realizados para a forma da onda de pressão arterial mostraram resultados satisfatórios. Resultados extraídos pela segunda derivada da forma do fotopletismograma para avaliação da rigidez arterial mostraram excelente concordância com os valores encontrados na literatura.

Palavras-chave : Rigidez arterial, Platforma multicanal, Parâmetros hemodinamicos, Interface gráfica.

Contents

List of Figures

List of Tables

Acronyms

ABP	Arterial Blood Pressure
AIx	Augmentation Index
APW	Arterial Pressure Waveform
AU	Arbitrary Units
BMI	Body Mass Index
CCA	Common Carotid Artery
CVD	Cardiovascular Diseases
DAQ	Data Acquisition
DBP	Diastolic Blood Pressure
DN	Dicrotic Notch
DW	Dicrotic Wave
ECG	Electrocardiogram
FN	False Negative
FP	False Positive
GEI	Electronics and Instrumentation Group
GUI	Graphic User Interface
HEE	Human Expertise Engineer
HR	Heart Rate
HRV	Heart Rate Variability
LVET	Left Ventricular Ejection Period
LPWV	Local Pulse Wave Velocity
MCU	Microcontroller Unit
MRSSD	Mean Squared Differences of Successive Interpulse Intervals
NI	National Instruments®
Nidaq	National Instrumental Data Acquisition Board
NN	Mean Interpulse Interval
PCB	Printed Circuit Board

Pi	Point of Inflection
pNN50	Proportiion of Sucessive Interpulse Intervals which exceeds the 50 ms
PPI	Peak-to-Peak Intervals
PPG	Photoplethysmogram
PPV	Pulse Pressure Variability
PVC	Polyvinyl Cloride
PWV	Pulse Wave Velocity
PZ	Piezoelectric
RMSE	Lowest Root Mean Square
RPWV	Regional pulse wave velocity
RRI	RR Intervals
SBP	Systolic Blood Pressure
SD1	Short Term Beat-to-Beat Variability
SD2	Long Term Beat-to-Beat Variability
SDNN	Standard Deviation of the Interpulse Intervals
SDPTG	Second Derivative of the finger Photoplethysmograph
SNR	Signal-to-Noise Ratio
SP	Systolic Peak
S/H	Sample-and-Hold Circuit
TP	True Positive
TT	Transit Time
WHO	World Health Organization

1. Introduction

1.1 Motivation

According to the World Health Organization, cardiovascular diseases (CVD) are one of the major death causes in the world. In 2008, an estimated 17.3 million people have died from CVD representing 30% of all global deaths and it has been predicted that the CVD mortality will increase up to 23,6 millions in 2030 [1]. There are some devices capable of detecting CVD factors, but they are quite expensive and hard to expertise. Therefore, the development of a simple, reliable and noninvasive methods is fundamental for the early detection of arterial stiffness, within therapeutic intervention can be a major beneficial [2].

Arterial stiffness (lack of elasticity) has been investigated as a good tracker of CVD, such as hypertension, atherosclerosis, coronary heart disease and stroke [3, 4]. Over the past years, more attention has been paid to arterial stiffness, where many studies proven arterial stiffness as an independent predictor of all-cause and cardiovascular mortality in hypertensive patients, in elderly people and in patients with end-stage renal disease for CVD diagnosis [5-12].

The more used noninvasive methods to assess the arterial stiffness is the arterial pressure waveform (APW) analysis, which can comprises parameters such as augmentation index (AIx) and pulse wave velocity (PWV). A few years ago, it was reported an acquisition technique using piezoelectric (PZ) sensors to acquire APW. This technique revealed a good performance in consequence of the high signal-to-noise ratio (SNR) as well as a high sensitivity in in vivo acquisitions [13]. In the last years, several prototypes based on this technology were also developed in *Electronics and Instrumentation Group* (GEI), namely: a double headed probe (DB) for the estimation of the local pulse wave velocity [14, 15] and a suitable single-headed PZ probe for measure the APW at the carotid artery [16, 17].

Another developments also included the development of a photoplethysmogram module [18]. This simple device measures blood volume changes at peripheral sites. Nevertheless, a large number of physiological parameters can be derived from it. Heart rate variability, vascular assessment, blood saturation and cardiac output measurements are some examples of his applications in health care [19].

All these modules were incorporated in a single platform – The multichannel platform, where it was also of interest to implement an electrocardiogram (ECG) module. This module, so often used in health care intuitions, gives important information about the heart activity. The ECG can also be used for PWV measurements, where the ECG is used as a time reference.

Although the invasive methods to access the central pulse pressure are accurate and precise, it is an expensive and painful method. The multichannel platform has the potential to extract important information regarding the cardiovascular conditions of the patients, through the noninvasive acquisition of different parameters. Thus, the multichannel platform can be a great advance in hemodynamic assessment, and its applications are widespread, where full characterization of the patients can be done according to the parameters acquired.

1.2 Previous work

The hemodynamic condition assessment has an important role at GEI, where many methods based on different recent technologies have been developed with the same goal –the noninvasive hemodynamic assessment.

Studies reporting the use of electromechanical-based technologies as a solution for pulse wave non-invasive assessment have been presented [9, 20]. A project led on GEI using PZ showed good agreement between values obtained of the PWV and the augmentation index (AIx) with the literature [21]. Subsequently, the PZ sensors were studied and then new PZ probes - single and double headed - were developed for APW and PWV acquisitions, respectively. Great advances have been made over the past years, whether on the development of algorithms capable of extract important information from the APW acquisitions, whether on the hardware developements [16, 17, 22, 23] . The PZ double headed probe used for measure the PWV has also been widely characterized on test bench. It was demonstrated a good performance on these tests [14, 15]. Afterwards, validation tests were also performed in pre-clinical trials, where it was also found the best algorithm to measure the PWV from the pressure signals [24].

Another important device previously developed, was a photoplethysmographic (PPG) probe for arterial blood pressure (ABP) assessment at peripheral sites [25].

The present work is a continuity of various projects developed at GEI, where the main concern of this project was to incorporate all of them in one single platform, allowing the noninvasive assessment of important physiological measurements. Moreover, all the modules incorporated can be acquired at the same time. Each of the modules can give important information about the cardiovascular condition, being possible the correlation of different retrieved hemodynamic parameters.

1.3 Goals

This project has as goal the development of DAQ software tools for the management of the modules that integrate the multichannel platform. The validation of the work is accomplished by a set of hemodynamic studies that comprise the synchronized data acquisition.

1.4 Thesis contents

This dissertation is divided in seven chapters. In the first chapter **(Introduction)** the motivation of this thesis, the goals and a short overview of the previous work is presented. Finally, the chapter-by-chapter structure of the entire thesis is briefly explained.

In the second chapter **(Theoretical Background)** it is presented the main concepts of the cardiovascular system, arterial stiffness and its factors, the main methods for noninvasive arterial assessment are also explained. The main concepts of the electrocardiography and the photoplesmography are also here described.

The third chapter **(Hardware)** focuses on all the previously developed hardware present on the multichannel platform.

In the fourth chapter **(Interface)**, the Graphic User Interface (GUI) used to acquire the signal presented on the multichannel platform is explained, where some details are briefly described. The existence of the database -*Cardiocheck* – is also referred.

The fifth chapter **(Methodology)** focuses on all the procedures to extract information from the data is fully explained. Here, the protocol made for the validation tests and the APW, PPG and ECG signal analysis are described.

The sixth chapter **(Results and Discussion)** is directed to the presentation and discussion of the results obtained from the validation test on group of the multichannel platform. An example of the two different acquisitions setup is demonstrated. A study using the PPG as a surrogate of the ECG regarding the heart rate variability assessment is exhaustive presented and discussed. The evaluation of the algorithms for the ECG and PPG is subject of study. A study regarding the second derivative of the PGG is performed.

In seventh and last chapter **(Conclusion and Future Work)**, finals remarks from the developed work are done. Suggestions of possible studies and features to be developed in the future work are presented.

2. Theoretical Background

2.1 Cardiovascular system

The cardiovascular system is composed by the heart, blood and vessels. The heart takes place as the pumping station of the cardiovascular, where the blood is the working fluid which travels along a complex branching configuration of blood vessels. This working system enables the exchange of energy, momentum and products between cells and their surrounding environment, by keeping the blood flow at an appropriate value [26]. Figure 1 shows a cross section of the human heart.

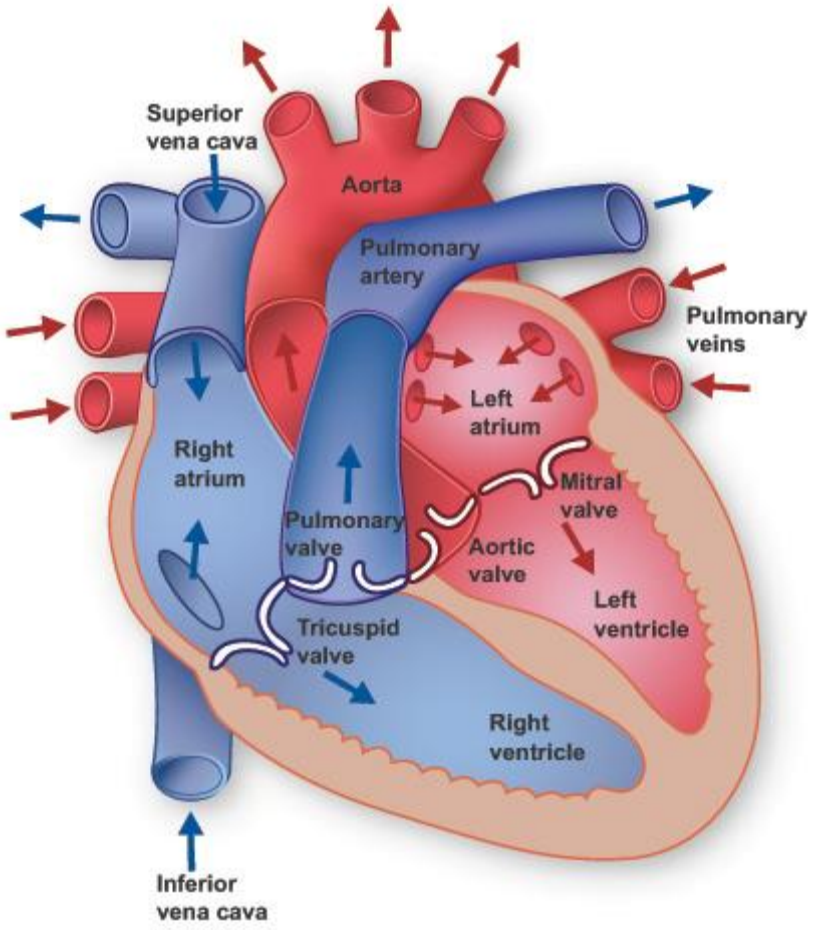

Figure 1 - Cross section of the human heart with the course of the blood flow. Taken from [27].

2.1.1 The heart

The main function of the heart is to pump blood into and through vessels to and from all parts of the body. The heart has four chambers. The upper chambers are called the left and right atria, and the lower chambers are designated as the left and right ventricles. Septa, a muscle wall, separate the heart in two sides, the left heart and right heart, where each has an atrium and a ventricle. The atrium receives the blood and pump it into their respective ventricle, while the ventricle is responsible to pump the blood to the lungs (right ventricle) or remainder part of the body (left ventricle) [28].

There are four valves which regulate the blood flow on heart and restrict the blood flowing backwards[28]:

- The tricuspid valve controls blood flow between the right atrium and right ventricle;
- The pulmonary valve controls blood flow from the right ventricle into the pulmonary arteries, where it will be oxygenated;
- The mitral valve regulates blood flow from the left atrium into the left ventricle;
- The aortic valve lets the oxygen-rich blood go through the aorta, and there to the rest of the body expect the lungs.

The right ventricle functions at low- pressures (< 40 mmHg gauge) because of the anatomic proximity of the lugs to the lungs. Thus, the right ventricle does not have to work hard to pump the blood to the lungs. On the other hand left ventricle works at high pressures (up to 140 mmHg gauge or even more) to ensure the blood flow is driven on whole systemic circulation [26].

2.1.2 Common carotid artery

The major source of blood to head, neck and brain is given by the left and right common carotid artery (CMA). Both common carotid arteries bifurcate into internal and external carotid arteries. The left and right common carotid artery has the same course, however they have different origins. The left common carotid arises from the aortic arch in the superior mediastinum, while the right common carotid originates in the neck from the brachiocephalic artery [29].

In the Figure 2 can be seen the arteries present on the head and neck.

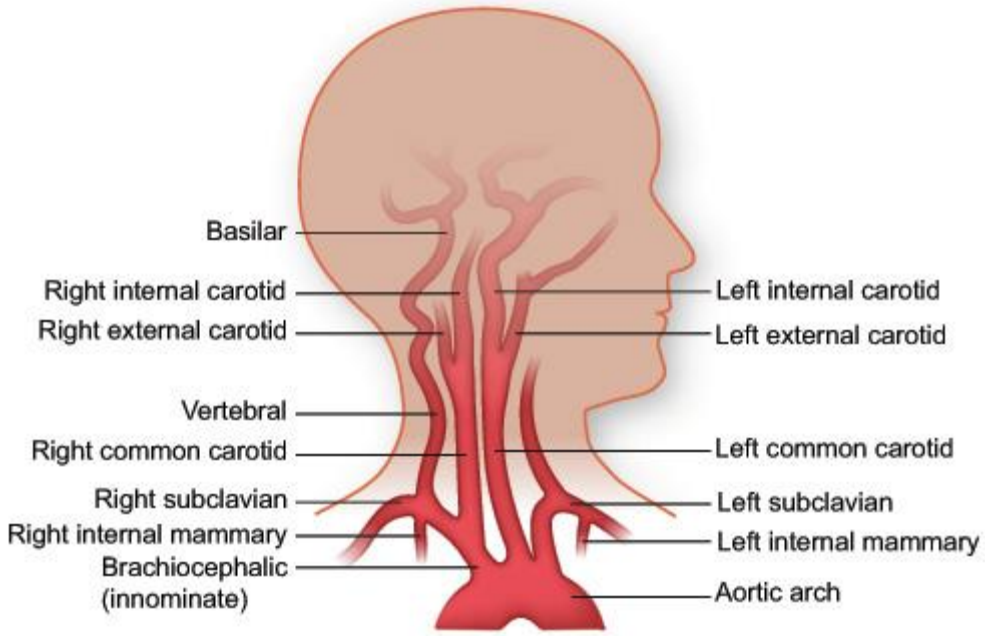

Figure 2 - Arteries of the neck and head. Taken from [30].

2.2 Arterial stiffness

The heart pumps the blood into the arterial system in a series of strong bursts. The arterial walls have to stand the pressure caused by the injected blood from the left ventricle causing distension and contraction for a proper functioning of all the cardiovascular system.

Arterial stiffness measures the lack of elasticity within the arterial wall, providing important information about the properties of the wall material independent of the geometry [9, 31, 32]. Nowadays, arterial stiffness has been strongly related with the development of CVD [5-12].

Arterial stiffness increases the velocity at which the pulse wave travels through the vessels. It is responsible to cause a premature return of the reflected waves in late systole, increasing the systolic blood pressure (SBP), and subsequently the central pulse pressure (PP). Thus, the load on the ventricle is raised, reducing ejection fraction, which increases the myocardial oxygen demand [6, 31, 32]. Another reason for the increase of the SBP is due to the lack of distensibility and elasticity of stiffer arteries. Stiffer arteries cannot accommodate the ejected blood by left ventricle, and for the same stroke volume, this result in an increase of the SBP and central PP [33].

2.2.2 Proximal and distal arterial stiffness

As consequence of the different molecular, cellular, and histological structure along the arterial tree, the elastic properties of conduit arteries change along the same. While the proximal arteries are more elastic, distal arteries are stiffer. The result is that the amplitude of the pressure wave is higher in the peripheral arteries than in the central arteries (Figure 3) [9].

A pressure wave propagating along a viscoelastic tube is progressively attenuated, with an exponential factor, however a pressure wave which is propagated along a viscoelastic tube with numerous branches (like a human arterial tree) due to the reflected waves it is progressively amplified from the proximal to distal arteries. This effect is denominated by "amplification phenomenon", which results in higher amplification of the pulse pressure in the peripheral arteries, comparatively to the central arteries [9]. Thus, it is inaccurate to use the common brachial PP as a surrogate of central PP, mainly in young subjects [6].

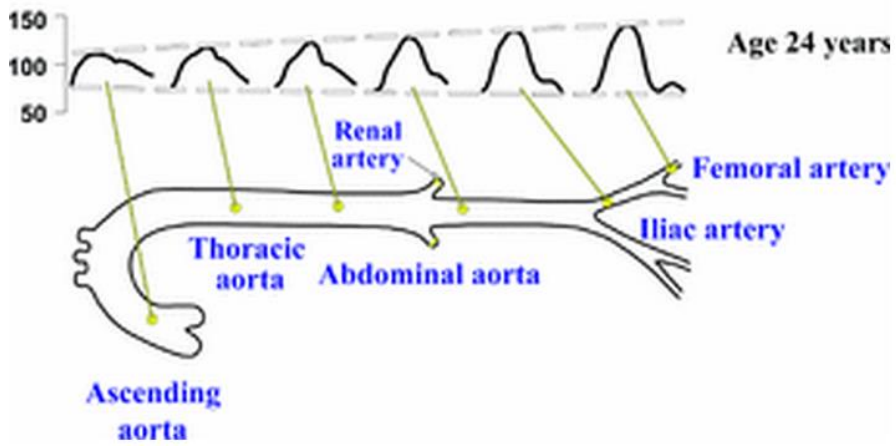

Figure 3 - Propagation of the ABP through the arterial tree – "Amplification phenomenon" [34].

2.2.3 Arterial stiffness factors

There are a vast amount of pathophysiological conditions that can lead to the increase of the arterial stiffness. For example, there are studies reporting the obesity has a precursor of arterial stiffness regardless the age of patients [35]. Those pathophysiological conditions are reported on the following table.

Table 1- Factors that affect arterial stiffness [9].

Ageing	Risk Factores	CVD
Other physiological conditions	Obesity	Coronary heart disease
Low birth weight	Smoking	Congestive heart failure
Menopausal status	Hypertension	Fatal stroke
Lack of physical activity	Hypercholesterolaemia	Primarily non – CVD
Genetic background	Impaired glucose tolerance	End – stage renal disease
Parental history of hypertension	Metabolic syndrome	Moderate chronic kidney disease
Parental history of diabetes	Diabetes type 1 and 2	Rheumatoid arthritis
Parental history of myocardial infarction	Hyperhomocyteinaemia	Systemic vasculitis
Genetic polymorphisms	High C – Reactive Protein (CRP)	Systemic lupus erythematosus

2.2.3.1 Aging

Age is one major causes of arterial stiffness. In normal aging process peripheral muscular arteries changes are minimal. However, in large arteries age has a great influence, which can be accelerated by coexisting cardiovascular risk factors, like hypertension and diabetes.

The longstanding arterial pulsation is responsible by changes on the structural matrix proteins, collagen, and elastin in the arterial, disrupting of muscular attachments and causing elastin fibers to fatigue and fracture. Accumulation of advanced glycation end-products on the proteins alters their physical properties, calcium deposition are others causes which results in arterial stiffness [33]. The major contribute for arterial stiffness is the progressive elastic fiber degeneration [9, 33, 36].

2.3 Arterial pressure waveform

The APW morphology contains important key points that allow the hemodynamic parameters assessment. Nowadays, many methods are used to acquire the APW, invasive methods like catheterization, and lately, noninvasive such as applanation tonometry or PZ probes [37].

The APW can be measured at central or peripheral level. The central level is preferable for the APW acquisition, since central level, like ascending aorta, surrogates the true load imposed to central large artery walls and left ventricle. For measurements at peripheral levels, such as radial, brachial or femoral artery, for the same pressure the APW has a different pulse

pressure and wave shape than the APW acquire on the central level, due to changes in arterial elasticity and dimensions along the arterial tree (Figure 3). However, the relation between central and peripheral pressure can be quantified and it can be used a transfer function to reconstruct aortic waveform [38]. Carotid and central arteries have similar waveforms, thus a measurement at carotid arteries is desirable since it does not need to use a transfer function. These leads to an increases the data precision, even though, it requires a higher degree of technical expertise [39].

2.3.1 APW morphology

The APW is composed by two types of waves: a forward travelling incident wave, resulted by the ejected blood by the left ventricle during systole, and the backward reflected wave from the periphery, caused by arterial tree branch points or sites of impedance mismatch [36, 37].

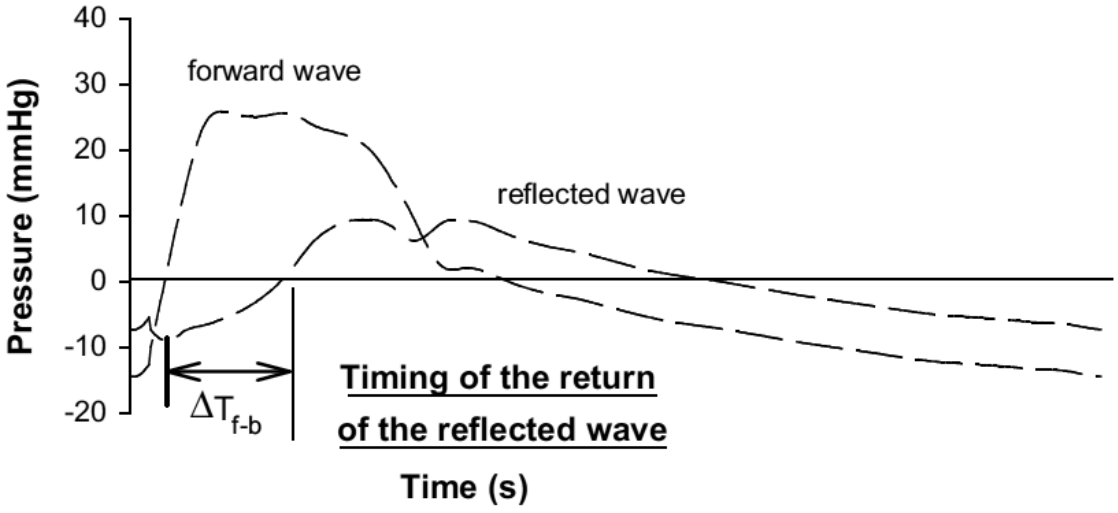

Figure 4 -The arterial pressure waveform as a result of the sum between the incident and the reflected pressure wave. Adapted from [40].

2.3.1.1 Incident wave

The capacitive of the ascending aorta, which receives the blood pumped by the left ventricle, gives origin to an incident wave [38]. Thus, the characteristics of the incident wave rely on the left ventricular ejection and stiffness of the aorta [36].

There are two points of interest in the incident wave: the systolic peak (SP) and the diroctric wave (DW), also called incisura. The SP is the point of highest pressure of the APW, while the DW is the result of the closure of the aortic valve. DW is commonly used to determine the left ventricular ejection period (LVET) parameter [38, 41].

2.3.1.2 Reflected wave

The blood injected pump by the left ventricle towards the peripheral arteries, finds bifurcations on its path, which blocks its flow, causing a reflection of the PP which travels back to the heart [42]. However, due to the gradual increase of stiffness and decrease in size from the central to the peripheral arteries, wave reflections do not just occur at specific sites of impedance mismatch, but are continuously and diffusely generated all along the arterial tree [31]. The characteristics of the backward reflected wave are influenced by the distance to reflections sites and the reflection coefficients and elastic properties of the arterial tree [36].

The sum of the reflected wave with the incident wave induces a momentary rise of the pressure on APW – the point of inflection (Pi).

2.3.2 APW types

Murgo et al. (1986) proposed a APW classification based on his morphology [43], where the morphology is determined by the reflected wave location. This classification considers four different waveform types, as depicted in Figure 5.

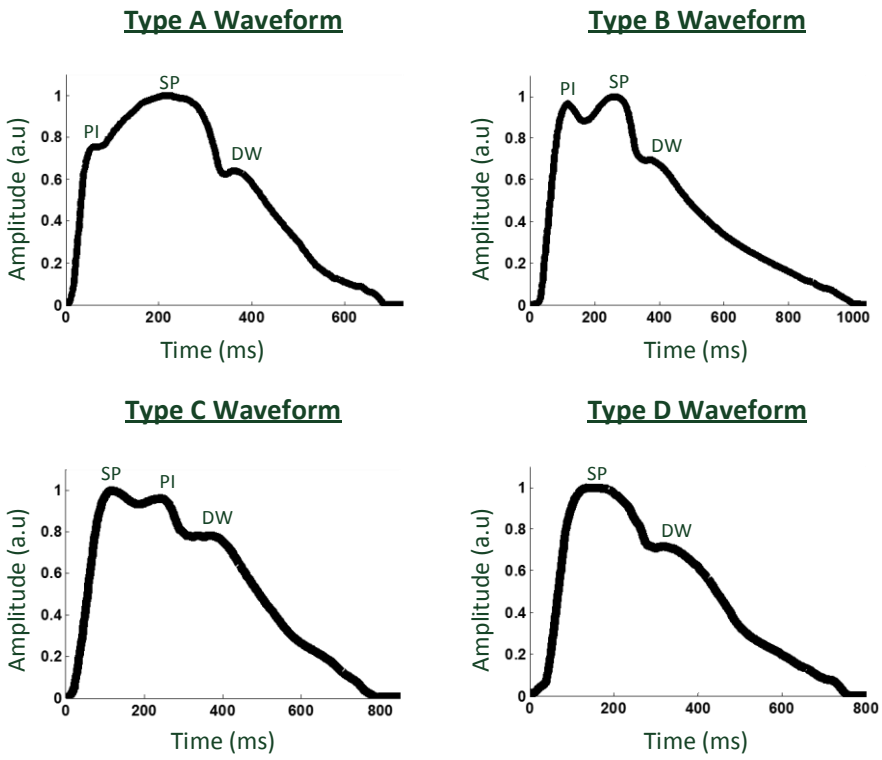

Figure 5- APW classification according to Murgo el al., where Pi is the inflection point, SP is the systolic pressure and DW is the dicrotic wave [39].

2.4 Noninvasive assessment of arterial stiffness

Arterial stiffness can be quantified through different hemodynamic parameters. The measurement of arterial stiffness gives relevant information about the cardiovascular risk of the patients.

In this section it will be discussed the most used parameters for arterial stiffness assessment.

2.4.1 Pulse pressure

Pulse pressure (PP) is simply the difference between systolic and diastolic pressure. It is a valuable marker for arterial stiffness and is an independent predictor of cardiovascular risk in general population [44]. PP is determined by the interaction of cardiac factors (stroke volume and ejection time) and vascular factors (arterial stiffness and arterial wave reflections) [37]. It is known that PP increases with advanced age [45].

PP is commonly measured at the cuff brachial artery using a sphygmomanometer. However, this measurement does not always accurately reflects the true central PP, since there is an amplification of the pressure along the arterial tree, which constitutes a potential source of error [31, 32, 38, 39]. Nevertheless, there are numerous studies reporting the brachial PP as good marker of arterial stiffness for elderly people (more than 50 years old) [46, 47]. The accuracy of the brachial PP for elderly people occurs due to the decrease of differences between carotid and brachial PP for these populations [48]. This can be explained by the decrease of pulse wave amplification over the age [37, 47].

2.4.2 Arterial compliance and distensibility

To record these hemodynamic parameters it is necessary a device capable to record the maximum and minimum arterial diameter, such as a magnetic resonance imaging (MRI) or an ultrasound. The use of ultrasound has the disadvantages of the limited resolution, which can be a problem to detect small changes in vessel diameter, and it is technique hard to expertise [37].

Arterial compliance (C) traduces the elastic properties of the arteries and it is defined as the change in volume for a given pressure, reflecting the change in artery diameter caused by left ventricular ejection. The arterial distensibility (D) is proportional to arterial compliance (as we can see on the equation below), and is the quotient of the C by the initial volume.

$$C = \frac{\Delta A}{PP}\ , \tag{2.1}$$

$$D = \frac{\Delta A}{A_d PP}, \tag{2.2}$$

with ΔA is pulse cross-sectional area ($\Delta A = A_s - A_d$), where A_s stand for systolic cross-sectional are and A_d for diastolic cross-sectional area [39].

Reduced arterial compliance and distensibility is a consequence of loss of arterial elasticity.

2.4.3 Augmentation index

Augmentation index (AIx) is frequently considered to be an index of arterial stiffness, and thus, a predictor of cardiovascular risk [36, 49]. AIx measures the contribution of the reflected wave relative to the total APW, and is equal to the difference between the second and first peaks as a percentage of PP [39]. The Figure 6 illustrates how the AIx can be retrieved by the APW.

Many factors influences AIx, such age, PWV, traveling distance of pressure waves (body height) and reflective properties of the arterial system [44, 50]. AIx is also influenced by blood pressure, and more importantly, by heart rate [51]. The AIx is determined by the following equation:

$$AIx = \frac{AP}{PP} = \frac{P_2 - P_1}{PP}, \tag{2.3}$$

Where AP stands for augmentation pressure, and P1 and P2 are the first and second pressure peaks, respectively.

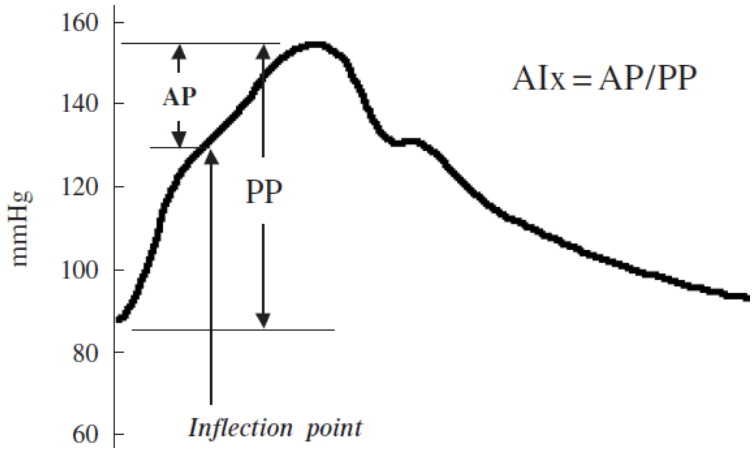

Figure 6 - Augmentation pressure (AP) as the difference between the systolic pressure and the inflection point pressure and pulse pressure (PP) measurements [47].

As it is perceptible, the AIx value depends if the reflected wave occurs prior or after the systolic peak. Thus, the AIx is computed according to the APW morphology as described in Table 2. The AIx is the proportion of central PP that results from arterial wave reflection.

Table 2 - Classification of the different APW according to the inflection point position and AIx calculus, where P_s is the systolic pressure, P_d the diastolic pressure and P_i the pressure in the inflection point [39].

APW Type	APW Properties	AIx calculus
A	The inflection point occurs before the systolic peak. The AIx is positive, and indicates high arterial stiffness.	$\frac{P_s - P_i}{PP} \times 100\%$
B	The inflection point occurs shortly before the systolic peak, indicating small arterial stiffness.	$\frac{P_s - P_i}{PP} \times 100\%$
C	The inflection point occurs after the systolic peak. The AIx value is negative, and indicates an elastic and healthy artery.	$\frac{P_i - P_s}{PP} \times 100\%$
D	The inflection point cannot be recognized because the reflected wave arrives in early systole and merges with the incident wave.	-

The AIx of the APW type D (Table 2) cannot be calculated, since the inflection point is not visible. The APW type D can occur for young people, where the reflected wave coincides with the diastolic pressure, but also for elderly subjects, where the reflected wave arrives earlier overlapping with the systolic pressure [47].

Typically, AIx is negative in healthy young people, but with aging, AIx becomes increasingly positive, due to significance change in the APW morphology. Several studies reported the relationship of AIx with ageing, where AIx becomes higher with the aging process [36, 52, 53].

In some recent studies AIx has predicted mortality for patient with a normal PWV (less than 11 m/s), which highlights the importance of assessing arterial wave reflection, over than the pulse wave velocity (PWV) [54].

2.4.4 Pulse Wave Velocity

Pulse wave velocity (PWV) is the speed at which the APW generated by cardiac contraction travels from aorta through the arterial tree, and so, a higher coefficient of arterial stiffness corresponds to higher PWV values [55].

While AIx is an indirect surrogate of arterial stiffness, PWV is a direct measure of arterial stiffness and also the most used technique for arterial stiffness assessment. PWV is simple, reproducible and robust noninvasive technique. Several studies have reported PWV as an independent predictor of CVD [9, 54, 56, 57]. However, PWV increases with an increase in blood pressure, which can be lead to less accurate values of PWV [47].

According to Moens and Korteweg (1878) [58], PWV can be related with arterial stiffness by the flowing equation:

$$PWV = \sqrt{\frac{E \,.\, h}{2r\rho}}, \tag{2.4}$$

where E is the elastic modulus of the vessel wall, h is the wall thickness, r is the radius and ρ is the blood density. For this equation, it is assumed that there is no significant change whither in vessel area, whither in wall thickness. Bramwell and Hill [59] proposed some alterations on the previous equation. This alternatively shows the relationship of the PWV with the arterial distensibility.

$$PWV = \sqrt{\frac{dP\ .V}{dV\ .\rho}} = \sqrt{\frac{1}{\rho D}}, \tag{2.5}$$

where P is the pressure, V is the volume, ρ is the blood density, D the volume distensibility of the arterial segment and dP . V / dV stands for volume elasticity.

PWV depends on geometric (h and r) and elastic (D) properties of arteries, as the previous equation shows. Thus, since the arterial tree varies along (as mention in Section 2.2.2) the PWV will also have different standard values for each site.

Practical PWV assessment, as described in the following equation, is defined by the distance between the two sites and the time delay (Δt) between the two pressure waves recorded in arterial system. This two measurement sites should lie on a peripheral artery that can be palpated from the body surface [47]. The distance is determined on the body's surface between the recording sites, which can lead to inaccurate PWV measures, since it does not correspond to the real distance [56].

$$PWV = \frac{distance}{\Delta t}, \tag{2.6}$$

many arterial segments have been used in literature , such as, radial-tibial, brachial-ankle, carotid-radial, brachial-radial and femoral-tibia, but the most commonly used and considered as the "gold-standard" is carotid-femoral segment [9, 40]. The carotid-femoral is the best surrogate of the aortic PWV, which has high clinical value for evaluation of the arterial stiffness. Aortic PWV values greater than 13 m/s represents a strong predictor of cardiovascular mortality in hypertension [60, 61].

2.4.4.1 Regional pulse wave velocity

Regional pulse wave velocity (RPWV) measurement is when PWV is acquire over a long segment of the arterial tree with different mechanical characteristics (elasticity, wall thickness and diameter) [40]. The RPWV results in an average PWV over a long arterial segment often composed both from elastic and muscular arteries, and therefore, it is not as accurate as the local pulse wave velocity [62].

To measure the RPWV it is needed to calculate the transit time (TT) and the distance between the two sites, where the devices are placed.

Currently, different methods are used to calculate the arterial tree segment distance, such as depicted in Figure 7[9, 56].

- Measure the distance between the measurement sites on the surface body (L_{direct});
- Subtract the distance from carotid location to the sterna notch with the distance between sterna notch and femoral artery site of measurement (L_{sub}).

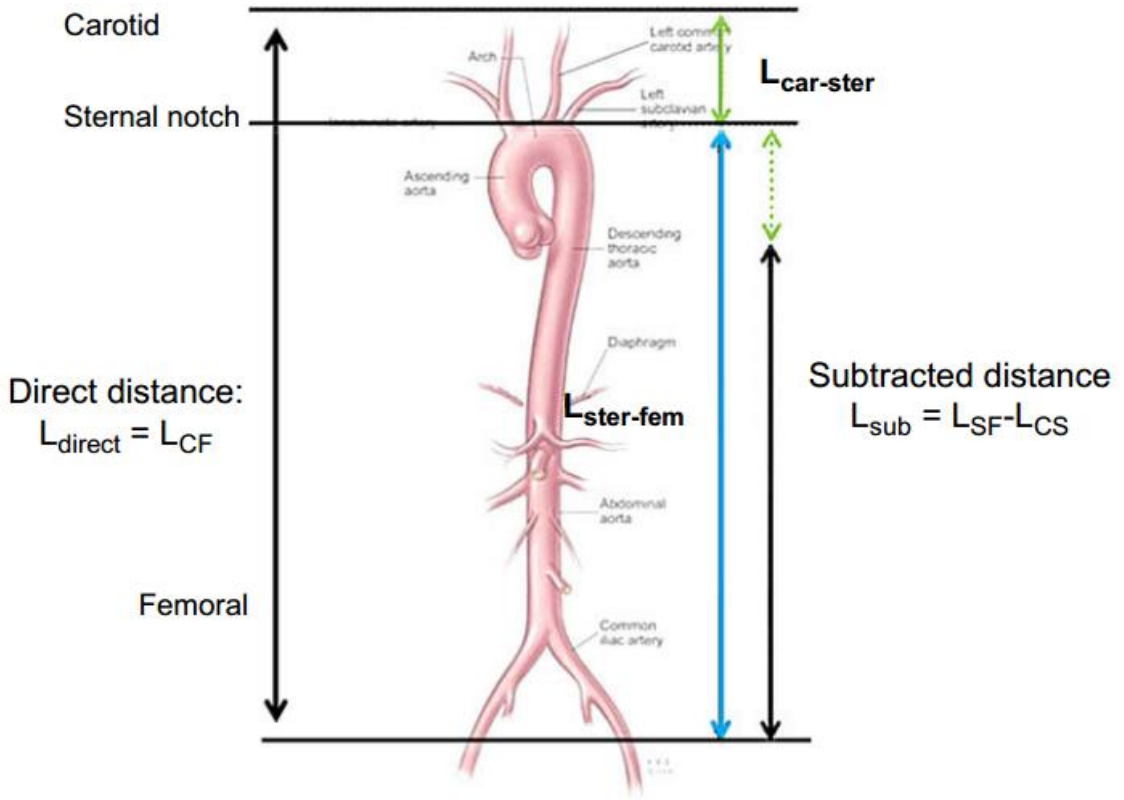

Figure 7 - Different method to measure the path length [56]

Although the first method is simpler, the second method is a more accurately approach to the real distance, since it takes in count that carotid and femoral pulses waves travel in opposite directions [62]. Therefore, the second method is preferable between both. Nevertheless, there is not yet a precise method to calculate the distance, due to the trajectory and curvature of vessels in the arterial tree [56].

There are many methods used to measure TT, but most of them are based on the same principle: to detect a characteristic point of the wave over the two sites recorded.

As the wave travels through the arterial system, its waveform is changed because of the differences in arterial wall properties along the path. Thus, the characteristic time-point used to identify the reference of the wave can be shifted to a different position within the waveform, which results in inaccurate estimation of the TT [62]. There are many references point on the pulse wave, such as, the systolic upstroke also known as 'foot' point or the SP. The systolic

upstroke is more commonly desirable to be chosen among all the references points, since it is hardly affected by the wave reflections, enabling a more accurately measure of the TT [56, 62]. The Figure 8 shows an example the measurement of the carotid-femoral PWV.

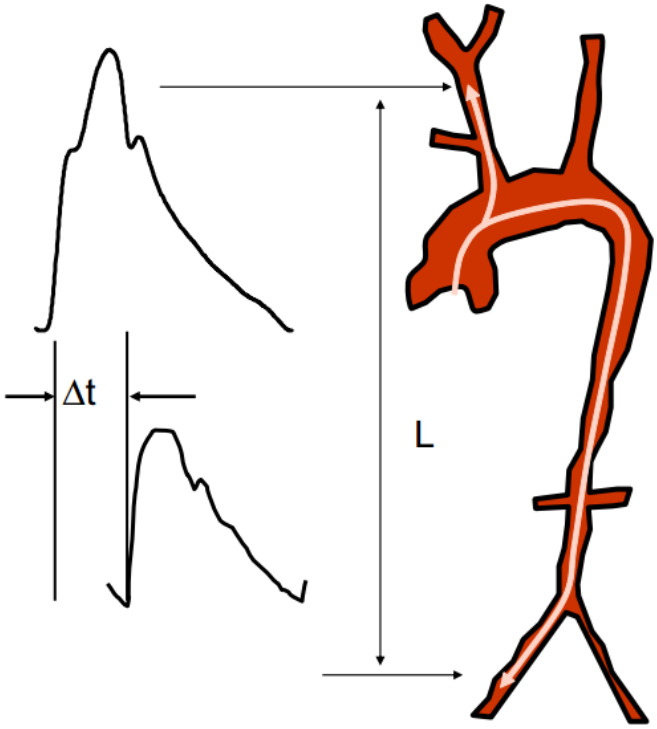

Figure 8- Measurement of carotid-femoral PWV [56].

Another method to calculate the TT is to gate the separated recordings to a fixed point in the cardiac, usually the R wave of the ECG (as it is described on Figure 9) [37, 54].

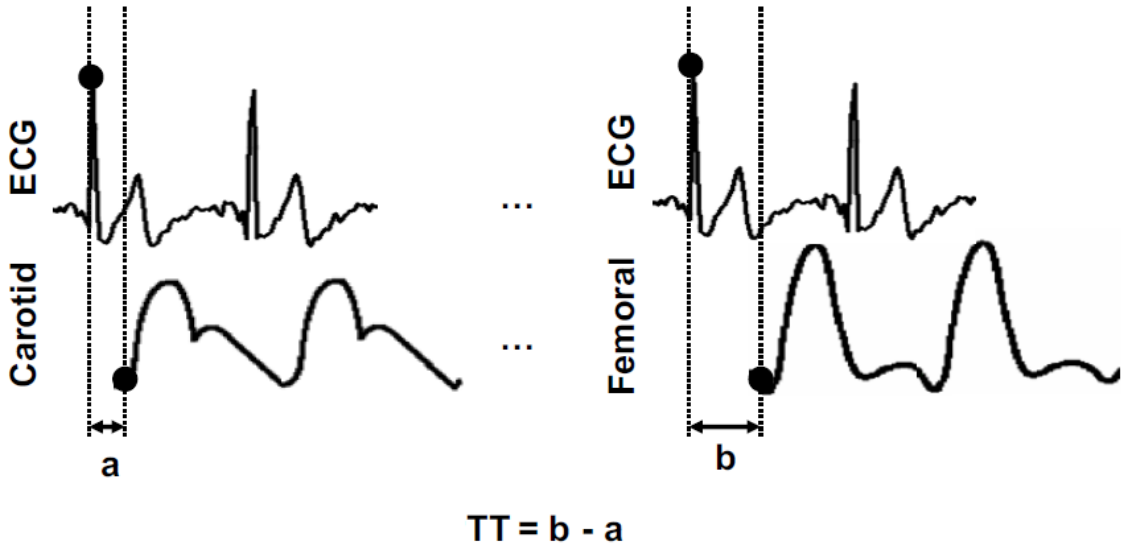

Figure 9 - Transit time measure with an ECG as reference [61].

2.4.4.2 Local pulse wave velocity

In contrast with RPWV, the local pulse wave velocity (LPWV) is measured over a short segment of an artery. As mention on the equation 5 there is an relationship between LPWV and distensibility. Therefore, it is possible to determine the LPWV from a local distensibility measurement (through assessment of local pulse pressure and diameter) [40]. Another way, to measure the LPWV is from a simultaneous measurement of APW by two sensors at close positions. Where, the distance between the two sensors is known and the TT is measured by the time delay between the two recorded waves [61, 63].

An advantage of LPWV regarding the arterial stiffness at common carotid artery, is that it measures the only PWV of common carotid artery, whereas the RPWV measures the average PWV along a segment with different proprieties. Thus, LPWV gives relevant information about the local arterial condition, however, because it is calculated by short the distance between two recordings sites, it has a greater absolute error in determining the TT [9, 37].

A new technology based on PZ sensors have recently been reported for LPWV assessment [14, 15].

2.5 Photoplethysmogram

The photoplethysmogram (PPG) is a simple and low-cost optical technique used to detect blood volumes changes in microvascular bed of tissues, like the arteries at the finger. PPG has various applications in various physiological conditions, such as vascular assessment, clinical physiological monitoring and automatic function study [64].

2.5.1 Operation Principle of PPG

PPG is compounded by a light source to illuminate the tissue and a light detector that measures the transmitted or reflected light [64].

To detect the changes in volume a wavelength in the visible (red) and near infrared (IR) is used. At these wavelength spectrum one of the main absorbers of light in this spectrum is the haemoglobin, which has two modes: oxyhaemoglobin (HbO_2) and reduced haemoglobin (Hb) [64]. Thus, the attenuation of light at the tissue is given by the following equation:

$$I_L = I_H e^{-[\varepsilon_{Hb}(\lambda)c_{Hb}+\varepsilon_{HbO_2}(\lambda)c_{HbO_2}]\Delta d}, \qquad \text{[Equation 2.7]}$$

where, I_L is the minimal light intensity received (occurs at systole), I_H is the maximal received light received (occurs at the end of diastole), $\varepsilon(\lambda)$ is the extinction coefficient or absorptivity of the medium for a particular wavelength, c is the concentration of the absorbing substance, Δd is the change in optical path length during the cardiac cycle (Figure 10) [25]. A more detailed explication and the demonstration on the previous equation was presented by Santos, P. [25].

Volume at blood vessels is constantly changing, due to the heart's activity. In systole, the blood is ejected by the ventricles though the arteries trees causing an increase in blood pressure and consequently an increase in volume at blood vessels. Then during diastole, the blood returns again to the heart leading to a decrease in blood pressure and volume in the blood vessels. This blood volume variance alters the amount of light which is detected at the detector of the PPG [64].

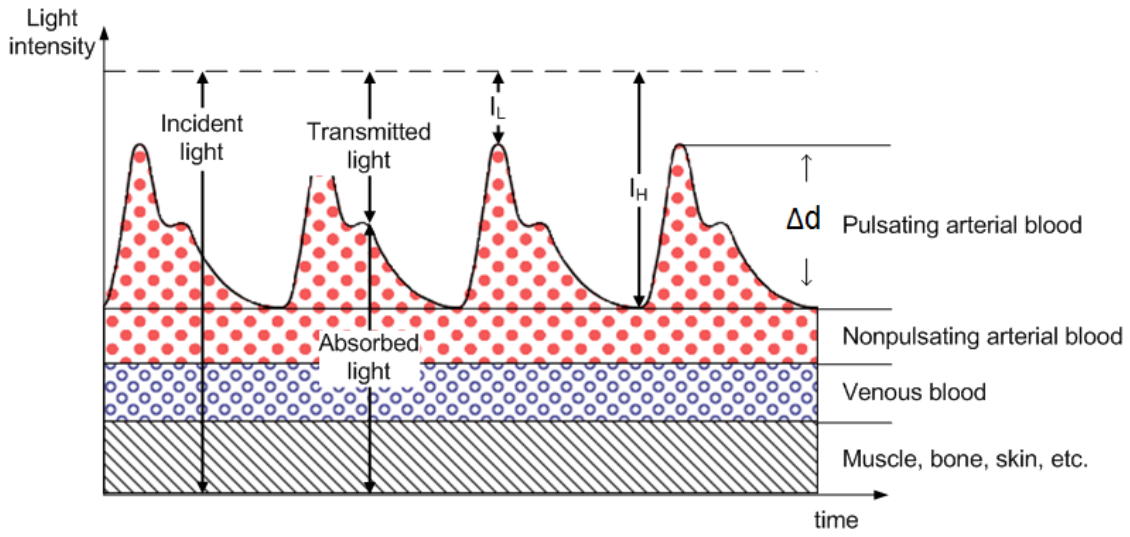

Figure 10 - Absorbed and transmitted light in pulse oximetry [25].

The PPG waveforms can be divided in two parts: a pulsatile component (AC) and a continuous component (DC). The AC component it is related to the blood volume, which is constantly changing due to the cardiac cycle and it has typically a low frequency (around 1 Hz). On the other hand, the DC component it is due to the constant light absorption by tissues (muscle, bone, skin among other) and the average blood volume [64].

Thus, the PPG measures volumetric blood changes, since the blood absorbs the infrared or red light many times more strongly than the remaining skin tissues.

2.6 Electrocardiogram

The heart contraction is triggered by an electrical wave which passes through it. This electrical propagation has a coordinated pattern and leads to a changes of the electrical potential on the surface of the body. The electrocardiogram (ECG) has the ability to measure the electrical potential difference between two electrode placed in different parts of the human body [65].

2.6.1 Cellular electrophysiology

The negative potential of the cardiac cells, at resting stage, with respect to surround extracellular fluid is maintained by a series of ion channels. Those ion channels controls the cell membrane permeability of specific ions, such as, Na^+, K^+, Ca^+ and Cl^-. These ions are pumped in and out of the cell to maintain the electronegativity of the cardiac cells [65].

Therefore, the electrical potential can be controlled by the opening or closure of the ionic channels. When an ionic channel opens the ions movement creates an extracellular potential field creating a depolarization wave at macroscopic level, due to cell-to-cell

propagation of the electrical event. However, when ionic channels closes, this ionic flow is interrupted and the membrane potential returns return to its resting stage (repolarization). The cardiac cycle is initiated by the cardiac cell depolarization, also known as P wave [65].

2.6.2 PQRST complex

The P wave is the first wave of the ECG and represents the spread of the electrical impulse through the atrial musculature (depolarization). This electrical impulse is then conducted from the atria through the A-V node and the His-Porjinje system. Then, the ventricles are excited and they contract forming the most important complex in ECG, the QRS, where Q wave is the initial downward deflection, R wave is the initial upward deflection and S wave is the terminal downward deflection. The last wave is known as the T wave as represents the ventricular repolarization [66]. In the following figure it is possible to observe all the previously compounds described.

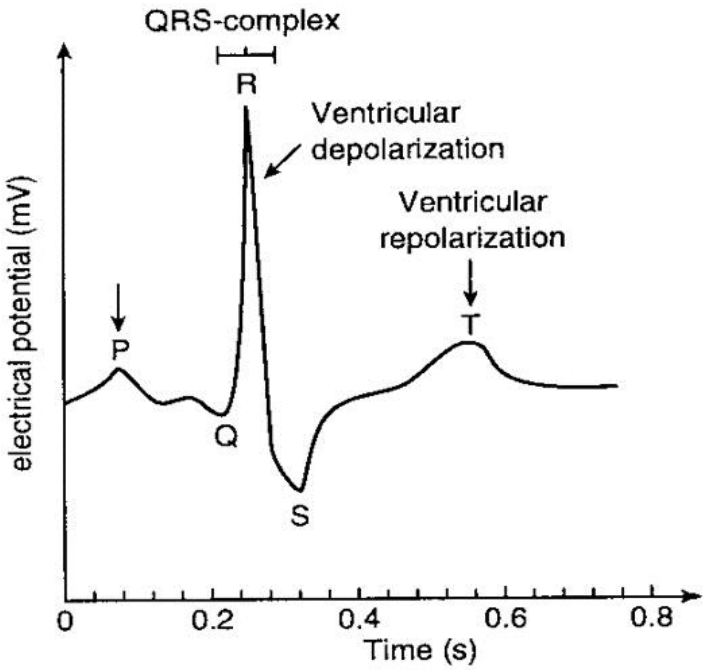

Figure 11 - One cycle of a typical ECG signal [67].

2.7 Commercial devices for noninvasive of arterial stiffness assessment

Currently, several non-invasive methods are used for vascular stiffness assessment. While, local and regional arterial stiffness can measured directly at various sites along the arterial tree, systemic arterial stiffness can only be estimated from models of circulations [9].

The main features of devices and methods currently used according to Laurent et. al (2006) are described on the following table:

Table 3 - Devices and methods used for arterial stiffness measurements and wave reflections [9].

	Device	Methods	Measuring site
Local Stiffness	WallTrack®	Echotracking	CCA[b],CFA,BA
	NIUS®	Echotracking	RA
	Artlab®	Echotracking	CCA[b],CFA, BA
	Various vascular ultrasound systems	Echotracking	CCA[b],CFA, BA
	MRI device	Cine-MRI	Ao
Regional Stiffness	Complior®	Mechanotransducer	Aortic PWV[a]
	Sphygmocor®	Tonometer	Aortic PWV[a]
	Walltrack®	Echotracking	Aortic PWV[a]
	Artlab®	Echotracking	Aortic PWV[a]
	Ultrasound Systems	Doppler probes	Aortic PWV[a]
Systemic Stiffness (waveform shape analysis)	Area method	Diastolic dexay	
	HDI PW CR-2000®	Modif. Windkessel	
	SV/PP	Stroke volume and pulse pressure	
Wave Reflections	Sphygmocor®	AIx	All superficial arteries
	Pulse Tracer®	Finger photoplethysmography	Finger

Ao, aorta; CCA, common carotid artery; CFA, common femoral artery; BA, brachial artery; RA, radial artery; SV/PP, stroke volume/ pressure.

[a] Aorta, carotid-femoral, also carotid-femoral and femoro-tibial PWV

[b] All superficial arteries, including particularly those mentioned

3. Hardware

3.1 Multichannel platform

The Multichannel Platform has incorporated four modules for hemodynamic assessments and one other dedicated to the synchronization mechanism. There is also a data acquisition board (DAQ) and a power supply +12V in it. The 12V from the battery is used to supply others stages from the different modules (see Table 4).

Table 4 - Power supply requirements for each modules

Module	Power
ECG module	+5V / -5V
APW module	+3.3 V, +5V/-5V
PWV	+15V / -15V
PPG	+3.3 V, +5V/-5V
Nidaq Power Supply	+5V

The multichannel platform integrates the following modules:

- The arterial pressure wave (APW) module for pulse wave contour analysis developed for CCA measurements (Figure 12 - B).
- The electrocardiogram (ECG) module to record the hearts activity. At this module is also couple a synchronization module to determine the delay between the modules which receives the data through a RS232 connection and the modules which data is transmitted through the NI6210 DAQ module (Figure 12 – C).
- The pulse wave velocity (PWV) module for local pulse wave velocity assessment at CCA (Figure 12 – D).
- A photoplethysmography (PPG) module to acquire the blood volume pulse at the peripheral arteries (Figure 12 – E).
- NI6210 DAQ module (Figure 12 – F).

Figure 12 - Multichannel Platform. (A) Power Supply; (B) APW module; (C) ECG probe integrated with synchronization module; (D) PWV module; (E) PPG module; (F) NIdaq-6210

3.1.1 Acquisitions system

On the acquisition system there are two different of acquisitions module: the APW acquisition module (PIC33FJ256GP710) and a dedicated data acquisition board (DAQ) module.

The APW acquisition module is efficiently capable of acquire the pulses from the subject and to send the data acquired to the laptop by a RS232 connection with a sample rate of 1 kHz. However, the others modules (such as the ECG, PPG or PWV) need a dedicated module - the DAQ module - to send the data acquired to the PC through a USB cable.

The DAQ used was a National Instruments® (NI) NI6210 (Figure 13) with 16 analog inputs, 16-bit resolution and it can sample up to 250 kS/s. The data acquisition and analysis was done using Matlab – a powerful instrumentation and analysis programming language for PCs. All the signals were sampled at 20 kHz [68].

Figure 13 - DAQ -NI USB 6210

3.1.2 Schematic

The current set up of the BUS lines of the Multichannel Platform is presented on the Figure 14.

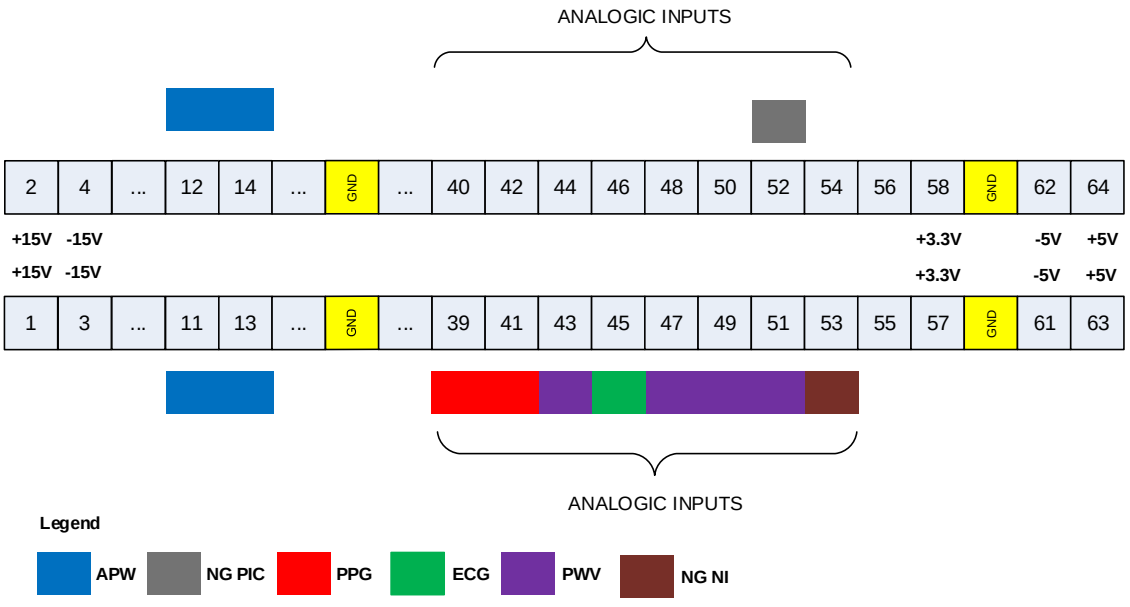

Figure 14 – Schematic of the Multichannel Platform

Where the synchronization module is represented as NG (noise generated), and PIC stands for the microcontroller presented on the APW module. All the modules, except the APW are acquired though the National instrumental data acquisition board (Nidaq).

3.3.1 Arterial pressure waveform module

The arterial pressure waveform (APW) module (Figure 15) is able to record and storage the waveform in a digital format, enable future processing of the data acquired. This module consists of one PZ transducer probe and a signal conditioning, responsible to filter and amplify the signal.

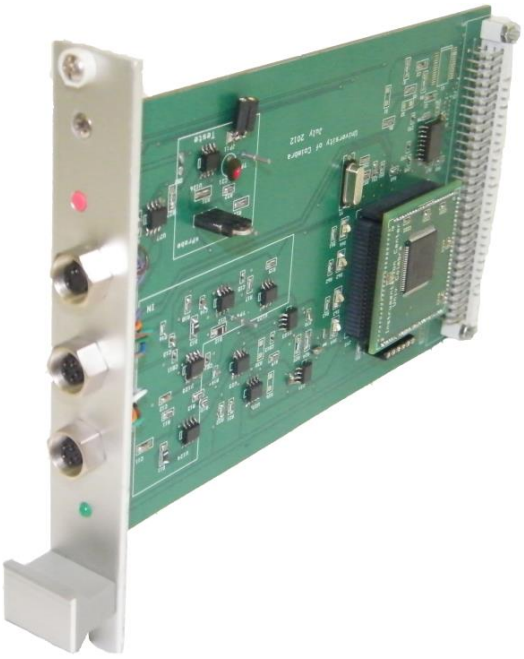

Figure 15 - APW module

3.3.1.1 Piezoelectric sensor

Piezoelectric (PZ) sensors are able to measure pressure, acceleration, strain and force into a proportional measurable voltage signal. Some peculiar characteristics of the PZ sensors are their low cost, high rigidity, high sensitivity and high SNR. Those characteristics made them a desirable sensor for hemodynamic purposes. These sensors have been widely used for the hemodynamic parameter assessment, such as to APW analysis [16, 17] and PWV measurements [14, 15].

The single PZ probe used on APW (Figure 16) is compounded by one PZ transducer bonded to a plastic block that supports bending under normal use. A mushroom interface was assembled over the PZ element.

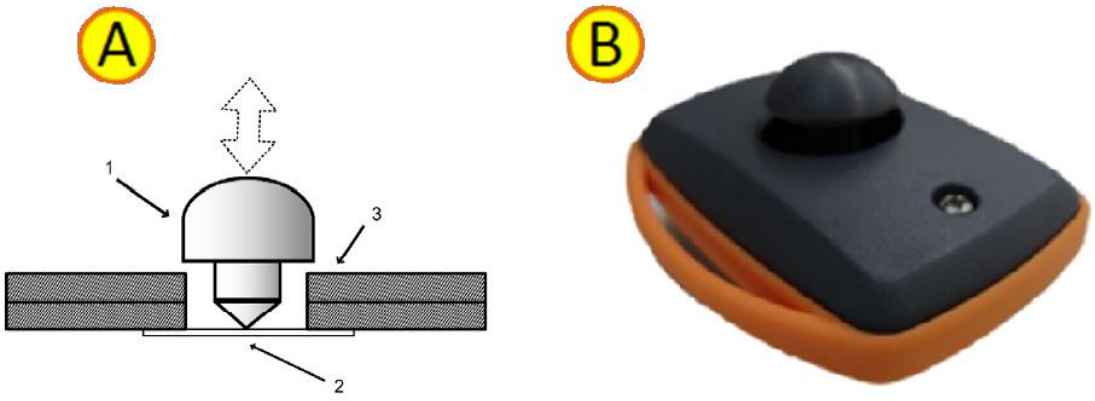

Figure 16 - PZ sensor. (A) Probe elements in cut, (1) mushroom - shaped interface, (2) PZ disc sensor and (3) printed circuit board (PCB). (B) Outer upper view of the single headed PZ probe [16].

A study executed by Almeida *el al* (2011) proved that a pointy probe, which contacts directly with the sensor, has best performance over a flat and an intermediate probe. The pointy probe selected showed the lowest root mean square (RMSE) variance among all the three PZ probes [16].

3.3.1.2 Signal conditioning circuit

The signal conditioning circuit architecture consists of three main parts: a power supply module, a first amplifying stage and a processing module. The power supplied via an USB cable is connected to a personal computer. In the first amplifying stage, an active differentiator mode amplifier amplifies the raw signal. Afterwards in the processing module, a peak detector with a timer is used to extract the reference time signal associated to the signal peak [16]. Due to the nature of the signal obtained, which is a time derivative of the physiological signal, it must, therefore, be integrated by a Microchip® (Chandler, Arizona, USA) dsPIC33 microcontroller.

3.3.2 Pulse wave velocity module

The pulse wave velocity (PWV) module (Figure 17) allows the assessment of two signals: the derivate of the pressure waveform (obtained by the piezo-electric effect – the PZ signal) and the arterial blood pressure waveform (integrated PZ signal). Those signals are recorded and saved in a digital format, allowing future data processing.

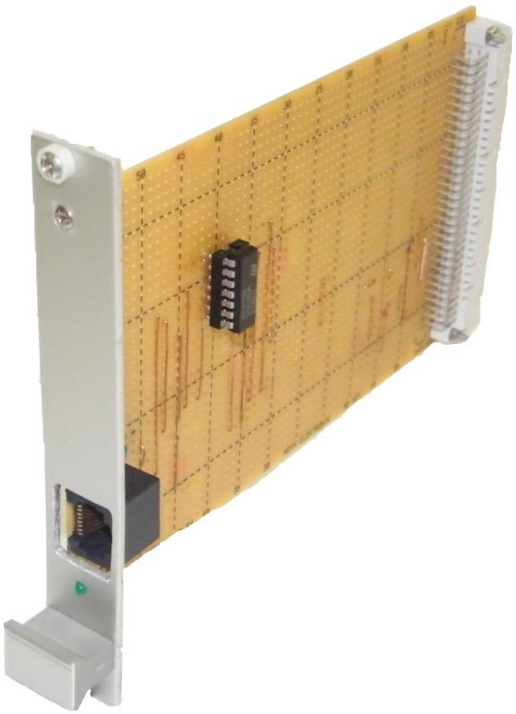

Figure 17 - PWV module.

This module consists of one double headed PZ probe transducer probe within a signal conditioning, responsible to filter and amplify the signal.

3.3.2.1 Double PZ Headed probe

Figure 18 - Double headed probe. (1) Thin film PZ sensors.

The PZ probe is a double headed probe, which consists of two circular-shaped PZ sensors (MURATA 7BB-12-9 Sounder, 12mm of diameter), placed 23mm apart. This new conception of a thin film PZ was assembled regardless the previous mushroom-shaped PVC,

since it is more manageable. This characteristic was desirable, because of the difficult to place the double PZ sensor over the CCA [14, 15]. The same setup of PZ sensor were also referred in literature for hemodynamic assessments [20].

A RJ45 connector allows connecting the double PZ sensor to the multichannel platform.

3.3.3 Photoplethysmography module

The photoplethysmography (PPG) module (Figure 19) is able to connect a PPG probe and it is also setup for use of accelerometers. The accelerometers have important role to prevent the distortion of the PPG signal due to the movement of the subject.

Figure 19 - PPG module.

The PPG system has five important modules (Figure 20): LED driver, photodetection, sample-and-hold, transimpedance and an low pass filter.

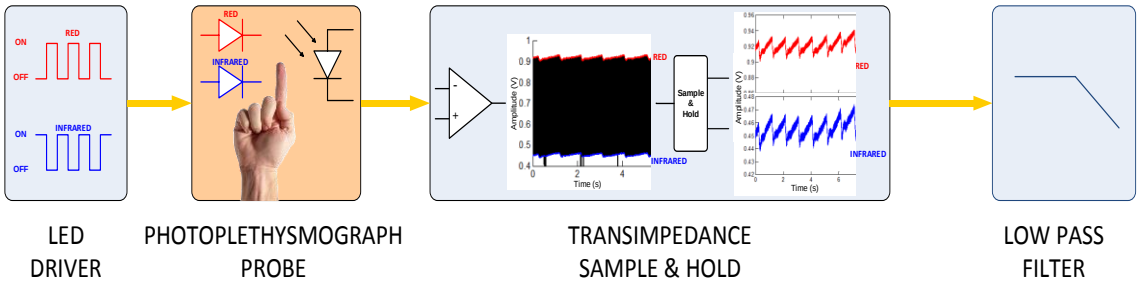

Figure 20 - Schematic of the hardware on the PPG.

The photoplethysmographic module employs two wavelengths red and infrared. The PGG was assembled with those two wavelengths, useful to oxygen saturation measurements. Due to the existence of only one photodetector, the two LEDs are used in opposite phase. Thus when the red is ON, the infrared is OFF and *vice-versa*. A microcontroller unit (MCU) defines which LED is ON and which is OFF, thus, just one LED is polarized each time. Those LEDs are supplied with a constant current source, maintaining a constant brightness [18].

Within the finger probe, the LEDs emit a beam on the finger, which it is detected by a silicon photodiode on opposite side of the LEDs. This photodiode is coupled with a transimpedance, to convert the light received by the photodiode into a voltage proportional to the light received [18].

The LEDs used have different optical power and the extinction coefficients of the involved tissues are different for both, and so it is convenient separate the two signals. Therefore, a sample-and-hold ciruit (S/H) was used. The function of S/H is to sample the voltage of the analogue signal and then hold that voltage for a certain period of time. An S/H is compounded by a circuit with an input voltage buffer, an interrupt, a capacitor and an output buffer. [18].

Then, after the signals being separated by the S/H, it is possible to filter the signal in order to remove some undesirable components, typically noise. This noise is a high filter, and so, to remove it a low-pass filter with a cutoff frequency of 20 Hz was implemented. This filter also helped to prevent aliasing. For more details about the PPG hardware see P. Santos [25].

3.3.4 Electrocardiogram and Synchronization module

The module illustrated in the Figure 21 has both components the ECG and the Synchronization.

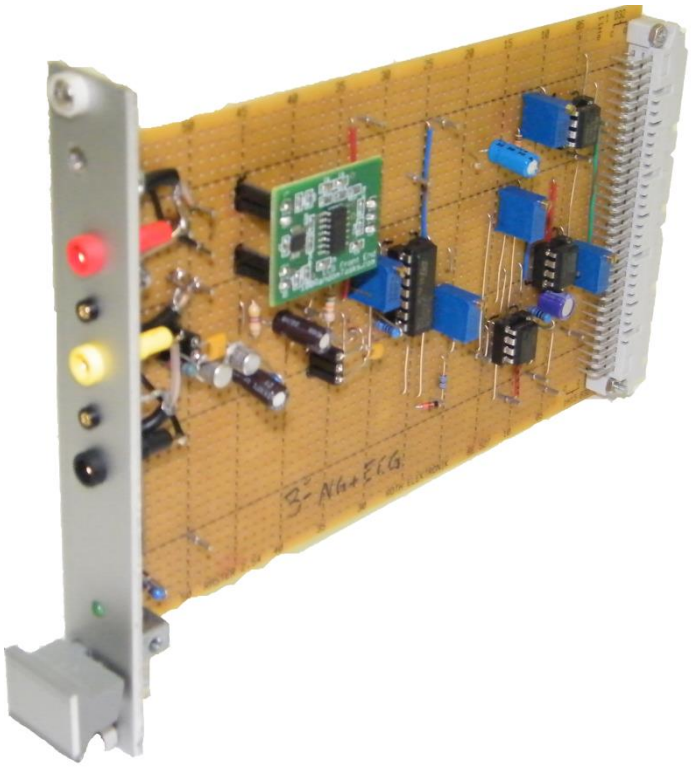

Figure 21 - ECG and synchronization module.

3.4.4.1 Synchronization

Since the communication from all modules is not the same, a synchronization module was developed to determine the delay between the acquisitions made through the two different DAQs. The synchronization module is a simple noise generated which is then amplified. Both DAQs acquired this signal in order to know the shift between both DAQs. By matching the signal acquired from the two different DAQs it is possible to measure the time delay between, and put the same reference time on the signals acquired by the different DAQs.

3.3.4.2 Electrocardiogram

The ECG signal is acquired through the Nidaq (Figure 14). Afterwards the signal is record and storage in a digital format, allowing future data processing.

The configuration used for the ECG was a three leads. On this configuration, three electrodes are placed on the surface of the body, one on each arm and the last one on the left leg, forming the triangles of Einthoven. The ECG records the voltage difference between any two

electrodes. And so, on this configuration it is possible to form three different leads (Figure 22) [26].

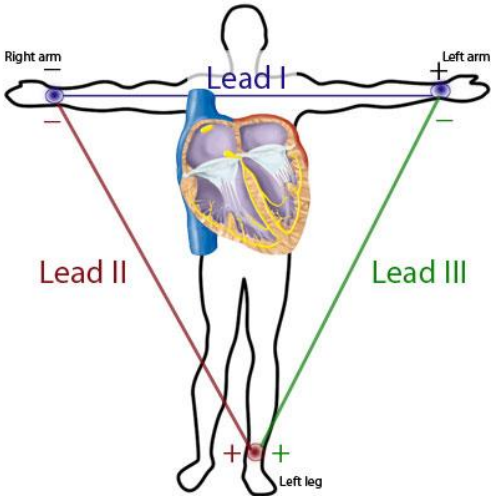

Figure 22 - Proper placement of the limb electrodes for a 3-lead ECG [69].

$$\text{LEAD I} = V_{\text{LEFF ARM}} - V_{\text{RIGHT ARM}}$$

$$\text{LEAD II} = V_{\text{LEFT LEG}} - V_{\text{RIGHT ARM}}$$

$$\text{LEAD III} = V_{\text{LEFT LEG}} - V_{\text{LEFT ARM}}$$

The Biopac® disposable Ag-AgCl electrodes (EL503) (Figure 23) were the electrodes chosen for the ECG acquisitions. This type of electrodes is appropriate for short-term recordings, because of their peculiar characteristics. They are high chloride and pre-gelled electrodes with a circular contact area diameter of 10 mm, a backing diameter of 35 mm [70]. These electrodes convert the ionic current flow over the surface of the body to the electron flow of the metallic wire.

Figure 23 - Biopac® disposable Ag-AgCl electrodes [67].

In order to remove some noise on the ECG it was implemented a low pass filter with a cutoff frequency of 106 Hz.

4. Interface

4.1 Interface - main menu

A graphical user interface (GUI) was developed in order to record, visualize and store all signals presented on the multichannel platform. This Interface was developed in Matlab® and it was assembled to be as simple and intuitive as possible.

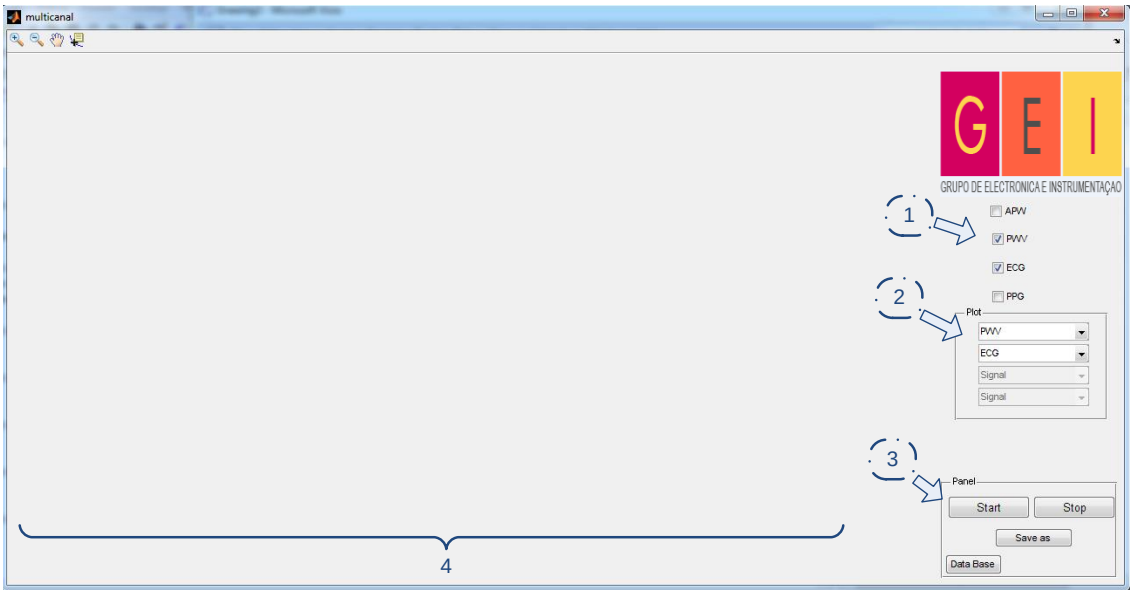

Figure 24 - Graphical user interface of the multichannel platform. The GUI has the following filed: (1) signals to acquire, (2) signal to display, (3) start/stop/save the acquisition and (4) display window.

First the operator must select the signal to acquire (Figure 24 -1). Currently, the multichannel is prepared to have fours distinctive probes: APW, PWV, ECG and PPG, such as described in chapter 3. The communication of the APW module is made through a RS232 converter connected to the PC by a USB port, while all the others (PWV, ECG and PPG) are acquired by a USB port through the NI6210 module.

All the setup is made automatically when the operator chooses the signal. The APW is acquired at a sample rate of 1 kHz. On the other hand, the signals acquired through the NIDaq are acquired with a sample rate of 20 kHz. This discrepancy of sample rates is required by the PWV module. The PWV measurements require a high sample rate, since the two PZ sensors are placed apart with a small distance. Therefore, an accurate PWV computation, which is on order of 10m/s, requires a high sample rate.

The interface enables to acquire one signal but not to show if the operator so desires. On the checkbox it is selected the signal to record and on the pop menu (Figure 24 – 2) it is selected

the signals to visualize. Whenever a signal is selected to be acquired on the checkbox it is added the signal as option on the popup menu (Figure 25). This simple feature allows decreasing the time needed to setup the interface for the acquisition.

Figure 25 - Demonstration of the Popup feature developed.

The scheme on the Figure 25 shows the automatic setup of the popup menu for one acquisition by steps. From step 1 until the step 3 the user is selecting the signals to acquire and the GUI automatically selected signals by order on the various popup menus. Nevertheless, when the user unselect one signal to acquire (step 4 on Figure 25), the GUI delete this option from the popup menu and maintain the others options selected. This function was implemented on the GUI for the Multichannel platform to shorter the time needed to set up the GUI to acquire the signals, since commonly the signals that the user wants to acquire, also wants to see them.

4.1.2 Signals present on the multichannel platform

The ECG is composed by one only signal, whereas the PPG has two signals, one for the wavelength (red and infrared). For each PZ sensor there are two signals the PZ signal (derivate of the pressure waveform) and the integrated PZ signal (the ABP waveform). Since the PWV probe has two PZ sensors and the APW only one, the PWV acquisition results in four signals whereas the APW signal results in two signals. Because of the time shift between the APW and the others signals, caused by different medium of communication, a synchronization signal was added allowing to quantify the time shift between them. The synchronization signal is recorded

when an acquisition when two probes are selected, where mandatorily one of them is the APW. The following table resumes all the signals which can be acquired through the multichannel platform.

Table 5 - Signals acquired through the multichannel platform.

DAQ	Probe	Signals
PIC	APW	Pressure waveform derivate Integrated PZ signal
	Synchronization	Noise generated
NIDaq	ECG	ECG signal
	PPG	Red wavelength Infrared wavelength
	PWV	PZ1 - Pressure waveform derivate PZ1 - Integrated PZ signal PZ2 - Pressure waveform derivate PZ2 - Integrated PZ signal
	Synchronization	Noise generated

4.1.3 GUI signals display

In order to have a bigger temporal resolution, during the acquisition of the multiple signals only the last 5 seconds of each signal are displayed. Otherwise the signal would be continuously compressed into the window size (Figure 24 - 4), which leads also to a decrease in the time resolution. This option also saves the graphical resources of the laptop, since it only has to display the last 5 seconds of the signal, while the others part of the data is stored in the system.

Another issue about the signals display is related with the amplitude resolution. The amplitude resolution of the signal will be lower as more signals are acquired, since the size of the window panel to display the signal is limited. Nevertheless, only some signals are displayed for each probe when they are selected (Table 6).

Table 6 - Signals displayed on the Interface.

Probe	Signals Displayed
APW	Pressure waveform derivate Integrated PZ signal
PWV	PZ1 - Integrated PZ signal PZ2 - Integrated PZ signal
ECG	ECG signal
PPG	Infrared wavelength

For the APW is it shown the differential and the integrated signal of the PZ, whereas for the PWV the two integrated signals from both PZ of the double PZ sensor. The ECG has only one signal, which is displayed, and the PPG is only shown the infrared wavelength, since both wavelengths for visualization purpose have the same relevance.

In the Figure 26 is possible to observe different acquisition and to see how the graphs are displayed and the amplitude resolution changes according to how many signals are displayed.

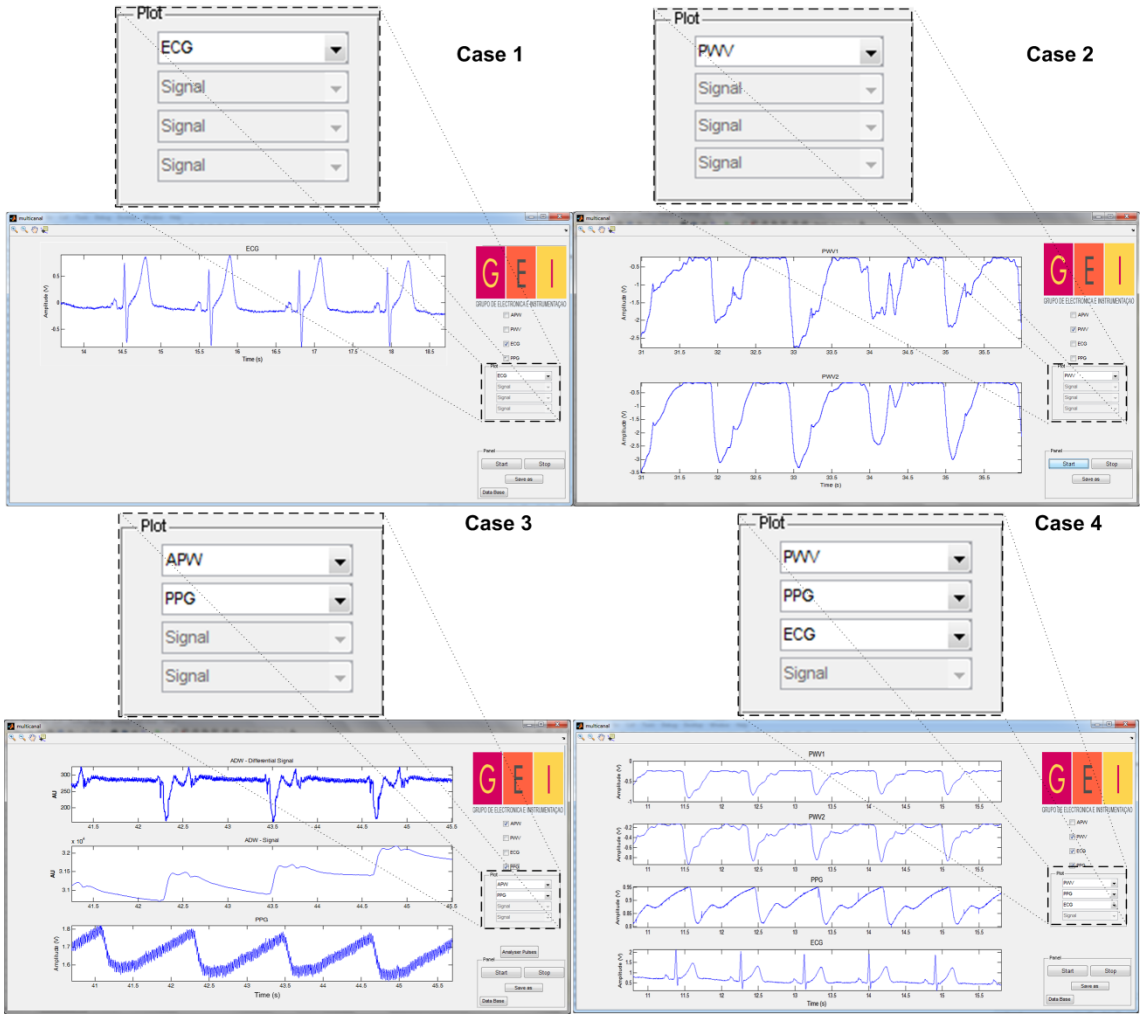

Figure 26 - Example of signals exhibit.

The popup menu which takes focus on the previous figure defines which signal will be displayed in the interface. It is demonstrated four different cases of acquisition. On case 1, in accordance with Table 6 for the ECG probe, just one signal is displayed. However, on case 2, even though just one probe is selected, it displayed two signals. The two signals showed are relative to the integrated PZ signal for the two PZ sensors presented on the PWV probe. Others cases are represented on the figure above, where the signals displayed are order by the order selected on the pop menu.

Assuming that the PWV and the APW probes are not acquired at the same time, the interface displayed a total maximum of four signals. Therefore, the lowest amplitude resolution is represented in Figure 26 on the fourth case.

4.1.4 Save data acquired

After the operator stops the acquisition it can store the data into the database. It was set a default folder to save all the files. The data, is then stored in a mat file with the name given by the operator.

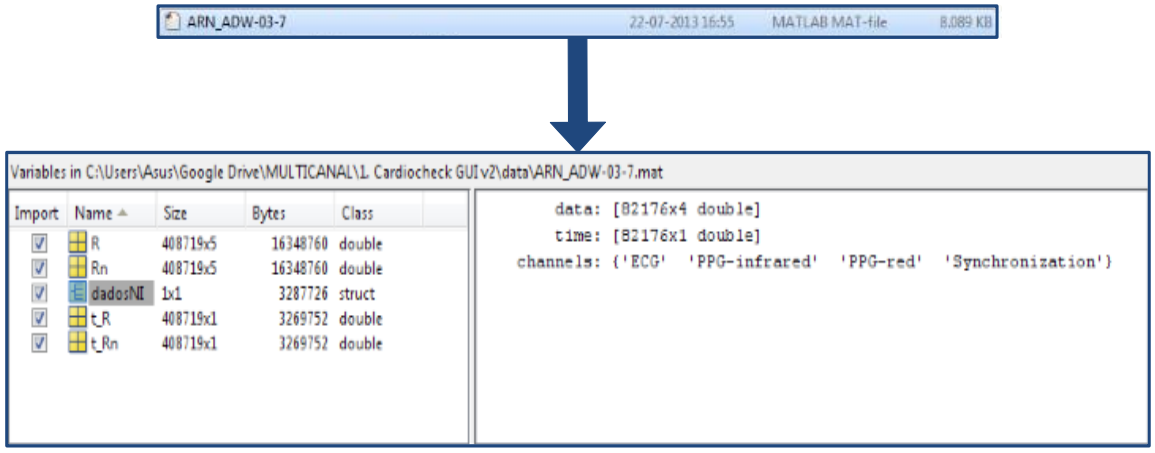

Figure 27 - Example of an acquisition file.

In Figure 27 it is possible to see the data is stored on the laptop on the *.mat file*, where it has all the data recorded during the acquisition. The files 'R', 'Rn', 't_R', 't_Rn' corresponding to the APW probe, whereas the 'dadosNI' is the file containing all the data acquired from the NIDaq (Table 5). Moreover, the file "dadosNI" has in it a file called "*channels*", which labels all signals stored from the acquisition into the *dadosNI.data* matrix. Thus, according to the "*channels*" the first column corresponds to the ECG signal, the second and third column is the infrared and red wavelength of the PPG, respectively. The last column corresponds to the synchronization signal.

4.2 Database - *Cardiocheck*

The previously GUI for the multichannel platform was incorporated into a database – *Cardiocheck* – developed by Pedro Santos [71]. A database is a collection of programs that manages the database structure, and enables the storage of the data, as well as the access to it. A presence of a database is essential for efficient validation tests, since it simplifies the organization and management of the acquisitions recorded.

The GUI of the database was developed on Matlab and uses the MySQL to store and manage the information on the database. On this database it is possible to insert patients and operators, change the personal information of the patients, among several others functions. In the Figure 28 is possible to observe the main menu of the *Cardiocheck* database.

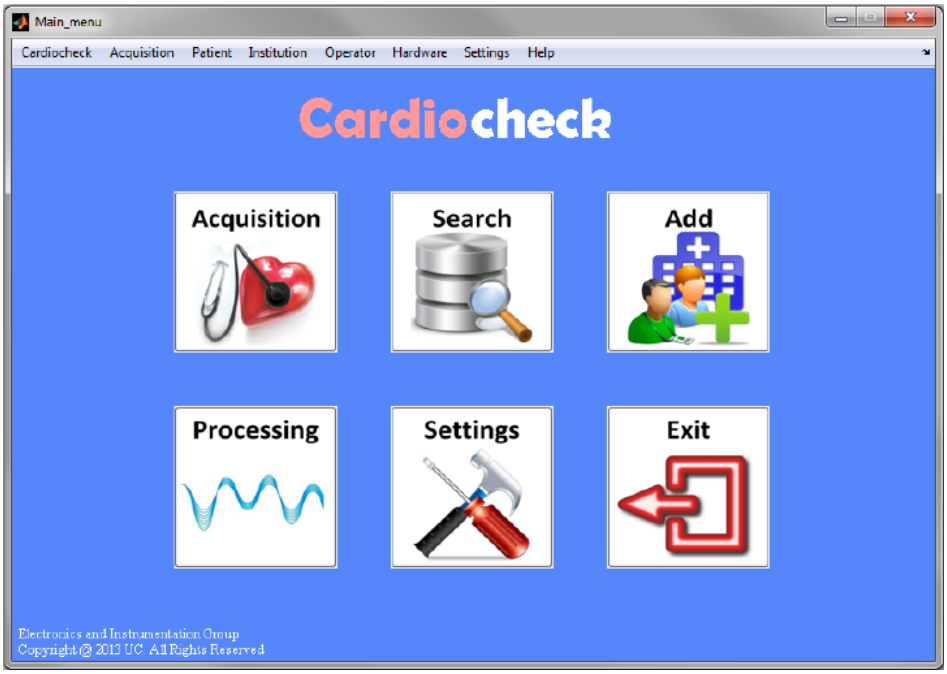

Figure 28 - *Cardiocheck* main menu appearance.

From this main menu is possible to execute different actions. Nevertheless, it will be briefly explained the steps needed to perform an acquisition.

The first step, if the subject still does not exist in the database, is to insert the patient personal data on the database at Figure 29.

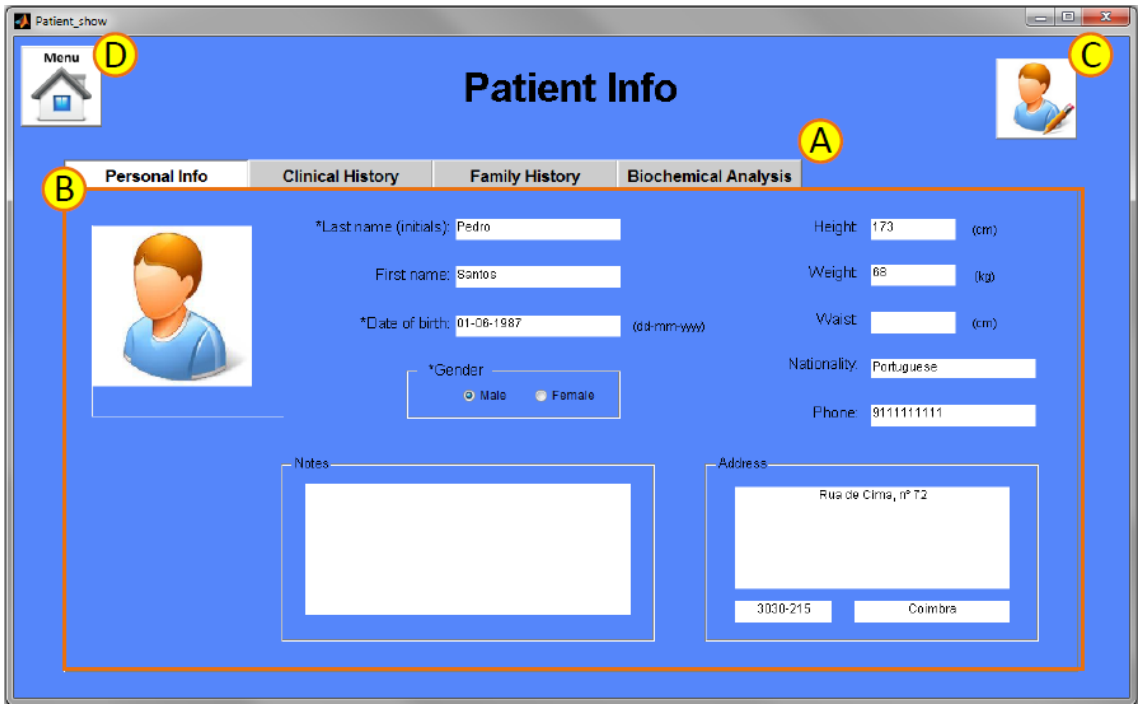

Figure 29 - Cardiocheck Patient Window : personal window tab. (A) tab selection, (B) personal info fields, (C) patient Edit/Save and Cancel buttons, (D) main menu button.

On this window it is type important information concerning the patients, such as age, height, weight. On the 'Clinical History' tab it is included important clinical information, such as: diabetes, cardiovascular disease, smoking habits, among other important information regarding clinical history. This information may be useful in formulation a diagnosis or to segment patients by these conditions in order to extract new health indicators through for example data mining techniques.

Afterwards, the acquisition procedure is initiated, where first some information about the acquisition must be selected (Figure 30) and then finally the acquisitions are made through the multichannel platform GUI developed (Figure 24).

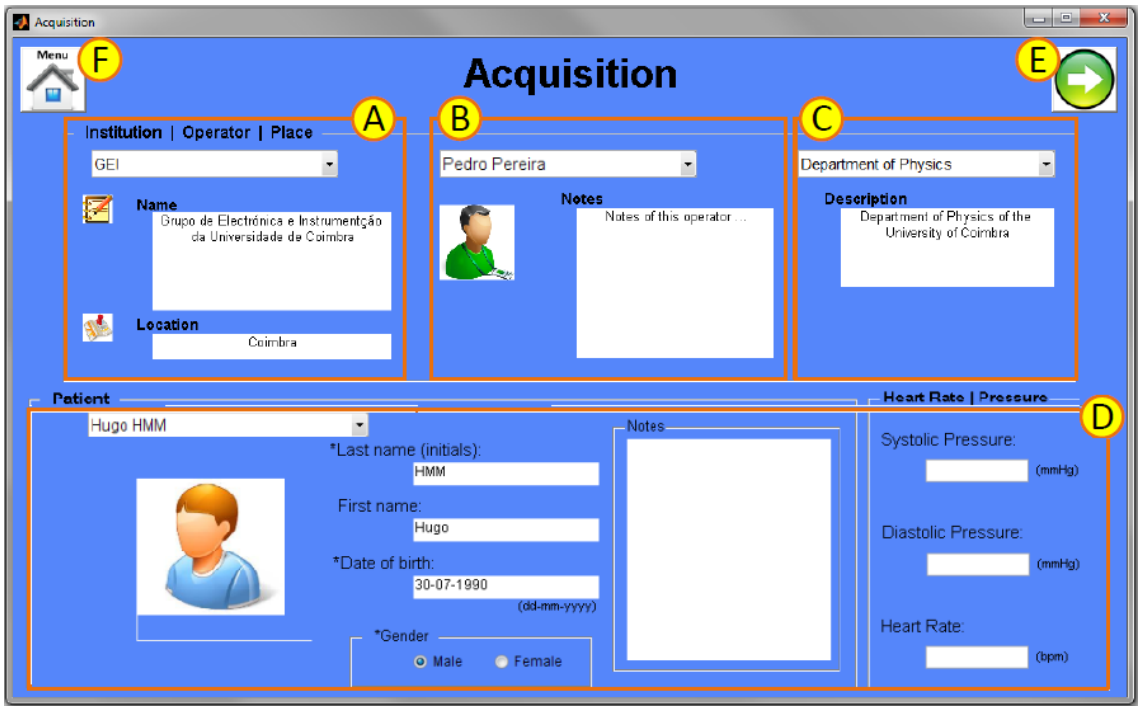

Figure 30 - Cardiocheck Acquisition window. (A) institution select pop-up; (B) Operator select pop-up; (C) place of acquisition pop-up; (D) Patient select pop-up and its basic information ; (E) proceed to multichannel platform GUI; (F) main menu button.

On the acquisition window first is selected the Institution (A), the operator (B) and the place (C) where the acquisition is going to be done and by whom. Then, the second part is regarding the patient, where it is selected one patient from the database, and important physiological parameters must be acquired (Systolic Pressure, Diastolic Pressure and Heart Rate). Then, by pressing the button 'E' it goes directly to the multichannel platform (Figure 24) where the acquisition data takes place.

4.3 Inter – communication between GUIs

When the GUI of the multichannel platform is performing an APW acquisition it is possible to inter-communication between the current GUI and with the APW Pulse Analyzer (Figure 31).

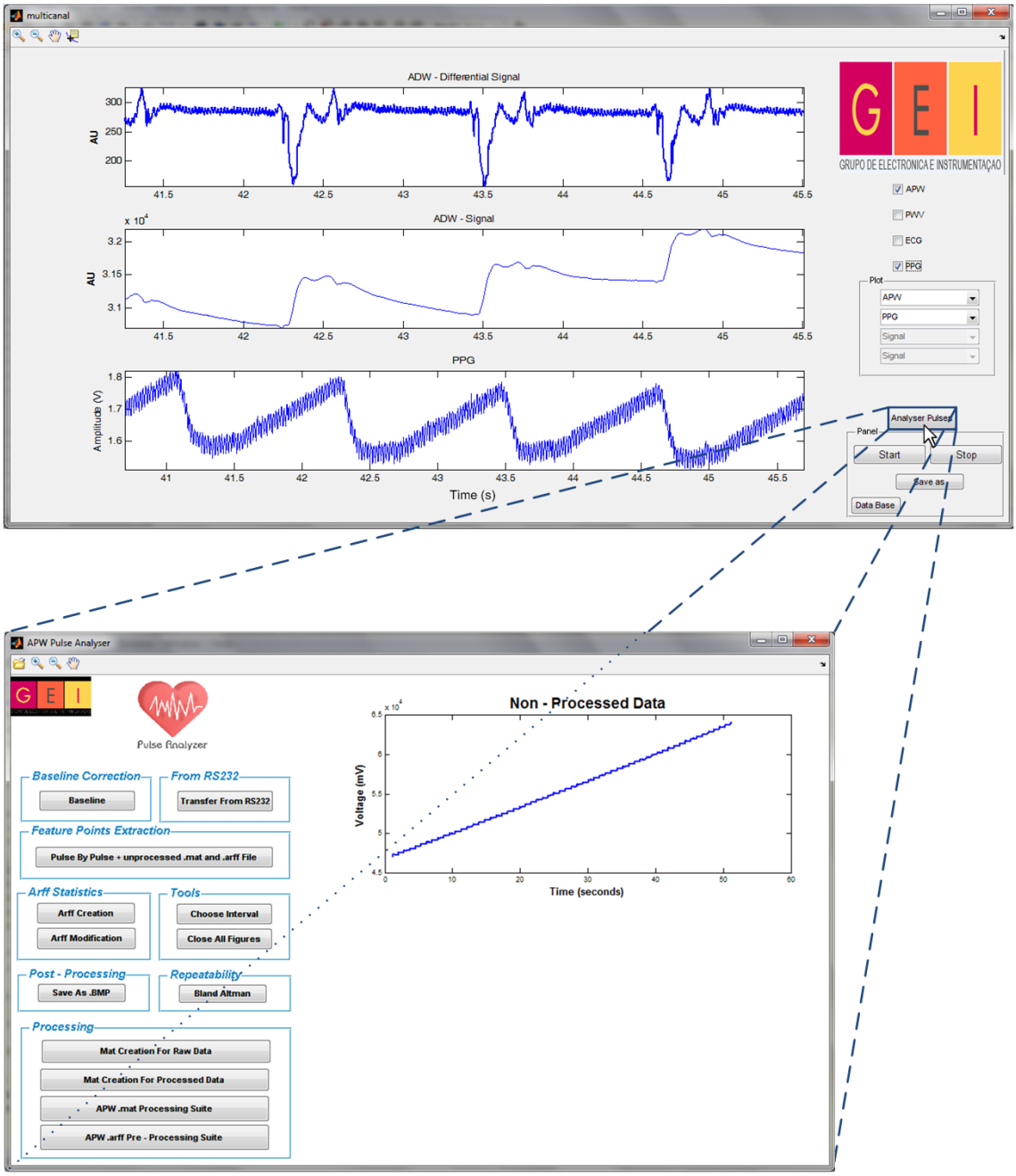

Figure 31 - Communication between the Multichannel Platform GUI and APW Pulse Analyzer Module.

This is a small improvement, and however, as a big importance for the acquisition procedures. This small feature enables to check during the acquisition of the acquired APW signal, if after the correct processing is possible to correctly extract the features points. Thus, another acquisition can be done, if due to internal or external factors the APW has poor quality, mainly dependent to the experience of operators.

As it is possible to see on the Figure 31 the button “Analyzer Pulses” shows up, which is responsible to transfer the previously acquired data to the APW Pulse Analyzer Module.

Then, on the APW Pulse Analyzer Module just by clicking on the “Transfer from RS232” it is possible to visualize and process the raw APW signal to check the quality of it.

5. Methodology

5.1 APW – Pulse Analyzer

After the APW signal is acquired, several steps must be executed before get valid information from it. A previously developed interface –The APW Pulse Analyzer [72] – was adapted and implemented on the multichannel acquisition system (Figure 31). This tool includes all the routines necessary to extract, from the arterial pulses, the features points that are necessary for sequential analysis. This tool also includes baseline noise removal and pulse segmentation routines, since the acquired raw APW may contain noise, artifacts and irregular waveforms and the pulses acquires are not segmented.

In order to analyze the data from the acquisition two files should be selected one with the data from the APW signal and other with important information about the subject. Since, the multichannel platform is storing all the data in the database, during this work, an update was done to get the information from the subject by a connection with the database. Therefore, it is only need to select the file with the APW data, instead of select the two files previously required.

All these tolls were already developed and discussed in previous works, which will be briefly explained on next sub-chapters [16, 73]. More recently, the APW Pulse Analyzer was developed where it was all those routines as well as some new features, such as a repeatability assessment [72].

5.1.1 APW on set calculation

The algorithm used to determine the onset of the APW, was based on Li et al. (2010) [74]. Accordingly to Li et al. the onset of an APW is related to a zero-crossing point before a maximal inflection of its derivative. First, in order to remove noises and artifacts, a third order low pass Bessel filter with a cutoff frequency of 30 Hz is applied to the raw signal. Then, a magnitude threshold is applied to the derivative signal to determine the local extreme, which is the maximal inflection point of each pulse. Finally, it is possible to determine the onset for each APW pulse, which corresponds to the first zero crossing point before each maximal inflection points.

5.1.2 Baseline noise removal

Before extract any features from a signal is fundamental to ensure the signals is clean of noise. Moreover, if the noise is not correctly removed it will lead to results with no clinical value, since there are not reliable. The baseline can be caused by electrical fluctuations, slow motions of the neck attached PZ probe, and motions artifacts due to patients breathing or by cough.

Although, the PZ probe has a real time baseline elimination based on a consistent baseline restorer [16], a baseline fit algorithm for baseline wander removal was also implemented to guarantee the validity of the APW signal. This algorithm determines the baselines index, which match to the onset and offset of each APW pulse. A baseline fit is interpolated from the baseline indexes points. Thus, a vertical adjustment for each sample between two successive baseline indexes is done, by matching those baseline point index to zero amplitude [73].

5.1.3 Morphological analysis

The morphological analysis is one important parameter, which must be carefully studied, since motion artifacts due to voluntary or involuntary movements of the subject lead to changes in APW volume. Those events are not associated with normal APW acquired in resting conditions, and so, it is important to remove the APW pulses which are affected from those artifacts. This algorithm measures the mean APW and the RMSE between the mean APW pulse and every individual pulse. Ultimately a criterion is used to evaluate each pulse by wide variations in amplitude and width pulse to flag and remove all APW pulse, which match at least one of the abnormality criteria [73].

5.1.4 Pulse segmentation and normalization

At this stage the processed APW beats should be erased of any time of noise which can corrupt any result. Then, the signal is segmented into individual pulses, and it is normalized to scale heterogeneous, so that their morphology can be appropriately compared. Morphological characteristics is the only parameter analyzed from the APW signal, since the acquired APW is not calibrated [73].

5.1.5 Spatial feature extraction

Several characters points can be extracted from each individual APW pulse. Almeida et al. (2011) [23] proposed a method for spatial feature extraction, where diverse APW characteristics points are determined, enabling to classy the APW type and to establish other parameters, which could have relevant clinical value in the future.

5.2 Electrocardiogram

In ECG, the P wave is related with the atria depolarization, and so, it does not represent any mechanical event from a physiological point view. Therefore, it does not have any value for APW analysis. Actually, the most interesting wave in ECG is the R wave, since it represents the physical contraction of the ventricles. Moreover, studies requested the R wave to be a time reference, in order to either determine more accurately the regional and local PWV [37, 54, 61], or for heart variability assessment [75-77] only the R wave from the QRS complex is needed. Thereby, an algorithm with a high precision and sensitive to the R wave detection is desirable.

To detect the R wave from the QRS complex it was a used an algorithm based on Pan and Tompkins [78]. This algorithm is based in three different types of processing stages: linear digital filtering, nonlinear transformation and a decision rule algorithm. The algorithm is compounded by band-pass filter, a derivative and a moving window integrator (linear digital filters) and amplitude squaring (nonlinear transformation) and a thresholds rule (decision rule algorithm).

5.3 Photoplethysmogram

Over the past years, it has been paid more interest in PPG in a wide range of clinical measurements, because of his prosperous potential in those areas. Furthermore, PPG is a reliable, low cost, simple to use and noninvasive method. These unique characteristics of the PPG make him an ideal instrument to be used worldwide. The PPG can providing information related to blood pressure, arterial compliance, heart rate variability, neurology, cardiac output, respiration and detecting arterial disease [19].

However, PPG signal is very susceptible to external factors. Motion artifacts, respiration, ambient light are one of the most common factors that affect the quality of the PPG signal (Figure 32). Thus, signal processing techniques are required to ensure the absence of noise on the PPG signal [19].

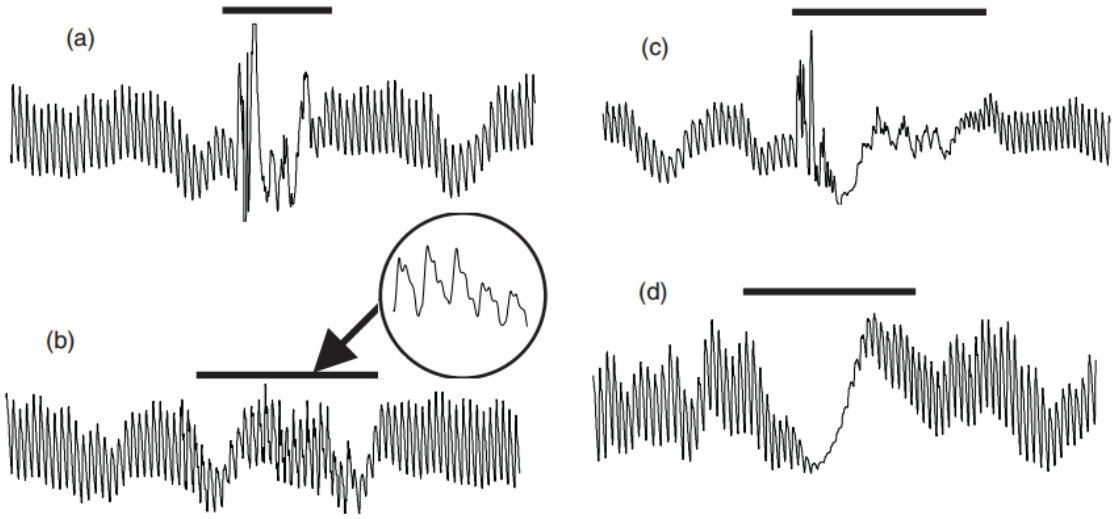

Figure 32 - Examples of artefacts present on the PPG due to: movement (a), finger tremor (b), bout of coughing (c) and breathing parttern (deep gasp or yawn) (d) [19].

In order to immune PPG signal from ambient light, the PPG has a cap to produce a light shade over measurement site.

As mentioned before, the PPG probe used has two diodes with different wavelengths and only one photodetector. A MCU is set just one diode at each time in order to measure each wavelength is opposite times. Nevertheless, while observing the measurement of one wavelength, it is perceptible the presence of some noise due to the second wavelength. The noise introduced by the second wavelength is similar to the "salt and pepper" noise. Thus, a median filter with a window size of 3 samples was the suitable option to efficiently remove this noise (chapter 6.2.3).

Two different algorithms were implemented to retrieved information from the PPG signal. Those two different algorithms are presented and described on the following sub-chapters.

5.3.1 Calculation of onset, systolic peak and dicrotic notch

The presented algorithm was based on the study of Li et al. [74] to characterize the arterial blood pressure (ABP) detected by the PPG probe.

First, as it is common in practice the PPG is inverted, and only then, the identification of the onsets, SP and dicrotic notches (DN) are done. The presented ABP delineator (Figure 34)

suggest by Li et al. [74] is based on a combination of ABP waveforms analysis with the first-order derivative (Figure 33) and some logical decisions.

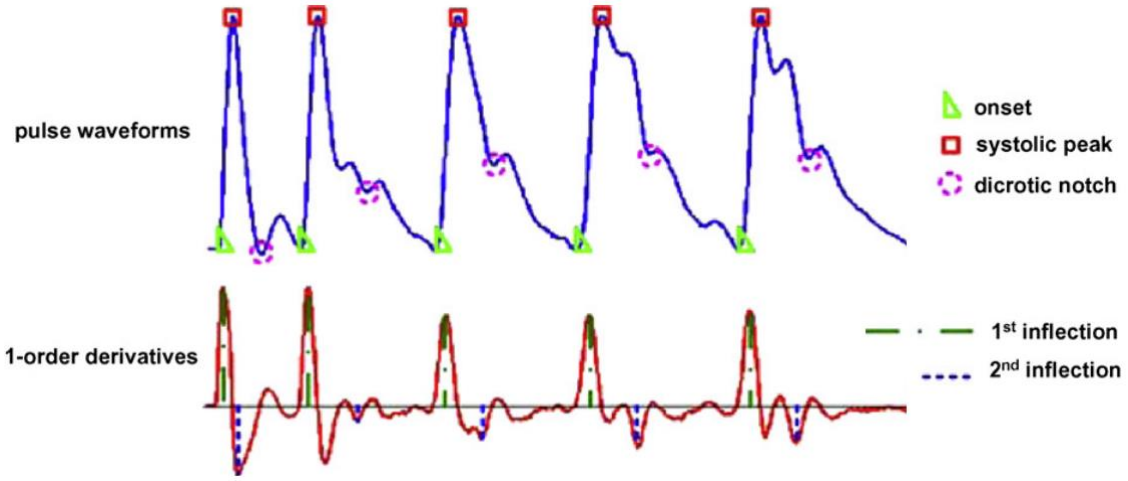

Figure 33 - ABP waveform and its 1st order derivative [74].

The onset of an ABP waveform is related with the zero-crossing point before a maximal inflection, while the SP is related with the zero-crossing point after a maximal inflection (Figure 33) [74].

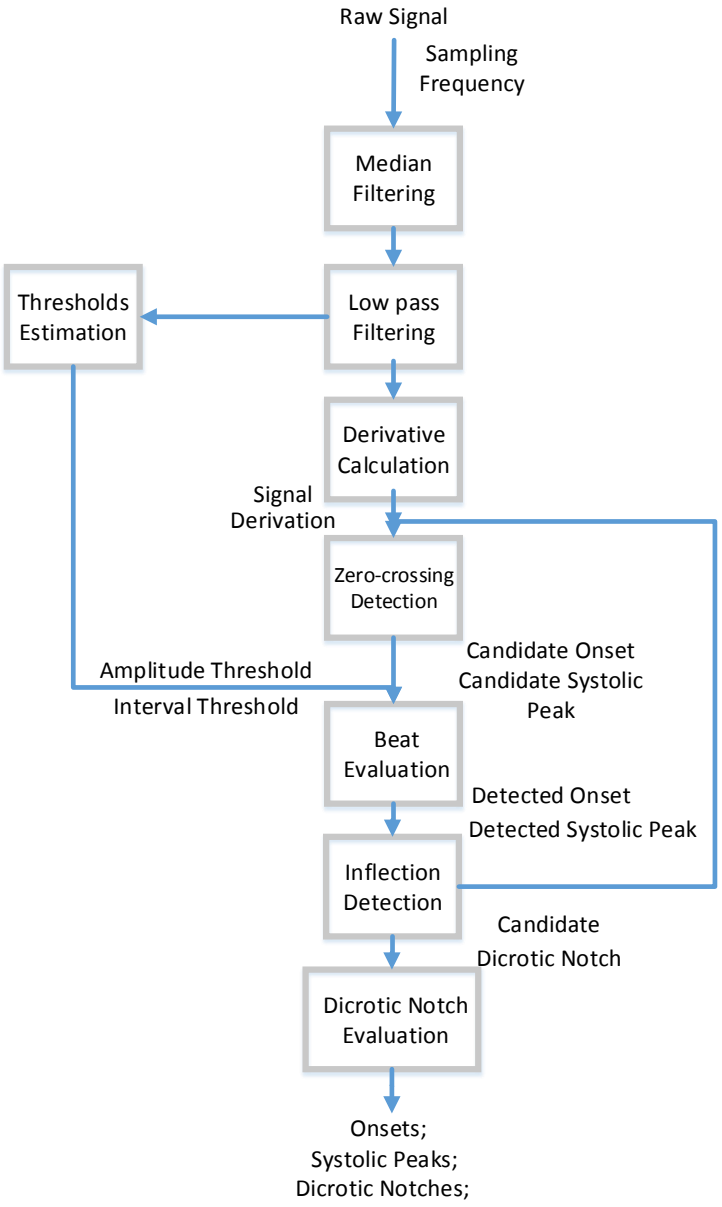

Figure 34 – Flowchart of the algorithm to detect the Onset, Peak Systolic and Dicrotic Notch. Adapted from [74].

PPG signal detected is very susceptible to be influenced by many factors. Therefore, a 3-order low-pass Bessel filter with a cutoff frequency of 30 Hz is used to suppress those factors.

The algorithm (Figure 34) divides the signal in windows of equal parts and it calculates its derivative and estimate a thresholds based on the amplitudes and pulses rates within those windows. Then algorithm seeks for the candidates for the zero-crossing points in the derivative. In other words, the algorithm searches for pairs of inflection points and zero-crossing points in the ABP derivative, where the zero-crossing point before the inflection point is the onset and after is the systolic peak. After a candidate is selected, it is evaluated on the ABP waveform by the amplitude and interval thresholds previously determined. If the candidate is qualified, the

algorithm proceeds to the DN detection. Otherwise, thresholds are adjusted and the algorithm starts over, and seeks for new candidates [74].

The presence of a DN is assumed to be after each SP detect, or at least, an incisura. The algorithm considers the first zero-crossing point after the second inflection point as the the DN. However, in some special cases when there is not a zero-crossing point, the algorithm settles an empirical point as the DN [74].

5.3.2 Second derivative of the finger photoplethysmograph

Studies [79-83] have reported the evaluation of the volume pulse wave contour by the second derivative of the photoplethysmogram waveform (SDPTG) (Figure 35). The contour of the PPG signal has important information regarding the central and peripheral arterial properties. This method enables a precise analysis of sudden changes in the waveform and time shifts.

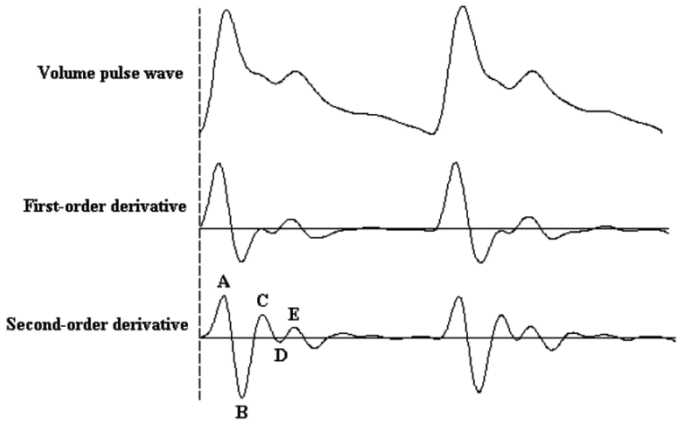

Figure 35- Photoplethysmogram waveform and its derivatives [79].

The SDPTG assumes the finger photoplethysmogram waveform is composed by five successive waves – A,B,C,D,E – where A,B and C waves occurs on early systole and D and E waves occurs on late systole (Figure 35). These indices have independently discriminated between hypertensive patients and healthy normotensive subjects, which shows the potential of this new method analysis. These indices are then normalized with A wave, and thus it can be obtained four ratios – B/A, C/A, D/A and E/A. Even though, there is not a physiological explanation for these ratios, strong correlation correlations have been done between those ratios with physiological and clinical characteristics. Strong correlations have been found between

some ratios with aortic AIx, as well as, with age, arterial blood pressure and carotid distensibility [79-81].

The presented algorithm (Figure 36) uses the same processing used to delete the noise present on the PPG signal mentioned on the previously algorithm are used. Therefore, the combination of the median filtering and the 3-order low-pass Bessel filter is first applied to the raw signal.

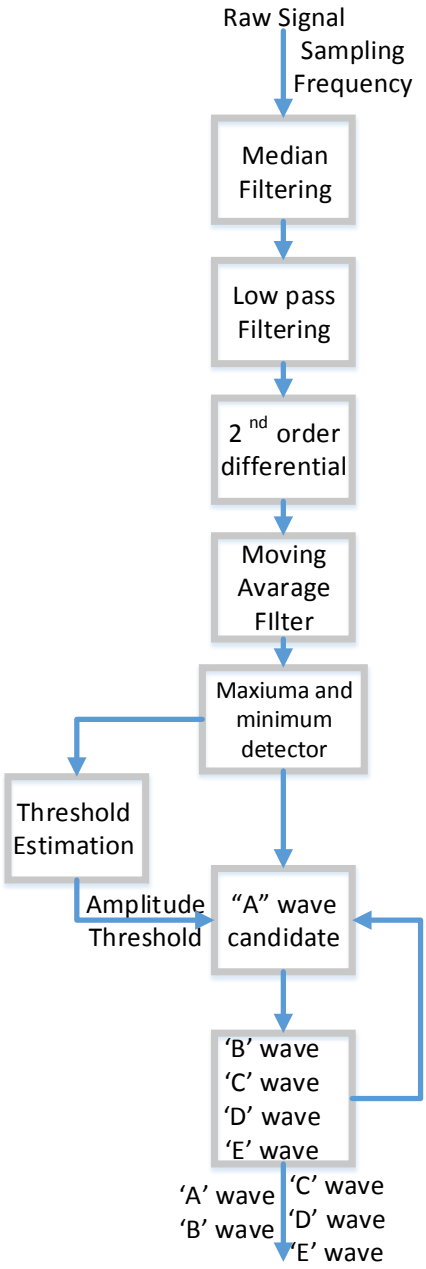

Figure 36 - Flowchart to determine the waves from SDPTG.

However, the differential function of second order amplifies any noise present in the sample. Thus, a higher degree of processing the data is required. Thus, a moving average filter is applied after the differential function, to guarantee the total absent of noise on the sample analyzed.

Then, maximum and minimum of the 2nd differential order are calculated. The threshold is set as a percentage of the maximum previously detected. By the application of this threshold the algorithm seeks for A wave candidates. If a B,C,D and E waves are successfully determined on a threshold interval, the pulse is stored. Otherwise, the algorithm skips the current pulse and goes for the next A candidate. The threshold interval is considered to be the time between to current and the next A wave candidates.

5.4 Multichannel platform acquisition

In this primary studies carried to evaluate the performance of the multichannel platform twenty and three volunteers (9 females and 14 males), aged between 19 and 28 years old were included. On this group were carried out 287 different acquisitions.

Before the proceedings for the various acquisitions through the multichannel platform all subjects gave informal consent after full explanation of the purpose, the used procedures and the risks inherent to the acquisitions. All acquisitions included additional data about the subjects was recorded. Therefore, before it each acquisition it was registered the: age, gender, weight, height, body mass index (BMI) smoking habits and diabetes history for each subject. With an automatic digital oscillometric sphygmomanometer (Omron M6 Confort, Kyoto, Japan) the SBP, DBP and HR values were also measured and saved on the database.

The patient acquisition protocol was based on the three different condition standardizations for hemodynamic assessment of Laurent et al., Van Bortel et al. and Boutouyrie et al. [9, 56, 84]. The full explanation of the procedure is very important to avoid any the surprise effect which can influence the acquisition data. All the subjects on this study were healthy volunteers, in others words, all subjects had no documented history of cardiovascular disorders.

Subjects remained quiet on their bed on a supine position, and were advised not neither to speak, to couch or to sleep. Acquisitions were made at similar time of the day, and in a controlled room temperature (22-23 ºC). It was also ensured that patient has not drunk any alcoholic drink or smoked within a time line of 3 hours before the acquisition. The acquisitions were made all by the same operator. A period rest of 10 minutes was done preceded to the

acquisitions, in an attempt to get BP, cardiac function, and vasomotor tone as close to basal resting conditions as possible. At least 2 or 3 acquisitions of more than 60 seconds were made per subjects, where all must be relative equal.

The double PZ sensor and the PZ probe could not be acquired at the same time, because of the limited area over the neck. Thus, two different acquisitions were made: one globing the single PZ sensor (Probe 1 in Figure 37), the ECG and ultimately the PPG, and another where it was used the double PZ sensor instead of the single PZ sensor (Probe 2 in Figure 37) with the ECG and PPG.

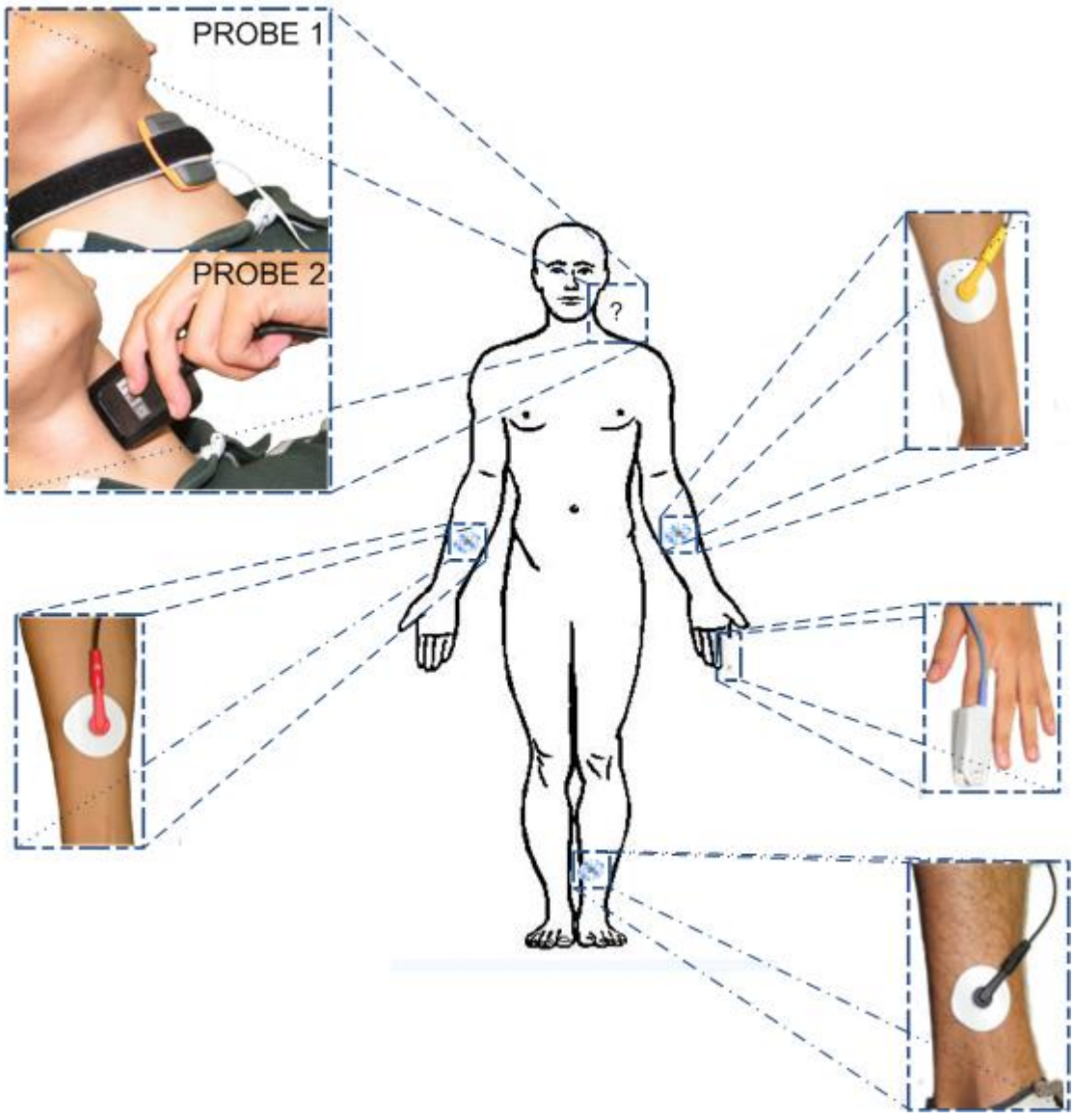

Figure 37 – The two different acquisitions set up.

The PPG sensor is placed were set on the indicator finger of the left arm. The ECG as explained previously (chapter 3.3.4.2) it is placed one electrode one the right and left arm and another on the left leg. The sensor of the PZ (both single and double headed) is placed over the left CCA. However, while the PZ single headed sensor is held by a collar to clench the sensor in the neck of the patient, the double PZ sensor must be hold by the operator. Thus, the double PZ sensor was hold the by the operation during the acquisition. This aspect turns harder to expertise double headed probe, requiring a high degree of expertise.

6. Results and Discussion

In this chapter, some of the results obtained will be presented and discussed. The studies carried out were attended to correlate the various signals acquired during the validation tests of the multichannel platform.

6.1 Results from acquisitions

Since both PZ probe could not be placed at the same time over the CCA, two different acquisitions were performed as illustrated on Figure 37.

6.1.1 Acquisition setup I

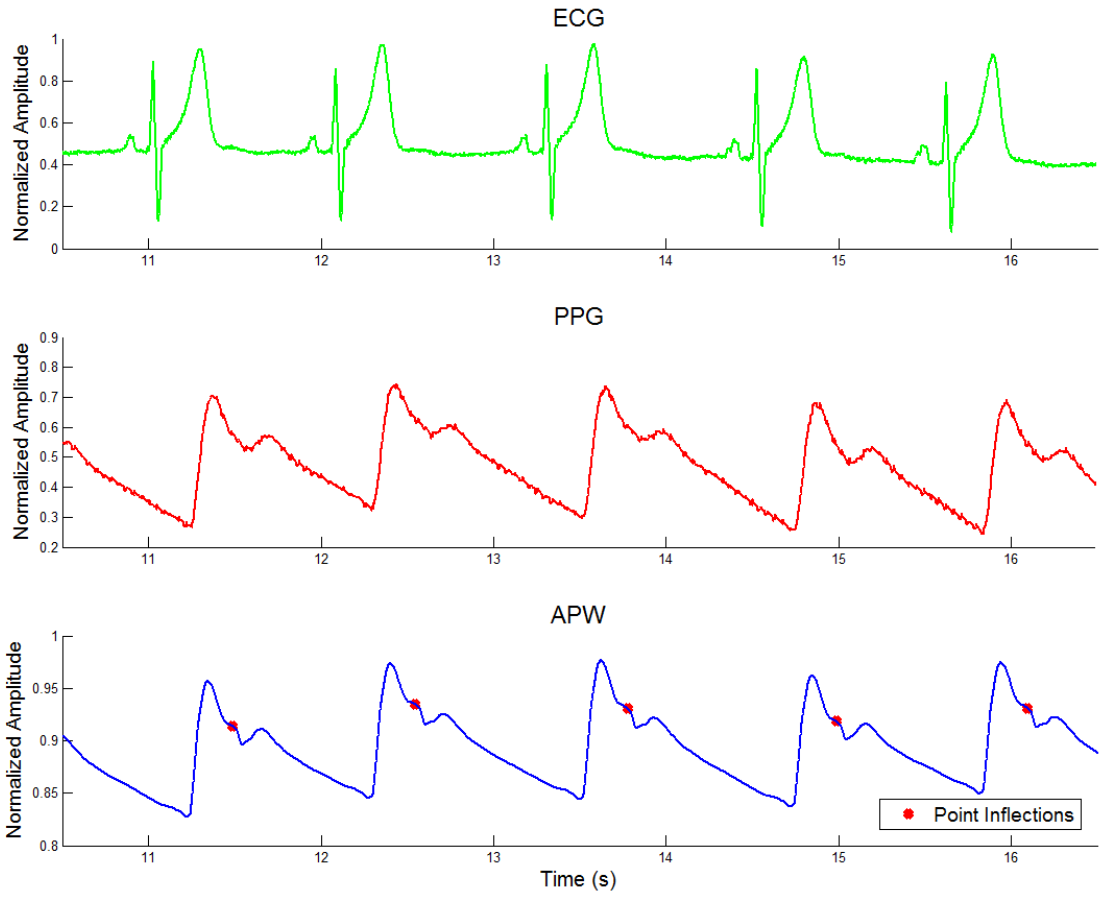

Figure 38- Acquisition setup I.

On the acquisition setup I the ECG, PPG and APW modules were used. In Figure 38 are represented the acquired signals for a one healthy subject. On the APW signal it is possible to

visualize a point of interest, the point inflection (Pi), which is the result of the sum of the reflected wave with the forward wave (signaled on the APW signal in the Figure 38).

Two observations can be done from a simple look at the signals. The first one is the late Pi, which occurs after the systolic peak, as it is normal from healthy subjects. Another important remark, it is the extinction of the Pi on the PPG signals, which although it measures the arterial blood pressure (ABP) at peripheral site, due the "amplification phenomenon" this point is lost along the artery tree. Nevertheless, the APW signal is acquired noninvasively at the carotid artery, which has a pressure similar to the central pressure, and thus, turns the APW signals a better choice to measure the central pulse pressure. However, the techinique of the APW (PZ sensors) requires a high degree of expertise, which, limits the possibility to use this technique as a widepread diagonises technique for CVD. The PPG compared to the APW in terms of ABP has the advantage of being easy to use and it has a big amount of information which can be retrived from it.

6.1.2 Acquisition setup II

The Figure 39 demonstrates the signals acquired from the second acquisition.

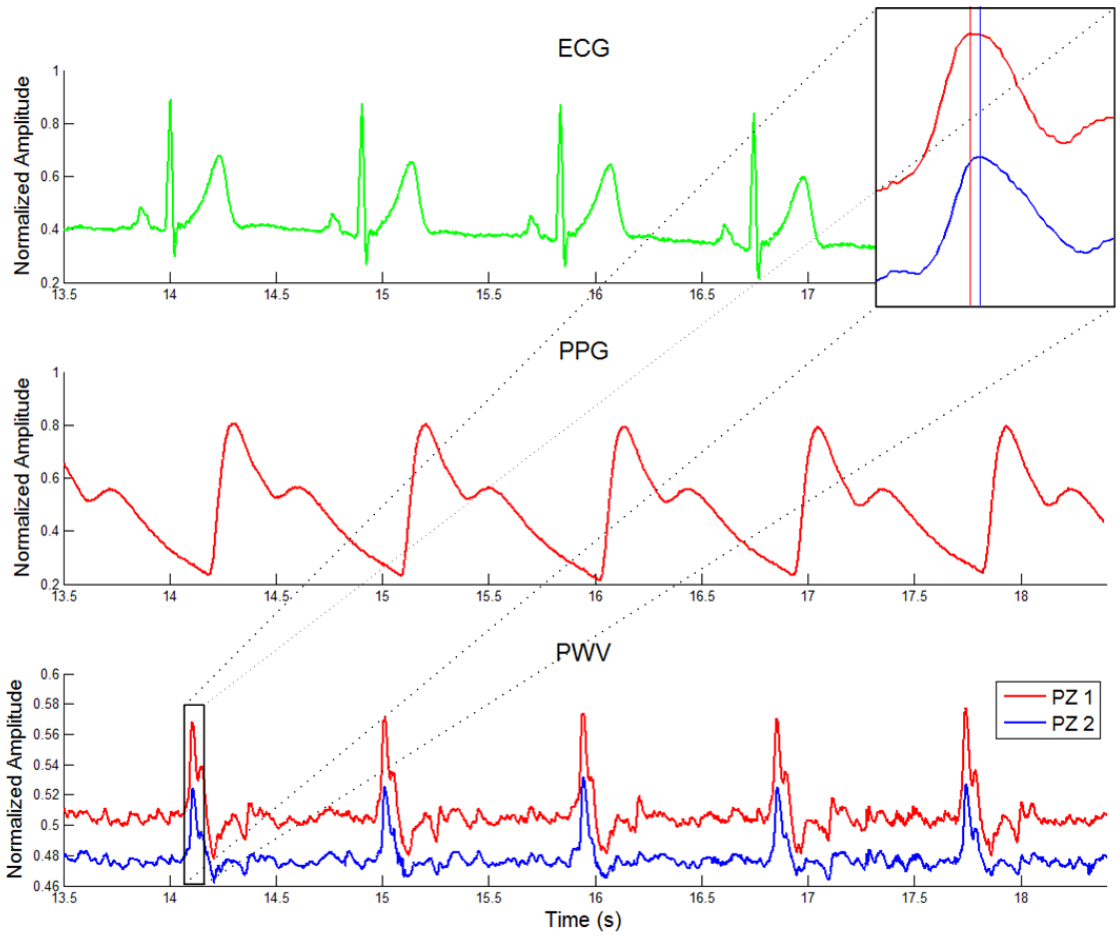

Figure 39 - Acquisition setup II.

The difference to the acquisition setup I is the use of the PWV module instead of the APW module, since both modules could not be acquired at the same time. The PWV acquired from the double PZ sensor has the arterial pressure waveform from two different PZ placed at a fixed known distance. Thus, measuring the time the blood flow takes to travels between the two PZ sensors – the TT - it is possible to determine the local PWV from the subject at the carotid artery. The TT is measured by the difference of a characteristic point of the pressure waveform over the two sites recorded. On the zoomed figure it is possible to observe the signal recorded from the PZ 1 and the PZ 2, where is marked the PZ maximum with a vertical line on both PZ signals, which corresponds to the maximum upstroke rise. The TT is determined by the time difference from those lines.

The example on the previous figure uses the maximum upstroke rise as the point reference to determine the TT. However, the best reference point to measure the PWV is the upstroke, since it is hardly affected by the wave reflections. The SP was used on this example, since it is more evident to explain how the PWV can be measured from these two PZ signals recorded at a distance known.

From this acquisition it is possible to use the most accurate method to measure the PWV. This method uses the ECG signal, where the R-wave used as a time reference to calculate the PWV.

6.1.3 Synchronization module

On the multichannel platform are implemented two different DAQ, the NI and PIC (used on APW acquisition). Signals acquired from different DAQ will not be synchronized in time, and may have different acquisitions rates. The use of a synchronization channel to determine the time delay between the DAQ is fundamental. On case of the acquisition which uses the two different DAQs the use of the synchronization is necessary. The Figure 40 illustrates the synchronization signal acquired from the two different DAQ boards presented on the multichannel platform, the NI and PIC.

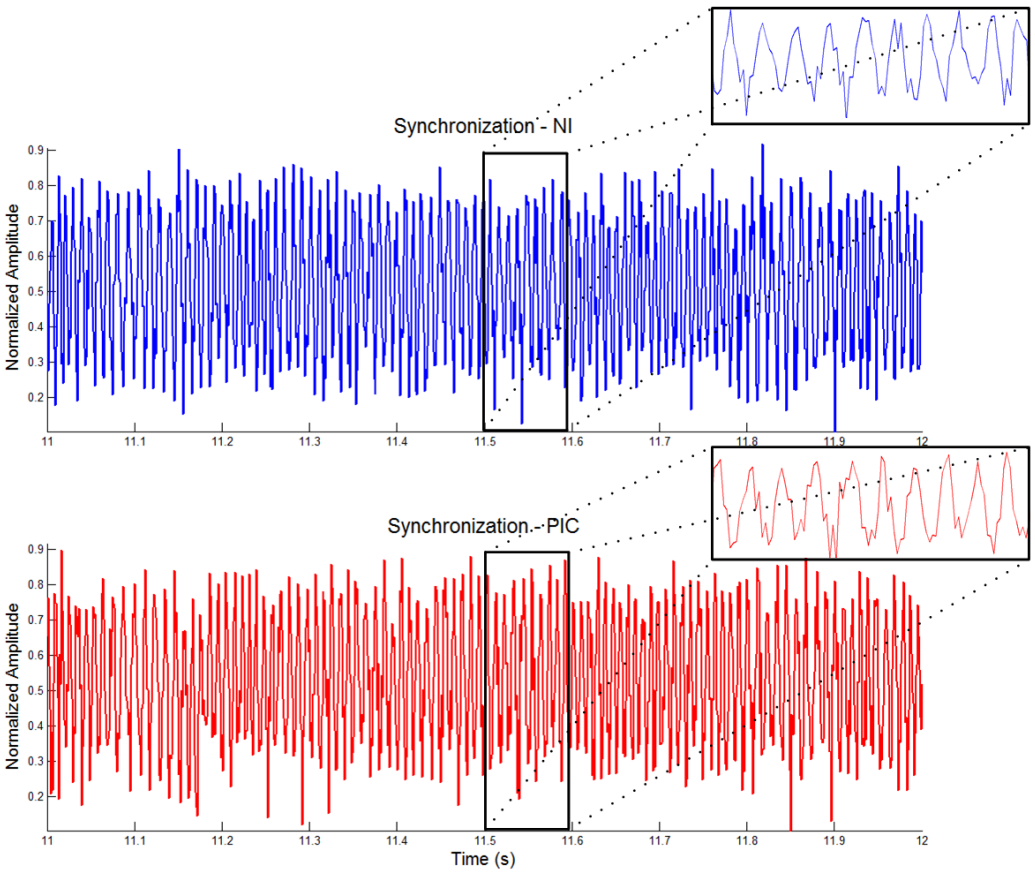

Figure 40- Synchronization acquired from NI and PIC.

Synchronization signal is a random signal (white noise) which is then acquired from both DAQ (dsPIC and NI6210). Applying an algorithm based on cross-correlation on the synchronization channel from each DAQ it is possible to determine the time delay. Thus, it is possible to put a common temporal reference in all signals acquired from the different DAQ.

6.2 Hemodynamic signals analysis

The first step to do any analysis is to retrieve valid information from the signals acquired during the data collected. Therefore, the implementation of a valid algorithm is fundamental. On this section it will be present and discussed some results obtained by the application of the processing algorithms.

Algorithms for the APW signals used will not be discussed since it was already been extensively analyzed and discussed on earlier studies, where it was proven their efficiency to retrieve valid information [72, 73].

6.2.1 APW analysis

6.2.1.1 Subject characteristics

In this section the parameters values for the group of studied subjects is presented (Table 7), as mean ± SD. Those values where retrieved from APW acquired during the acquisitions setup I (Figure 38) and from the general information regarding the subject. All this parameters can be found on the database – *Cardiocheck*.

Observing the Table 7 is possible to confirm that all the volunteers gather on this validation test have values of SBP (<130mmHg) and DBP (<84mmHg) considered normal, with no indices cardiovascular diseases [85]. Despite the high variability existence on the AIx values, the negative AIx is included in the margins of error for each subject. This also confirms the presence of typical healthy values, since negative AIx is related with no arterial stiffness, which is an indicator of CVD.

On this study it was only included the subjects for that it was possible to retrieve valid information from APW probe on both weeks of acquisition. If a number considerable of pulse was not detected on the APW Pulse Analyzer, this subject was excluded from the repeatability assessment.

We can observe a very homogenous group of test with similar characteristics, such as a low range of age (19 years old to 29 years old) and with similar BMI (body mass index). However, the aim of this primary studies is focused to validate the multichannel platform, where this group of test is enough.

In the Table 7 is noticeable big standard deviation of the AIx measured on the acquisition. Although, the algorithms used to calculate could lead to some increase of the variability in the AIx, another important, which must be mentioned is the operator. Even though, the acquisition were always made by same operator the probe has a high degree of expertise. Primary acquisitions were done by the operator to practice the placement of the PZ sensor over the CCA. However some variability can be influence by the operator, which realizes better acquisition on the last acquisitions in comparison with the first acquisitions, since the operator has low experience.

Table 7 - Test group characterization (mean ± standard deviation).

Subject #	Gender	Age	Height (cm)	Weight (Kg)	BMI	HR (bpm)	SBP (mmHg)	DBP (mmHg)	SP_t (ms)	Pi_t (ms)	AIx (%)	n
1	**F**	**20**	**156**	**45**	**18.5**	**80±5**	**107±6**	**68±4**	**142.8±40.6**	**187.3±33.6**	**-7.1±9.3**	**297**
2	**M**	**22**	**179**	**74**	**23.1**	**61±5**	**117±8**	**65±2**	**128.7±27.6**	**215.5±57.3**	**-21.9±15.8**	**356**
3	**F**	**23**	**169**	**52**	**18.2**	**80±5**	**102±7**	**68±11**	**134.1±34.0**	**163.6±55.0**	**-1.7±19.7**	**184**
4	**M**	**22**	**175**	**68**	**22.2**	**56±10**	**124±8**	**65±2**	**144.7±24.9**	**196.1±48.0**	**-8.6±18.5**	**108**
5	**M**	**23**	**175**	**73**	**23.8**	**59±2**	**125±4**	**74±1**	**142.8±7.3**	**111.0±61.2**	**26.1±27.8**	**124**
6	**F**	**22**	**165**	**54**	**19.8**	**86±8**	**125±2**	**83±1**	**186.1±36.5**	**188.1±78.7**	**8.5±20.6**	**152**
7	**M**	**19**	**180**	**67**	**20.7**	**83±7**	**125±1**	**67±1**	**119.2±13.5**	**222.8±30.6**	**-37.5±10.7**	**164**
8	**F**	**23**	**160**	**50**	**19.5**	**89±26**	**111±11**	**84±6**	**227.3±45.2**	**149.0±30.8**	**14.2±14.5**	**248**
9	**M**	**28**	**172**	**60**	**20.3**	**89±34**	**106±27**	**67±4**	**128.1±11.9**	**200.5±41.3**	**-20.4±14.3**	**183**
10	**M**	**24**	**173**	**69**	**23.1**	**76±33**	**106±19**	**64±7**	**176.2±65.9**	**171.6±51.9**	**5.5±22.5**	**232**
11	**F**	**22**	**161**	**49**	**18.9**	**82±6**	**106±7**	**71±5**	**167.8±51.4**	**51.2±60.2**	**12.0±24.4**	**129**

6.2.1.2 APW repeatability tests (agreement assessment)

As mentioned on chapter 5.4 all the acquisitions were done on the same period of the day. The protocol for the acquisition was elaborated to make the acquisition under the same conditions, to test the variability of the information acquired in an interval of time. Therefore, all external factors must be avoided, in order to prevent the influence of other factors than the variability of the probe.

The Figure 41displays a Bland – Altmand AIx plot of two measurements: on the first and second week and another realized on the third and fourth weeks.

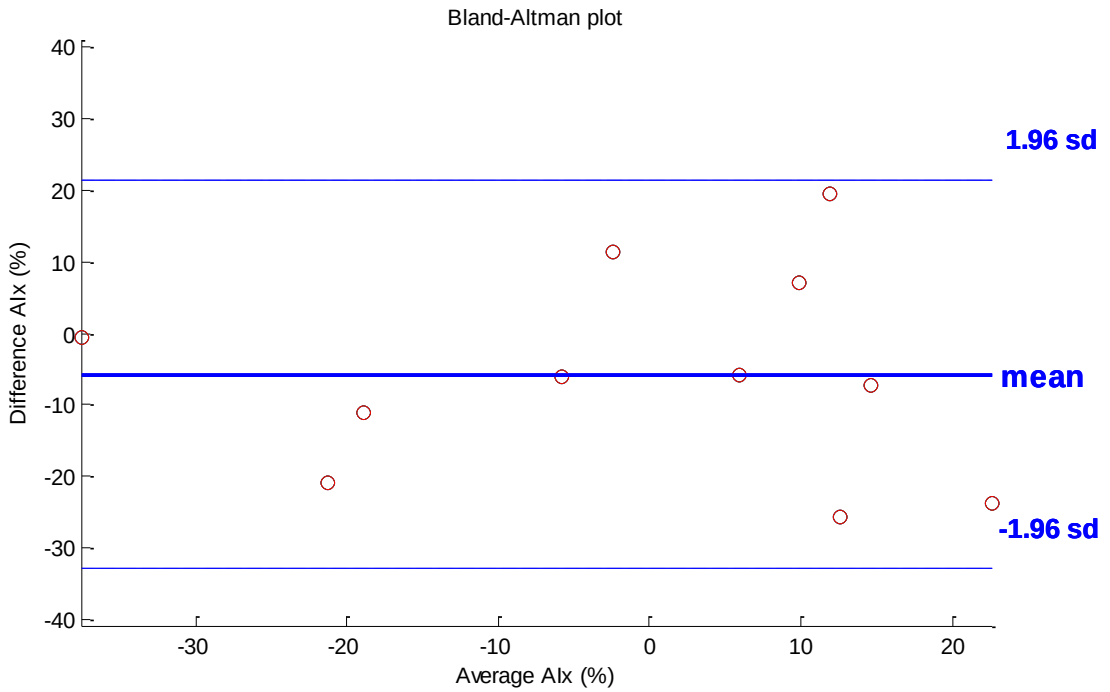

Figure 41 - Bland-Altman AIx plot between week the first 2 week and the last 2 weeks.

The mean difference from the AIx differs from zero by -5.47%. No patterns can be visualized and the variability seems consistent along the graphic. The upper and lower limits are 21.25% and -32.71%, respectively. All the differences between measurements between the first two weeks and the last two weeks lie within the limits of agreement.

A good agreement can be observed between those two weeks. The relative low mean difference (5.47%) demonstrates similar results on average. However, it be reminded that Bland-Altman assumes that 95% of measurements must be within the limits of agreement, which so, does not mean a total agreement.

Reasonable AIx variability between those two acquisitions was found, which reveals the good AIx repeatability between the two different weeks.

6.2.2 Electrocardiogram analysis

The purpose of the algorithm applied to the ECG was to accurately identify the R-wave, since it is the most common information retrieved from the ECG on hemodynamic studies. Therefore, an algorithm capable to correctly identify the R-wave on the ECG signal, despite all the noise the signal may contain, is desirable.

The ECG can be corrupted by artifacts with both origins, physiological and non-physiological. The most common artifact present or the ECG is due to the power-line interference, which is a sinusoidal wave with a frequency of 50 Hz. Other artifacts present on the ECG signal includes muscle noise, electrode motion, baseline wander and T waves with frequency similar to QRS complexes [26, 78]. In the Figure 42 is possible to see the raw signal acquired through the multichannel platform.

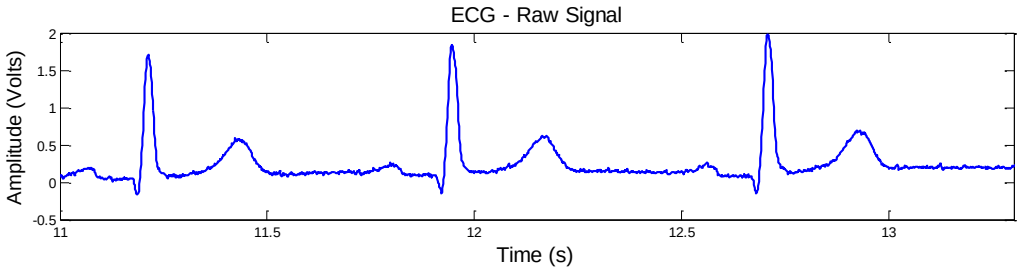

Figure 42 - Raw ECG signal.

The description of the algorithm based on Pan and Tompkins [78] is illustrated in the Figure 43.

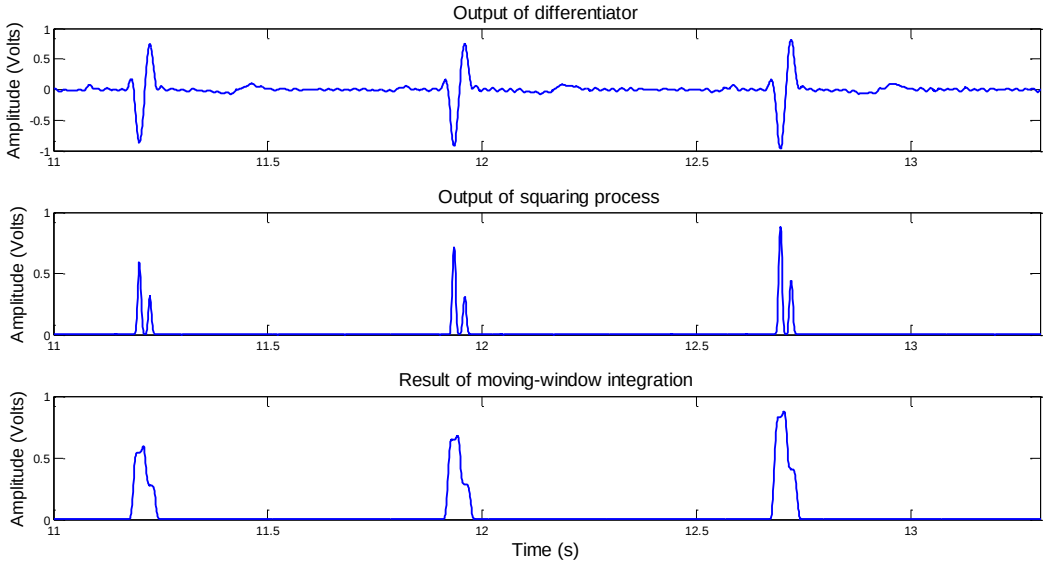

Figure 43- Digital Signal Conditioning.

The application of a band-pass filter with cutoff frequency from 0.25 to 40 Hz on the ECG signal has the goal to reduce the noise caused by muscle, the 50 Hz interference, baseline wander and T-wave interference. The band-pass filter increases the signal-to-noise ratios of the signal. Afterwards, the signal is differentiated providing important information regardless the QRS complex.

The square process emphasizes the high frequencies, in other words, it intensifies the slope of the frequency response of the derivative. This process is fundamental to ensure there is no false positive caused by T waves with high frequency, which have a similar slope as the QRS complex.

The last filter to extract fiducial points is a moving-window integrator. The output of this step gives information about the slope and width of the QRS complex. The QRS complex corresponds is based on the duration of the rising edge (width), allowing to distinguish the peak of the R wave from others maximal slopes [78].

Then the threshold equal to a fraction of the maximum ECG amplitude is applied to the result of the moving-window integration. This threshold identifies the position of the R point. The R point will be the maximum point calculated on the relevant window on the filtered ECG with the moving-window integration.

The Figure 44 is the result of the application of the algorithm to the acquisition represented on the Figure 42.

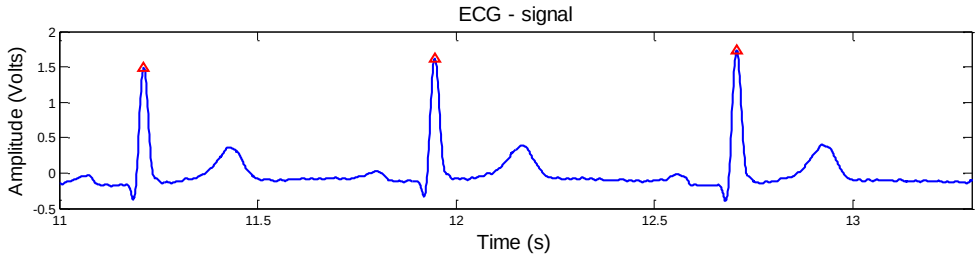

Figure 44 - Example of R wave detection

Nevertheless, before the information by the application of algorithms developed to the ECG signal, an evaluation of the performance of the ECG algorithm must be done. Therefore, the results of the identification of the R waves by the algorithm were visualized and inspected by a human expertise engineer (HEE). When the algorithm correctly calculates the R wave it is classified as true positive (TP), and as false positive (FP) when the algorithm incorrectly identify a R wave. On the other hand, when the algorithm does not identify the R wave in an ECG cycle it is classified as a false negative (FN).

From those values – TP, FP and FN – is possible to determine the sensitivity, positive predicted value or precision rate (P^+) and error of the algorithm by the following equations:

$$Sensitivity = \frac{TP}{TP + FN} \quad \text{Equation 8}$$

$$P^{+} = \frac{TP}{TP + FP} \quad \text{Equation 9}$$

$$error = \frac{FP + FN}{TP + FP} \quad \text{Equation 10}$$

Where sensitivity relates to the algorithm capability to identify the R wave, and precision rate measure the proportion of times the R wave are correctly identify by the algorithm. The Table 8 shows the results obtained for the performance evaluation.

Table 8 - Evaluation of the algorithm to detect R wave on the ECG signal

	N# of cycles	TP	FP	FN	P^{+} (%)	Error (%)	Sensitivity (%)
R wave	3257	3213	42	2	98.71	1.35	99.94

Forty random acquisitions made through the multichannel platform were chosen for the evaluation test. A total of 3257 cycles were within those acquisitions. The present algorithm demonstrates a high sensitivity and precision rate and a low error. This results made on a considerable sample test confirms the good performance of the ECG to retrieve the R wave from the ECG signal. The results obtained are according to the expected since the R-wave is the easier wave to detect. Nevertheless, it is the wave with more importance for hemodynamic studies as mentioned on chapter 5.2.

6.2.3 PPG analysis

In the PPG analysis, it was observed a noise signal. This may be produced by the interference of the second wavelength diode. A solution presented to solve this problem, since it has a similar behavior of a “salt and pepper” noise, is to apply a median filter (Figure 45).

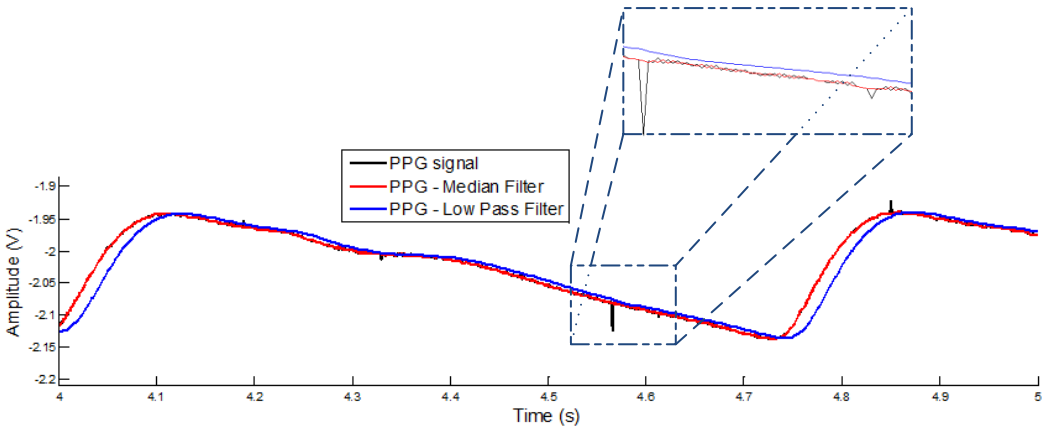

Figure 45 - Comparison of a median filter and a low pass filter

The Figure 45 represents the raw signal PPG after applying a butter low pass filter (LPF) with a cutoff frequency of 30 Hz and a median filter with size 3. Taking a close observation on the figure above is possible to affirm that the suitable choice is the median filter. The median filter perfectly eliminates the noise wanted without distorting the raw signal, while the LPF despite it also eliminates the noise it changes the form of the raw, which it is inconvenient.

Moreover, the raw PPG signal is almost imperceptible, since it relies precisely on the PPG signal filtered by the median filter. This fact suggests the choice the median filter as the most efficient filter to remove this noise.

After removing this precise noise from the signal the application of the processing algorithms can be correctly done.

6.2.3.1 Algorithm for onset, SP and DN detection

As explained on the chapter 5.3.1 the goal of delineator algorithm based on Li et al. [74] is to detect the onset, SP and DN from the PPG. The detection of these points is based on the first order derivative of the PPG signal. In the Figure 46 is possible to observe an example of the application of the delineator to an acquisition measured through the multichannel platform.

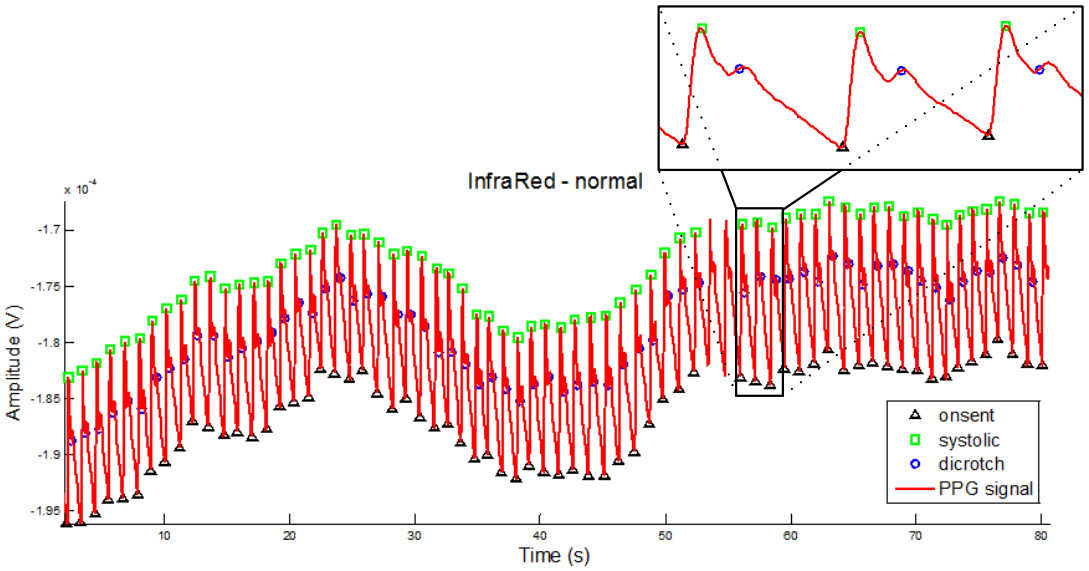

Figure 46 - Example of the waveform analysis based the delineator algorithm presented by Li et al. [74].

By a simple observation of this example, it can be seen the onset represented by black triangles and the SP marked as green squares are correctly identified on this example. However, the DN represented as purple circles does not have such good performance as the identification of the previously onset and SP points. Nevertheless, an evaluation of the performance of the implemented delineator algorithm based on Li et. al [74] is presented on the Table 9.

Table 9 - Evaluation of the algorithm to detect the Onset, SP and DN based on Li et al.

	TP	FP	FN	P^+ (%)	Error (%)	Sensitivity (%)
Onset	1301	20	6	98.50	2.47	99.54
SP	1293	28	6	97.88	2.57	99.54
DN	990	331	6	74.94	25.51	99.40

The procedure of the evaluation was the same as the evaluation for the ECG signal (Table 8). Although, fewer acquisitions were selected to evaluate, it is still a reasonable number for a test sample. A total of 17 random acquisitions, with a total of 1327 pulses, were selected among all the data presented on the database.

The onset and SP detection had similar results. They presented a good accuracy and sensitivity, with a low error. However, the results for DN detection are not as promising as the previous points. The DN detection showed a error more than 25%, which is relative high value.

Therefore, improvements of the detection of the DN must be done. Nonetheless, this point (DN) has only importance for subjects with heart valve diseases.

6.2.3.2 Second derivative of the finger photoplethysmograph

Takazawa et al. studied which application could the SDPTG waveform have in clinical areas. It was confirmed the useful of SDPTG to evaluate the vascular aging [82].

The Figure 47 represents the application of the algorithm explained on the chapter 5.3.2 to PPG signal. Two graphics can be observed. In the first graphic is the PPG signal, while the second graphic is the SDPTG of the first graphic, where five waves (A,B,C and D waves) are detected.

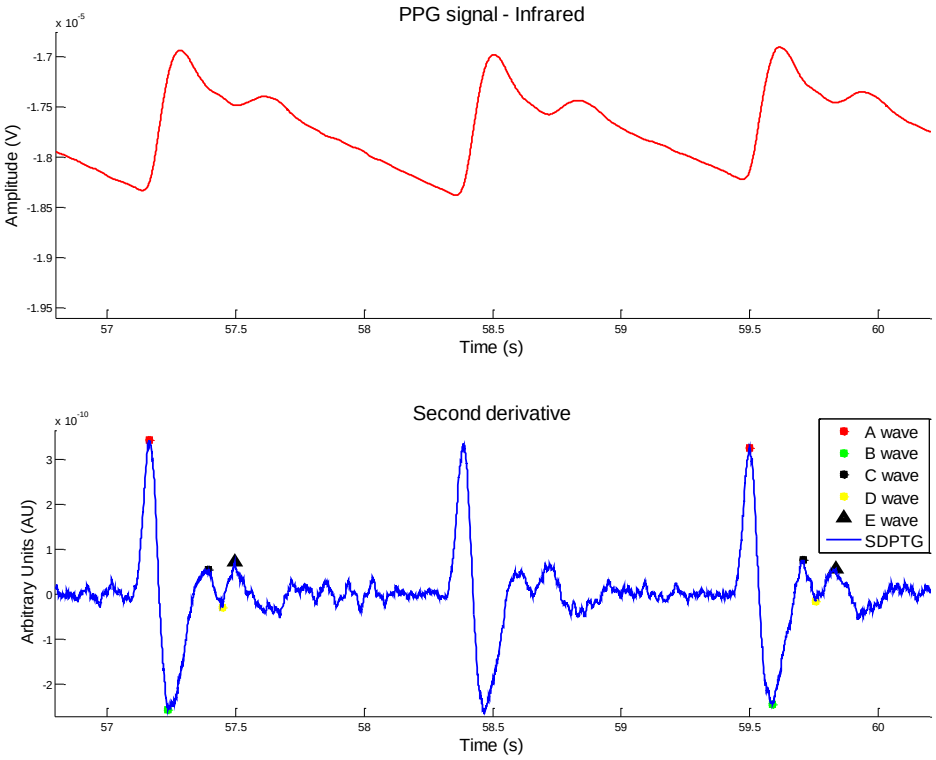

Figure 47 - Second Derivative of PPG and A,B,C,D,E waves.

These five waves characterize the contour of the SDPTG waveform. The identification all of those points is fundamental to analyze the SDTPG waveform. Thus, the algorithm only saves the pulses, where all five waves are identified. In the Figure 47 are represented three pulses, where on the second pulse the algorithm had skip it, because it did not detect all the fives within that interval.

After all waves are detected, the weight ratios of all waves respective to the A wave are calculated and saved.

6.3 Inter-signals Studies

This sub-section will reveal two performed studies. These two studies have as goal to use more than one signal acquired through the multichannel platform and to retrieve some clinical value from them.

6.3.1 Heart Rate Variability

The heart rate variability (HRV) is an indicative of the automatic regulation of the heart rate (HR). Currently, the main method to extract the HRV signal is to acquire the ECG signal and apply an appropriate QRS detection algorithm to locate the R wave and its peak, and thereby find the RR intervals (RRI). However, the ECG signals has methodological problems to record and analyze, which motivated a search of alternative methods to measure the HRV. Recent studies have suggested the possibility to use the PPG signal as a surrogate of the ECG to determine the HRV, since it also reflects the cardiac rhythm. The peak-to-peak interval (PPI) variability was showed a high correlation with the RRI of the signal [75-77].

The Figure 48 shows how the RRI and PPI are extracted from the ECG and PPG signals, respectively.

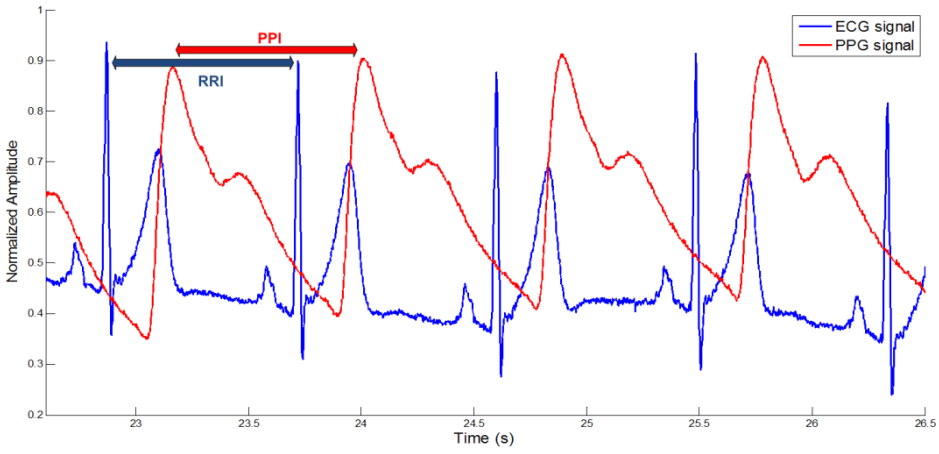

Figure 48 - Cardiac beat-to-beat interval extracted from PPG and ECG signals. RRI - R-R intervals, PPI P-P intervals.

To prove the feasibility of the PPG to measure the HRV the PPI values from PPG and RRI values from ECG were compared. For this study one hundred and twenty five different

acquisition (n=125), with a total of 10312 beats, were used as the sample test. The HRV is determined by the RRI from ECG, while the pulse pressure variability (PPV) was determined by the PPI from the PPG.

Firstly, it was applied the algorithm on the data in order to get the R points on the ECG and the SP on the PPG. Even though, the SP and R wave detection had a good accuracy (Table 8 and Table 9), it is vital to ensure that all the points are being properly detected by the algorithms, since any false points (FN or FP) can corrupt the results. Thus, all of the RRI and PPI time series underwent with an initial automated editing process before a careful manual editing performed by visual inspection.

6.3.1.1 Correlation Studies

On this chapter it is presented two different approaches: a time domain analysis and a non-linear analysis.

6.3.1.1.1 Time-domain analysis

Regarding the time domain of the HRV and the PPV, it is calculated four different parameters:

- the mean interpulse interval (mean NN) - Figure 49;
- the standard deviation of the interpulse intervals (SDNN) - Figure 50;
- the square root of the mean squared differences of successive interpulse intervals (MRSSD) - Figure 51;
- and finally, the proportion of difference of successive interpulse intervals which exceeds the 50 ms, also known as pNN50 - Figure 52.

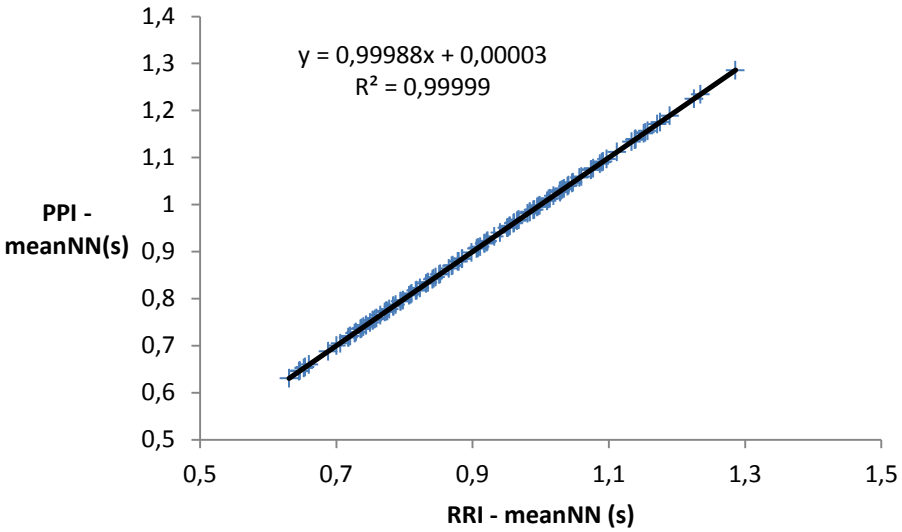

Figure 49 - Time domain regression analysis of the average of RRIs and PPIs.

The average of PPI and RRI shows a high correlation coefficient, close to a 1 (r=0.99). As we can see from the equation it has a proportion of almost 1:1, which is the expected. On the figure it is perceptible a large quantity of points within a small area, endures high correlations between the two variables.

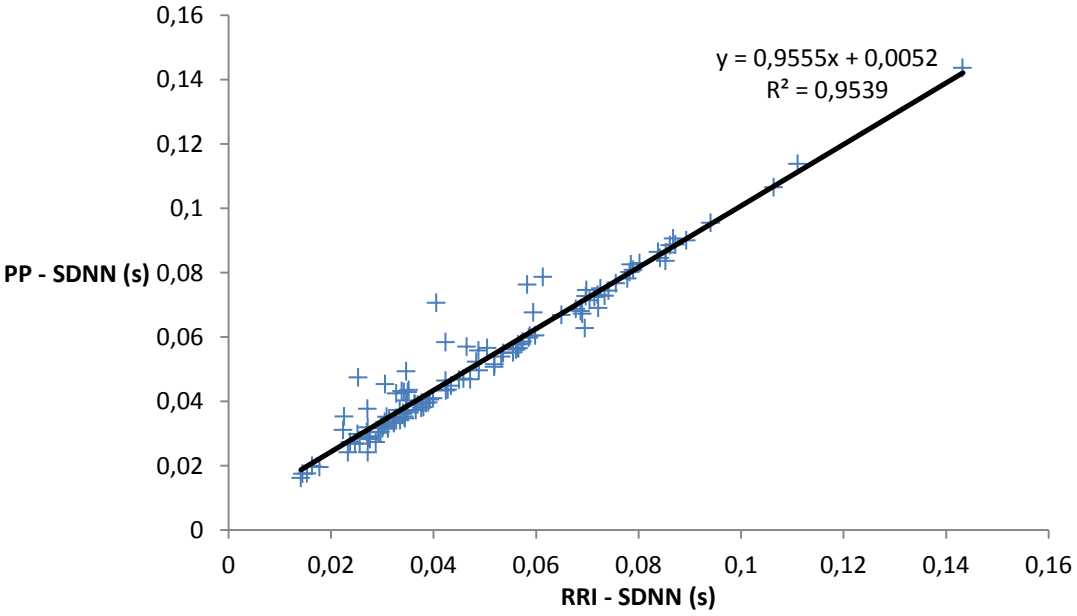

Figure 50 - Time domain regression analysis of the standard deviation of the NN from RRIs and PPIs.

As the previously correlation, the SDNN between the RRI and PPI has a slight lower coefficient, but still high (r=0.9555). Nevertheless, it is possible to see some discrepancies mainly for low standard deviations (0.02-0.06 seconds). Those differences can have some influence by deviations of the algorithms.

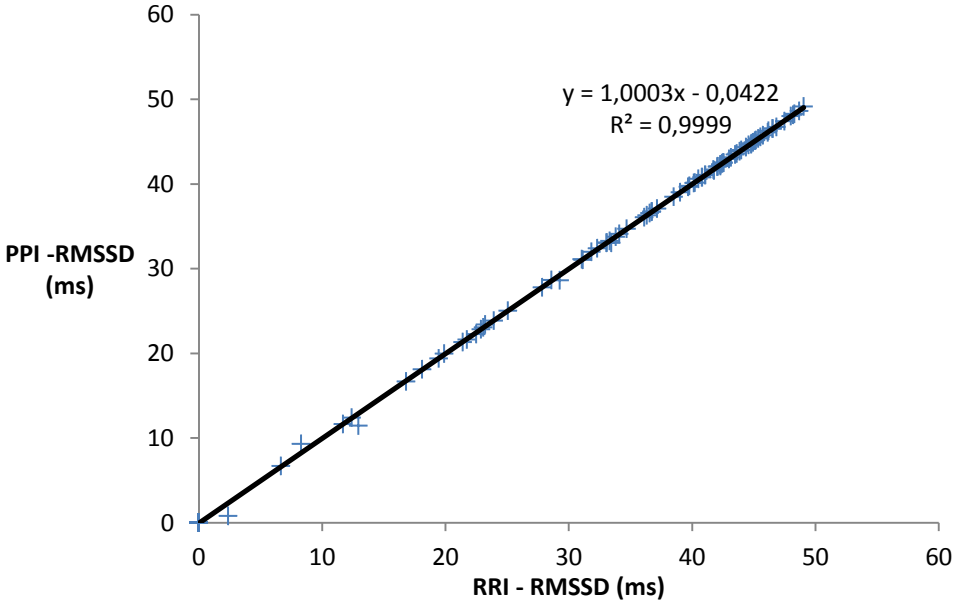

Figure 51 - Time domain regression of the RMSSD of RRIs and PPIs.

As is the case of average of the RRI and PPI, the RMSSD between the RRI and PPI also has a strongly coefficient correlation of r =0.9999.

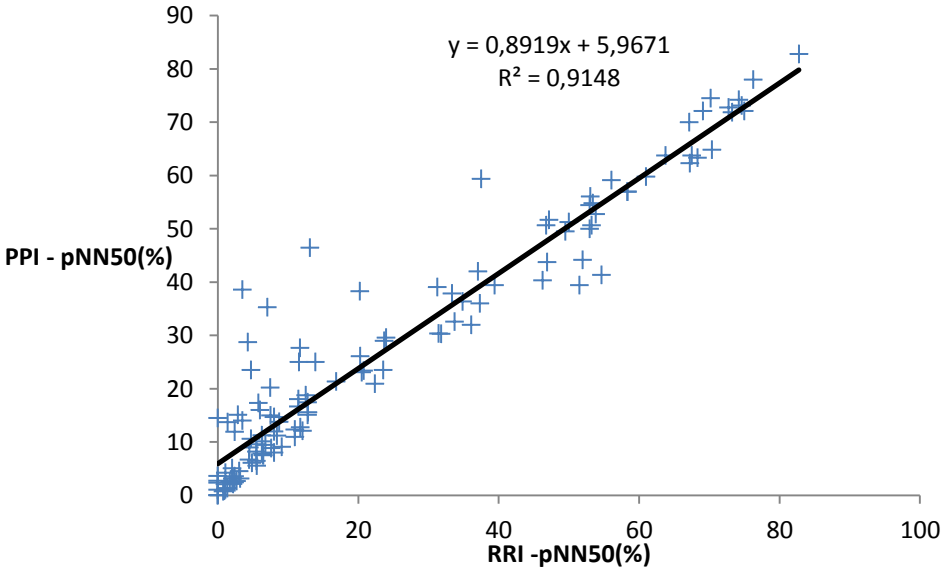

Figure 52 - Time domain linear regression analysis of pRR50 of RRIs and PPIs.

The last study in time domain is the pNN50(%). The pNN50(%) is obtained counting the number of successive NN differences which exceeds the 50 ms, and then divide that number from the total number of intervals on that acquisition. The coefficient correlation of pNN50(%) between the RRIs and the PPIs is the lowest from all the time domain parameters (r= 0.9148). Nevertheless, it is still considerable a good correlation between the pNN50(%) derived from the PPG and from the ECG.

While is a great source of error. Because the acquisition times are relatively low, small differences in the PPG and ECG has big impact on the overall of the sample, because it represents a larger proportion than if the time acquisition were longer. The time duration of 90 seconds per acquisition was chosen, because it set as a good time for CVD analysis. However, for HRV analysis longer duration should be done. Nevertheless, the results obtained were good.

6.3.1.1.2 - Non-linar analysis – Poincaré plot

One of the most used technique for nonlinear HRV analysis is the Poincaré plot. It is obtained by simply plot each intervals against the previously one. The Figure 53 and Figure 54 represent the Poincaré Plot derived by the HRV and the PPV, respectively.

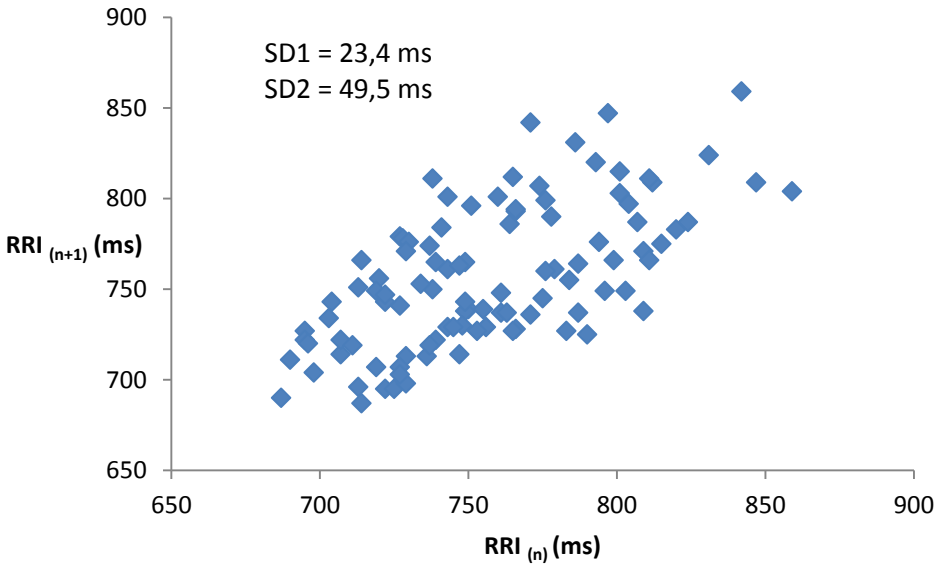

Figure 53 - HRV Poincaré plot from one subject.

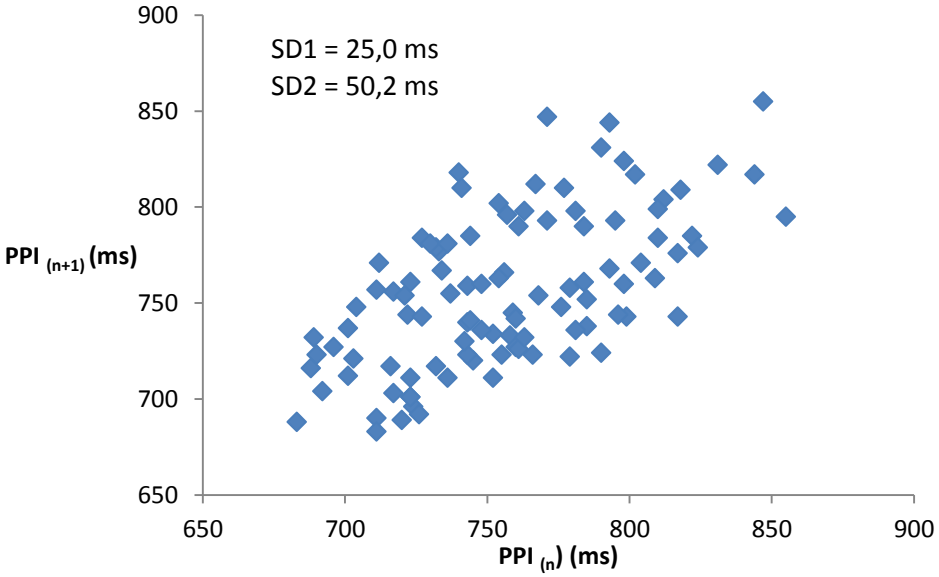

Figure 54 - PPV Poincaré plot from one subject.

From this plot two nonlinear parameters can be extracted the short term beat-to-beat variability (SD1) and the long term beat-to-beat variability (SD2). SD1 is the standard deviation of projection of the Poincaré plot on the line perpendicular to the line identify (y=-x), while SD2 is the standard deviation of the Poincaré plot on the line of identify (y=x) [86].

Figure 55 and Figure 56 shows the correlation between the SD1 and SD2 retrieved by the HRV and PPV.

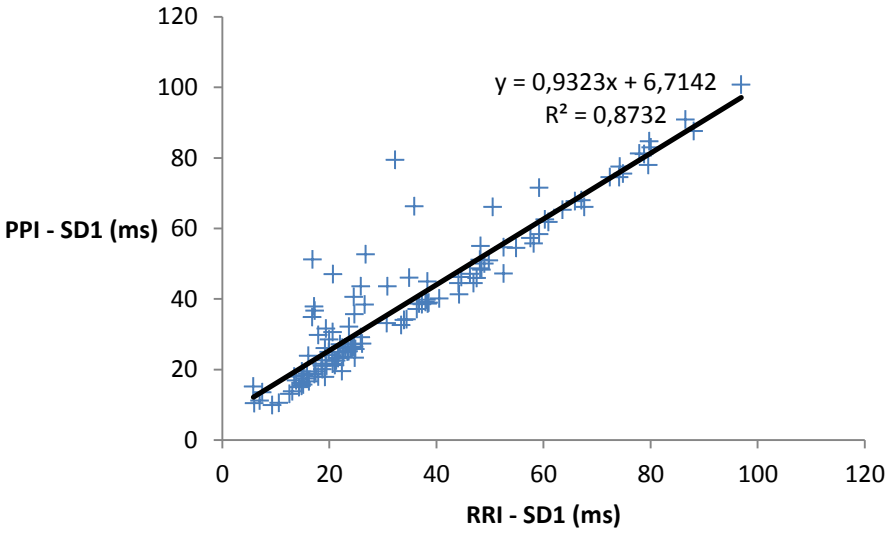

Figure 55 - Linear regression of SD1 from Poncaré plot derived from RRI and PPI.

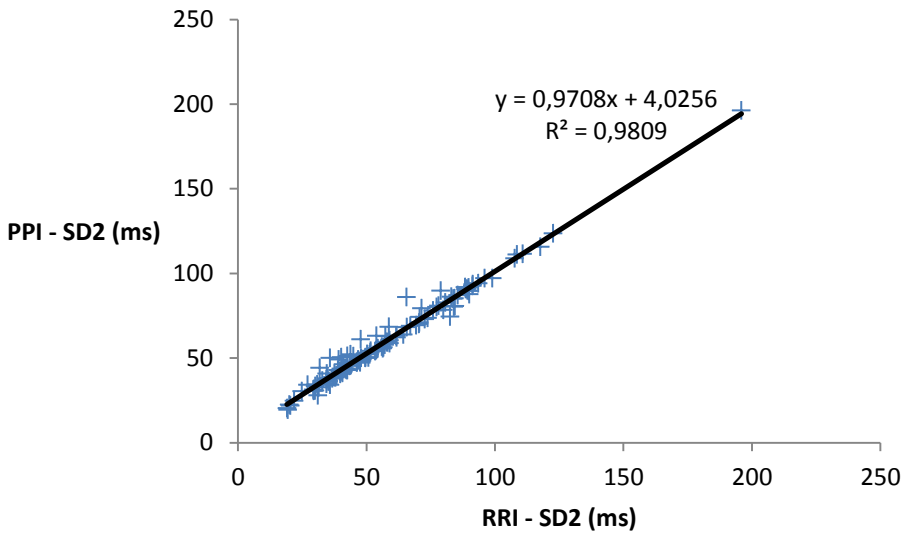

Figure 56 - Linear regression of SD2 from Poncaré plot derived from RRI and PPI.

A high correlation coefficient is observed between the HRV and the PPV for the nonlinear parameters SD2 (r=0.9809), while a lower correlation coefficient is seen for the SD1 parameter (r=0.8732). In the Figure 55 it can be clearly be seen some points with a big discrepancy to the regression line. This fact can be explained by the existence of some imprecision on the detection of the R and the SP. These fluctuations from the algorithm have bigger influence in short beats. This theory is endorsed by the result of SDNN showed on Figure 50.

On the other hand, the SD2 which represents the long term beat-to-beat variability derived by the PPG and ECG does not have the same problem, since some small imprecisions of the algorithms is very small relative to duration of the pulse.

6.3.1.2 Agreement assessments – Bland-Altmand tests

On this section it will be showed the results of the Bland-Altman plots about the NN and the SD ratio. The limits are considered to be 1.96 of the standard deviation of differences between the two samples, which corresponds to a confidence agreement of 95%.

Figure 57 displays a Bland – Altmand of NN intervals extracted from the ECG and the PPG.

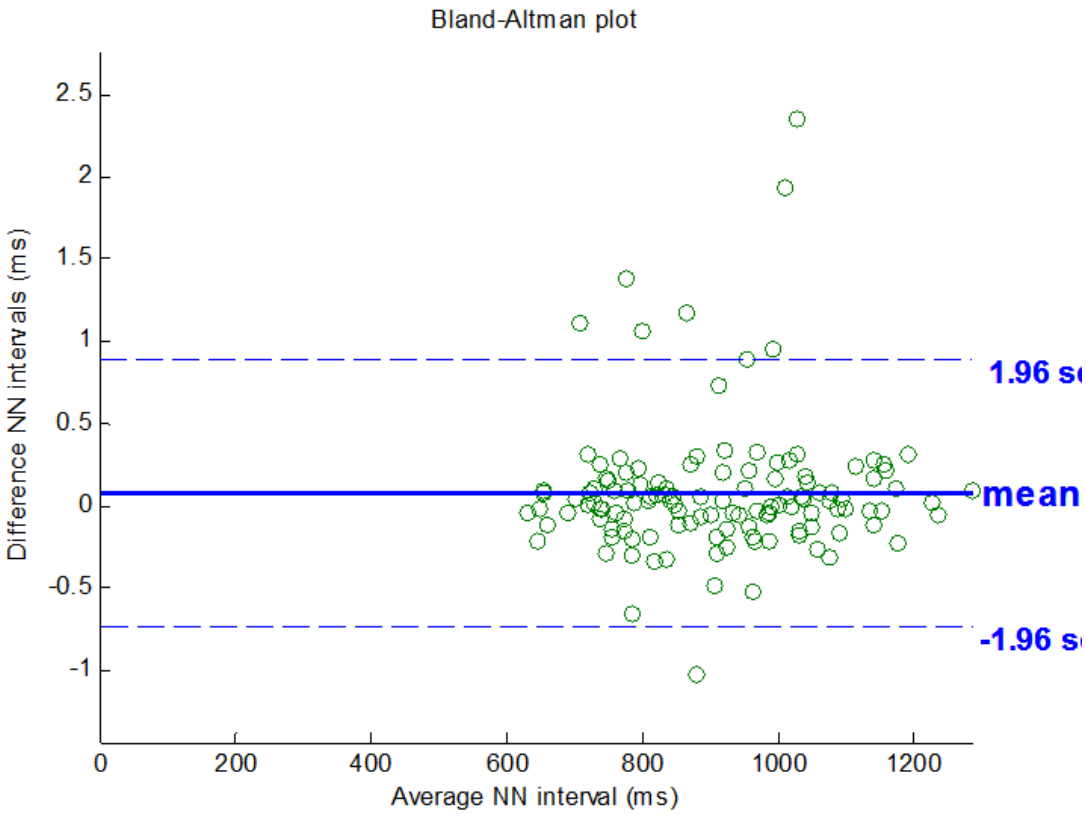

Figure 57 - Bland-Altman agreement analysis between NN from ECG and PPG.

The mean difference from the NN intervals showed was 0.0835% with the upper and lower limits of 0.892 % and -0.725% respectively. The difference between NN intervals derived by the PPG and the ECG presented low mean difference value (0.0835), which does not have clinical significance. The explanation can by the different nature of the ECG and PPG.

Only nine out of one hundred and twenty-five (7.2%) of the differences between measurements does not lie within the limits of agreement, which represents a relatively good agreement between the NN differences. No patterns can be visualized, and variability is consistent.

One reported non-linear parameter commonly extracted by the Poincaré plot for HRV analysis is the ratio between SD1 and SD2, denominated as SD ratio [86]. Figure 58 displays a Bland-Altman of the differences of SD ratios derived from PPG and ECG.

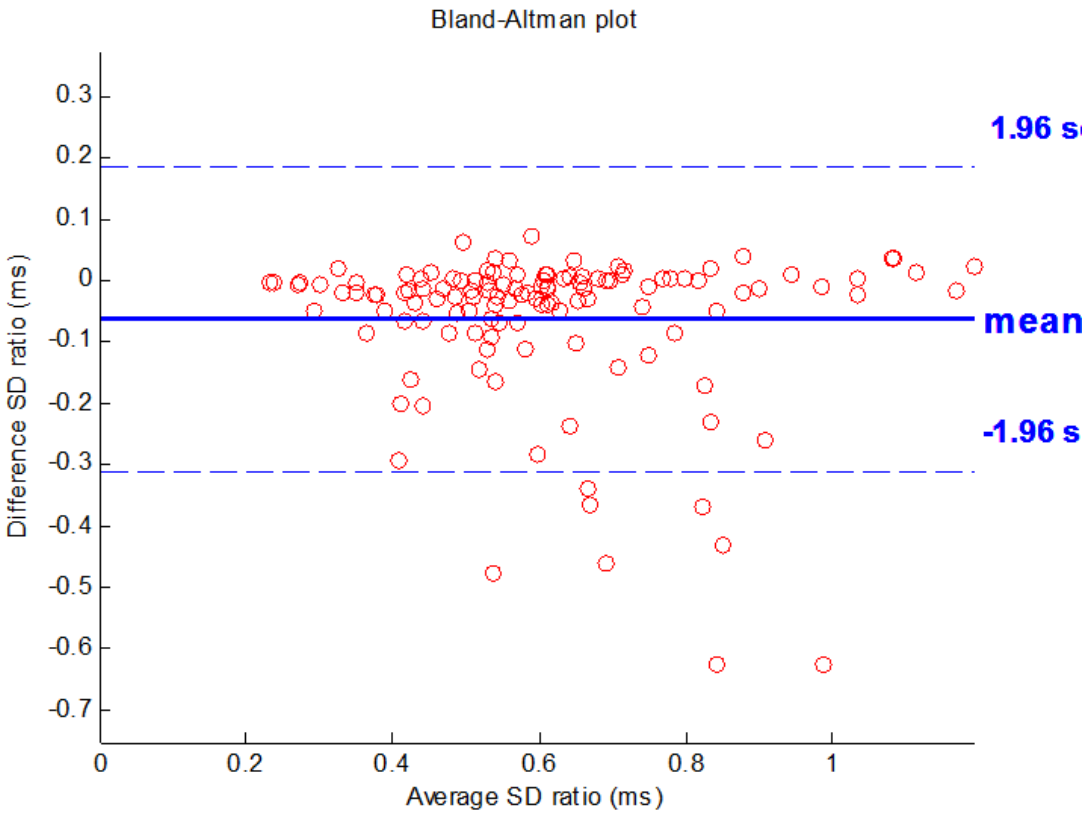

Figure 58 - Bland-Altman analysis between SD ratios derived from ECG and PPG.

The mean difference is of -0.0634% and the upper and lower limits are 0.184% and 0.311% respectively.

The differences between the two measurements, which lie within the limits of agreement is 92,8% of those differences. All the differences out of the limit are under the low limit of agreement.

6.3.1.3 Discussion of HRV

Both Bland-Altman plots (Figure 57 and Figure 58) show a low mean difference (6.34% and 8.35%) which indicates small discrepancies between the parameters extracted from the PPG and ECG. Moreover, the two Bland-Altman plots revealed a relative agreement between the two measurements of the NN intervals and the SD ratios with 92.8% of differences in both plots within the limits of agreements. This 92.8% of the differences is related to 95% of agreement, since the Bland – Altman assumes this value as the percentage of measurements which must be within to calculate his limits.

On both studies there is the same number of points outside of the range, which can suggest about the reliability of those acquisitions which could have been included by mistake into the sample test. If it is the case, it has decreased the level of agreement, which is still high, but it should be in fact bigger.

Nevertheless, a relative good agreement between the differences measurements of the NN intervals and the SD ratios is present on the Bland-Altman plots. Furthermore, the time domain and non-linear (Poincaré plot) parameters showed highs correlations coefficients, some of them almost 1. These results confirm fact the HRV can be reliably estimated from the PPG based on the PP intervals (PPV) in healthy subjects at rest, as some studies have already reported [75-77].

In order to ensure the PPG has valid method to measure the HRV, more studies need to me performed, since all this studies have been done in controlled ambient and only healthy subjects at rest. The correlation between HRV parameters derived from the ECG and PPG should be done with a wide range of age and with different healthy conditions. As the PPG measures the oscillations in blood volume at peripheral arteries, they are delayed in relation to the ECG. This delay depends on velocity which the flow blood takes from the heart to the recorded placed (TT). However, PTT shows beat-to-beat variations, which can be a great source of error in the measurement of the pulse intervals, and thereby can influence the HRV parameters derived by the PPG [87]. Nevertheless, the PTT variation is minimal in healthy subjects at rest, and thus, makes the measurement of HRV parameters reliable under these conditions, as suggested by the obtained results. More studies must be carried out in different conditions to evaluate the feasible to use the PPV as a surrogate of the HRV.

This method to measure the HRV has an important clinical value, since the PPG waveform can be easily recorded form the finger and will allow to avoid all the procedures needed to place the electrodes when an ECG is recorded. Moreover, PPG besides being very easy to record, it is also comfortable to the patient and thereby is suitable for long term studies.

PPG is very sensible to motion artifacts. However, an integration of accelerometers into the PPG enables to quantify the displacement of the sensor during the acquisition, and thus correct the PPG signal. This couple with the variety of signals which can be extracted from the PPG, such as blood oxygenation, ventilator rate and vascular assessments, makes it an ideal sensor for ambulatory acquisitions.

6.3.2 SDPTG for arterial stiffness assessment

Arterial stiffness can be assessed by the PPG using the second derivative of the finger photoplethysmograph (SDPTG) [79, 81, 88]. From all the ratio derived by this method D/A has the highest coefficient of correlation with the arterial stiffness index [88].

AIx retrieved from the APW also gives important information about arterial stiffness condition, where positive AIx values are associated with essential hypertension.

A comparison was performed for each subject between the AIx and D/A values derived from the APW and PPG, respectively. Nevertheless, no conclusive results were obtained from our test group. The reason which can explain this fact is the presence of a very homogeneous group of test and due to the variability of the AIx derived from the APW.

Nevertheless, the mean values obtained for D/A on the eighteen subjects for a total of 79 different acquisitions was -0.21 which is in accordance to values in literature [81]. This suggests the values of D/A derived from the SDPTG were correctly extracted by the algorithm described on chapter 5.3.2 (Figure 36).

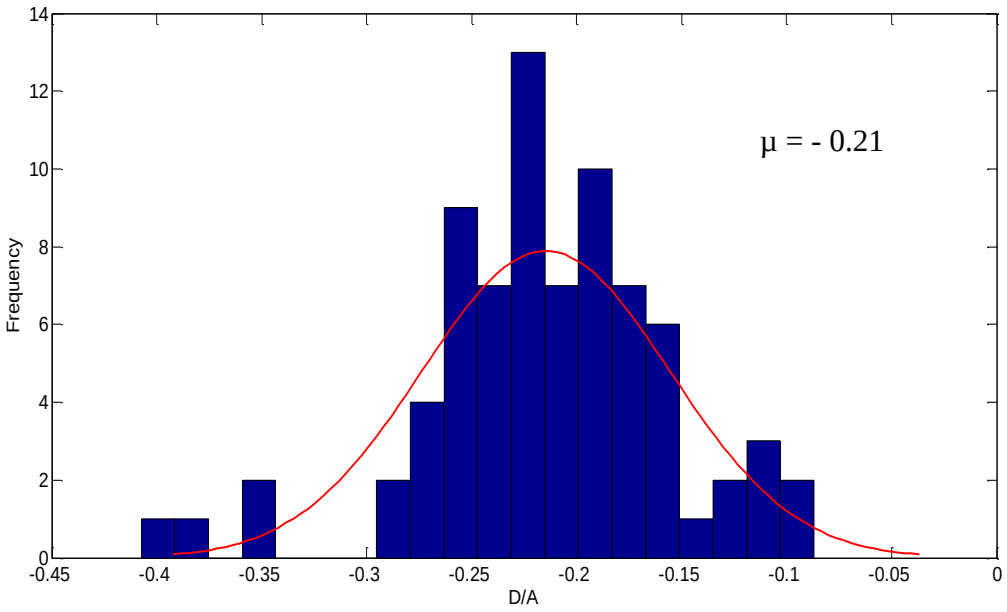

Figure 59 - Histogram with Gaussian of D/A values for the 79 acquisitions.

7. Conclusion and Future Work

7.1 Conclusion

The main goal of this thesis was the development of a DAQ software able to display and save all current modules present on the multichannel platform. The developed GUI was incorporated into a database – *Cardiocheck* – enabling an easy storage and management of all the data acquired through the multichannel platform and also general information about the subjects. The database also has general information about the subject, which may be important for the development of new methods of diagnosis. An additional synchronization signal was added to the multichannel platform due to the existence of two DAQs.

All acquired signals through the multichannel platform are in same time reference. Therefore, comparison between information about one parameter from different signals can be done. For example, it can be compared information for vascular aging assessment through the PPG and the APW.

The processing tools previously developed for the APW signals – APW Pulse Analyzer Module - were implemented in the GUI of the multichannel platform, allowing to check the quality of the APW signals at the time of the acquisition. An update was done to the APW Pulse Analyzer Module to communicate to the database and extract important information regarding the subject, once a file is selected for analysis.

An algorithm for the ECG analysis and a delineator algorithm for the PPG signal were also implemented and tested on the signals acquired. Both algorithms showed to be efficient in detecting the R wave in the case of the ECG signal, and the onset and the SP for the PPG signal. Improvements still need to be done to detect the DN, since it was verified a relative high error.

A new method for the analysis of PPG based on SDPTG was developed and implemented. However, since the acquired group of volunteers had very homogenous parameters, no relevant studies could be done in order to reveal the potential of this method.

A study performed to the use of PPV derived from the PPG as a surrogate of the ECG for HRV assessment, showed promising results at least for conditions equal to the acquisitions made. This relationship between the PPV and the HRV is in accordance to the literature, which validates the ECG and PPG acquired through the multichannel platform.

In the repeatability tests for the APW the Bland – Altman plots showed good agreement between weeks.

7.2 Future Work

It is crucial to develop a single GUI gathering all the tools and algorithms in order to retrieve important hemodynamic parameters from the signals present on the multichannel platform. This improvement will enable the extraction of hemodynamic parameters from the data present on the database in an easy, simple and reproducible way. Moreover, the automatic extraction of general information regarding the subject can be done through the implementation of the feature of communication with the database.

The enlargement of the current database is of high priority. The acquisition should be done at a large scale with a wide range of ages and different CVD conditions.

The development of a new algorithm to measure the AIx derived from the PPG should also be of interest. Then, comparison trials from the augmentation index derived both by the PPG and APW with results from a "gold-standard" device to evaluate and demonstrate the reliability of the PPG and APW.

Study the vascular aging assessment through different hemodynamic parameters, such as the SDPTG aging index, the AIx and the PWV.

Perform the same studies carried out to evaluate the PPG as a surrogate of the ECG for HRV assessment under different conditions. Test the reliability to use the PPG for HRV assessment in ambulatory cases will avoid all the methodologies to setup the ECG.

An exhaustive data mining with all hemodynamic parameters should be done with the purpose of studying new classification algorithms in order to find new diagnosis methods of the early detection of cardiovascular complications.

8. References

1. Mendis, S., P. Puska, and B. Norrving, *Global atlas on cardiovascular disease prevention and control*. 2011: World Health Organization.

2. Franklin, S., *Blood pressure and cardiovascular disease: what remains to be achieved?* Journal of hypertension. Supplement: official journal of the International Society of Hypertension, 2001. **19**(3): p. S3.

3. Arnett, D.K., G.W. Evans, and W.A. Riley, *Arterial stiffness: a new cardiovascular risk factor?* Am J Epidemiol, 1994. **140**(8): p. 669-82.

4. Weber, T., et al., *Arterial stiffness, wave reflections, and the risk of coronary artery disease.* Circulation, 2004. **109**(2): p. 184-9.

5. Mattace-Raso, F.U., et al., *Arterial stiffness and risk of coronary heart disease and stroke: the Rotterdam Study.* Circulation, 2006. **113**(5): p. 657-63.

6. Laurent, S., et al., *Aortic stiffness is an independent predictor of all-cause and cardiovascular mortality in hypertensive patients.* Hypertension, 2001. **37**(5): p. 1236-1241.

7. Boutouyrie, P., et al., *Aortic stiffness is an independent predictor of primary coronary events in hypertensive patients a longitudinal study.* Hypertension, 2002. **39**(1): p. 10-15.

8. Blacher, J., et al., *Carotid arterial stiffness as a predictor of cardiovascular and all-cause mortality in end-stage renal disease.* Hypertension, 1998. **32**(3): p. 570-574.

9. Laurent, S., et al., *Expert consensus document on arterial stiffness: methodological issues and clinical applications.* Eur Heart J, 2006. **27**(21): p. 2588-605.

10. Blacher, J., et al., *Impact of aortic stiffness on survival in end-stage renal disease.* Circulation, 1999. **99**(18): p. 2434-9.

11. Meaume, S., et al., *Aortic pulse wave velocity predicts cardiovascular mortality in subjects >70 years of age.* Arterioscler Thromb Vasc Biol, 2001. **21**(12): p. 2046-50.

12. Laurent, S., et al., *Aortic stiffness is an independent predictor of fatal stroke in essential hypertension.* Stroke, 2003. **34**(5): p. 1203-1206.

13. McLaughlin, J., et al., *Piezoelectric sensor determination of arterial pulse wave velocity.* Physiol Meas, 2003. **24**(3): p. 693-702.

14. Pereira, H.C., et al., *Characterization of a double probe for local pulse wave velocity assessment.* Physiological Measurement, 2010. **31**(11): p. 1449.

15. Pereira, H.C., et al. *Double Headed Probe for Local Pulse Wave Velocity Estimation-A New Device for Hemodynamic Parameters Assessment*. in *BIODEVICES*. 2011.

16. Almeida, V., et al., *Piezoelectric probe for pressure waveform estimation in flexible tubes and its application to the cardiovascular system.* Sensors and Actuators A: Physical, 2011. **169**(1): p. 217-226.

17. Almeida, V., et al. *A cardiac signal monitoring and processing system*. in *Bioengineering (ENBENG), 2011. ENBENG 2011. 1st Portuguese Meeting in*. 2011. IEEE.

18. Santos, P., et al. *Photoplethysmographic logger with contact force and hydrostatic pressure monitoring*. in *Bioengineering (ENBENG), 2013 IEEE 3rd Portuguese Meeting in*. 2013. IEEE.

19. Allen, J., *Photoplethysmography and its application in clinical physiological measurement.* Physiological measurement, 2007. **28**(3): p. R1.

20. Clemente, F., P. Arpaia, and P. Cimmino, *A piezo-film-based measurement system for global haemodynamic assessment.* Physiol Meas, 2010. **31**(5): p. 697-714.

21. Ferreira, E.S.B., *Assessment of hemodynamic parameters.* 2008.

22. Vieira, J.A.P., *Algorithmo development for physiological signals analysis and cardiovascular disease diagnosis-a data mining approach.* 2011.

23. Almeida, V., et al. *Hemodynamic Features Extraction from a New Arterial Pressure Waveform Probe*. in *BIOSIGNALS*. 2011.

24. Relvas, V.P.S., *Hemodynamic parameters assessment: Characterization of a new piezoectric probe.* 2011.

25. Santos, P., *Photoplethysmographic logger with contact force and hydrostatic pressure monitoring, Universidade de Coimbra, Setembro 2009.*

26. Bronzino, J.D., *The biomedical engineering handbook. 2*. Vol. 2. 2000: CRC press.

27. http://www.texasheartinstitute.org/HIC/Anatomy/anatomy2.cfm, *accessed on 1st August 2013.*

28. Publishing, B.E. and K. Rogers, *The Cardiovascular System*. 2010: Britannica Educational Pub.

29. Standring, S., *Gray's Anatomy: The Anatomical Basis of Clinical Practice*. 2008: Elsevier Health Sciences UK.

30. http://www.texasheartinstitute.org/HIC/Anatomy/head.cfm, *accessed on 1st August 2013.*

31. Nichols, W.W. and M.F. O'Rourke, *McDonald's blood flow in arteries: theoretical, experimental, and clinical principles*. 2011: CRC Press.

32. Cheung, Y.F., *Arterial stiffness in the young: assessment, determinants, and implications.* Korean Circ J, 2010. **40**(4): p. 153-62.

33. Schiffrin, E.L., *Vascular stiffening and arterial compliance. Implications for systolic blood pressure.* Am J Hypertens, 2004. **17**(12 Pt 2): p. 39S-48S.

34. http://www.clinsci.org/cs/116/0273/cs1160273f02.gif, *accessed on 8th August 2013.*

35. Nemes, A., et al., *Obesity is associated with aortic enlargement and increased stiffness: an echocardiographic study.* The international journal of cardiovascular imaging, 2008. **24**(2): p. 165-171.

36. Nichols, W.W., *Clinical measurement of arterial stiffness obtained from noninvasive pressure waveforms.* American Journal of Hypertension, 2005. **18**: p. 3S-10S.

37. Mackenzie, I.S., I.B. Wilkinson, and J.R. Cockcroft, *Assessment of arterial stiffness in clinical practice.* QJM, 2002. **95**(2): p. 67-74.

38. Avolio, A.P., M. Butlin, and A. Walsh, *Arterial blood pressure measurement and pulse wave analysis—their role in enhancing cardiovascular assessment.* Physiological measurement, 2010. **31**(1): p. R1.

39. Almeida, V.M.G.d., *Hemodynamic parameters assessment: an improvement of methodologies.* 2009.

40. Segers, P., et al., *Limitations and pitfalls of non-invasive measurement of arterial pressure wave reflections and pulse wave velocity.* Artery Research, 2009. **3**(2): p. 79-88.

41. O'Rourke, M.F., et al., *Clinical applications of arterial stiffness; definitions and reference values.* Am J Hypertens, 2002. **15**(5): p. 426-44.

42. Van Bortel, L.M., S.J. Vermeersch, and P. Segers, *Arterial waveform and central blood pressure: the complex links between large and small arteries.* Artery Research, 2010. **4**(4): p. 118-121.

43. Murgo, J.P., et al., *Aortic input impedance in normal man: relationship to pressure wave forms.* Circulation, 1980. **62**(1): p. 105-16.

44. London, G.M., et al., *Arterial wave reflections and survival in end-stage renal failure.* Hypertension, 2001. **38**(3): p. 434-8.

45. Franklin, S.S., et al., *Hemodynamic patterns of age-related changes in blood pressure. The Framingham Heart Study.* Circulation, 1997. **96**(1): p. 308-15.

46. Franklin, S.S., et al., *Does the relation of blood pressure to coronary heart disease risk change with aging? The Framingham Heart Study.* Circulation, 2001. **103**(9): p. 1245-1249.

47. Hirata, K., M. Kawakami, and M.F. O'Rourke, *Pulse wave analysis and pulse wave velocity: a review of blood pressure interpretation 100 years after Korotkov.* Circ J, 2006. **70**(10): p. 1231-9.

48. Kohara, K., et al., *Effect of reflection of arterial pressure on carotid circulation in essential hypertension.* Am J Hypertens, 1999. **12**(10 Pt 1): p. 1015-20.

49. Nürnberger, J., et al., *Augmentation index is associated with cardiovascular risk.* Journal of hypertension, 2002. **20**(12): p. 2407-2414.

50. Lemogoum, D., et al., *Validity of pulse pressure and augmentation index as surrogate measures of arterial stiffness during beta-adrenergic stimulation.* Journal of hypertension, 2004. **22**(3): p. 511-517.

51. Williams, B. and P.S. Lacy, *Impact of Heart Rate on Central Aortic Pressures and HemodynamicsAnalysis From the CAFE (Conduit Artery Function Evaluation) Study: CAFE-Heart Rate.* Journal of the American College of Cardiology, 2009. **54**(8): p. 705-713.

52. Kelly, R., et al., *Noninvasive determination of age-related changes in the human arterial pulse.* Circulation, 1989. **80**(6): p. 1652-9.

53. Cameron, J.D., B.P. McGrath, and A.M. Dart, *Use of radial artery applanation tonometry and a generalized transfer function to determine aortic pressure augmentation in subjects with treated hypertension.* Journal of the American College of Cardiology, 1998. **32**(5): p. 1214-1220.

54. Oliver, J.J. and D.J. Webb, *Noninvasive assessment of arterial stiffness and risk of atherosclerotic events.* Arterioscler Thromb Vasc Biol, 2003. **23**(4): p. 554-66.

55. Lee, H.Y. and B.H. Oh, *Aging and arterial stiffness.* Circ J, 2010. **74**(11): p. 2257-62.

56. Boutouyrie, P., et al., *Assessment of pulse wave velocity.* Artery Research, 2009. **3**(1): p. 3-8.

57. Hansen, T.W., et al., *Prognostic value of aortic pulse wave velocity as index of arterial stiffness in the general population.* Circulation, 2006. **113**(5): p. 664-670.

58. Korteweg, D., *Ueber die Fortpflanzungsgeschwindigkeit des Schalles in elastischen Röhren.* Annalen der Physik, 1878. **241**(12): p. 525-542.

59. Bramwell, J.C. and A.V. Hill, *The velocity of the pulse wave in man.* Proceedings of the Royal Society of London. Series B, Containing Papers of a Biological Character, 1922. **93**(652): p. 298-306.

60. Blacher, J., et al., *Aortic pulse wave velocity as a marker of cardiovascular risk in hypertensive patients.* Hypertension, 1999. **33**(5): p. 1111-1117.

61. Solà, J., S.F. Rimoldi, and Y. Allemann, *Ambulatory monitoring of the cardiovascular system: the role of pulse wave velocity.* New Developments in Biomedical Engineering, 2010: p. 391-424.

62. Hermeling, E., et al., *Measurement of local pulse wave velocity: effects of signal processing on precision.* Ultrasound in medicine & biology, 2007. **33**(5): p. 774-781.

63. Rabben, S.I., et al., *An ultrasound-based method for determining pulse wave velocity in superficial arteries.* J Biomech, 2004. **37**(10): p. 1615-22.

64. Allen, J., *Photoplethysmography and its application in clinical physiological measurement.* Physiol Meas, 2007. **28**(3): p. R1-39.

65. Reisner, A.T., G.D. Clifford, and R.G. Mark, *The physiological basis of the electrocardiogram.* 2007.

66. Wnek, G.E. and G.L. Bowlin, *Encyclopedia of Biomaterials and Biomedical Engineering*. 2008: Informa Healthcare USA.

67. http://www.biopac.com/disposable-electrode-100, *accessed on 6th August 2013.*

68. 6210, D.s.N.-U., *http://sine.ni.com/nips/cds/print/p/lang/pt/nid/203223*.

69. http://www.medicine.mcgill.ca/physio/vlab/cardio/setup.htm, *accessed on 10th August 2013.*

70. PRODUCT SHEET Biopac® Systems, I., *http://www.biopac.com/Product_Spec_PDF/EL500%20Series.pdf*.

71. Santos, P., *Development of a database - Cardiocheck - report , 2013.*

72. Borba, J., *Validation of non – invasive electromechanical sensors for cardiac monitoring, Universidade de Coimbra, 2012.*

73. Vieira, J., *Algorithm development for physiological signals analysis and cardiovascular disease diagnosis – A data mining approach, Universidade de Coimbra, 2011;.*

74. Li, B.N., M.C. Dong, and M.I. Vai, *On an automatic delineator for arterial blood pressure waveforms.* Biomedical Signal Processing and Control, 2010. **5**(1): p. 76-81.

75. Lu, G., et al., *A comparison of photoplethysmography and ECG recording to analyse heart rate variability in healthy subjects.* J Med Eng Technol, 2009. **33**(8): p. 634-41.

76. Selvaraj, N., et al., *Assessment of heart rate variability derived from finger-tip photoplethysmography as compared to electrocardiography.* Journal of medical engineering & technology, 2008. **32**(6): p. 479-484.

77. Bolanos, M., H. Nazeran, and E. Haltiwanger. *Comparison of heart rate variability signal features derived from electrocardiography and photoplethysmography in healthy individuals*. in *Engineering in Medicine and Biology Society, 2006. EMBS'06. 28th Annual International Conference of the IEEE*. 2006. IEEE.

78. Pan, J. and W.J. Tompkins, *A real-time QRS detection algorithm.* IEEE Trans Biomed Eng, 1985. **32**(3): p. 230-6.

79. Korpas, D., J. Halek, and L. Dolezal, *Parameters describing the pulse wave.* Physiol Res, 2009. **58**(4): p. 473-9.

80. Millasseau, S.C., et al., *Contour analysis of the photoplethysmographic pulse measured at the finger.* Journal of hypertension, 2006. **24**(8): p. 1449-1456.

81. Simek, J., et al., *Second derivative of the finger arterial pressure waveform: an insight into dynamics of the peripheral arterial pressure pulse.* Physiological research, 2005. **54**(5): p. 505.

82. Takazawa, K., et al., *Assessment of vasoactive agents and vascular aging by the second derivative of photoplethysmogram waveform.* Hypertension, 1998. **32**(2): p. 365-70.

83. Gonzalez, R., et al. *Photoplethysmographic augmentation index as a non invasive indicator for vascular assessments*. in *4th European Conference of the International Federation for Medical and Biological Engineering*. 2009. Springer.

84. Van Bortel, L.M., et al., *Clinical applications of arterial stiffness, Task Force III: recommendations for user procedures.* Am J Hypertens, 2002. **15**(5): p. 445-52.

85. Perk, J., et al., *European Guidelines on cardiovascular disease prevention in clinical practice (version 2012) The Fifth Joint Task Force of the European Society of Cardiology and Other Societies on Cardiovascular Disease Prevention in Clinical Practice (constituted by representatives of nine societies and by invited experts) Developed with the special contribution of the European Association for Cardiovascular Prevention & Rehabilitation (EACPR).* European heart journal, 2012. **33**(13): p. 1635-1701.

86. Piskorski, J. and P. Guzik, *Filtering poincare plots.* Computational methods in science and technology, 2005. **11**(1): p. 39-48.

87. Drinnan, M.J., J. Allen, and A. Murray, *Relation between heart rate and pulse transit time during paced respiration.* Physiological measurement, 2001. **22**(3): p. 425.

88. Kaibe, M., et al., *Arterial stiffness index: A new evaluation for arterial stiffness in elderly patients with essential hypertension.* Geriatrics & Gerontology International, 2002. **2**(4): p. 199-205.